A VORTEX WAKE ANALYSIS OF OPTIMUM HIGH BY-PASS RATIO DUCTED FANS

A THESIS

Presented to

The Faculty of the Division

of Graduate Studies

By

D. S. Janakiram

In Partial Fulfillment

of the Requirements for the Degree

Doctor of Philosophy

in the School of Aerospace Engineering

Georgia Institute of Technology

November, 1976

A VORTEX WAKE ANALYSIS OF OPTIMUM

HIGH BY-PASS RATIO DUCTED FANS

Approved:

Robin B. Gray, Chairman

James E. Hubbart

James C. Wu

Date Approved by Chairman: Nov. 22, 1976

ACKNOWLEDGMENTS

It is with a deep sense of gratitude that I wish to record here my appreciation of my teacher and advisor Dr. Robin B. Gray for his suggestion of the thesis topic and the wise counsel and guidance he has given me in my research work.

I would like to thank Professor James E. Hubbart and Dr. James C. Wu for their constructive criticism and careful examination of this manuscript.

I also wish to thank Miss Laura Royston for an immaculate job she has done in typing this thesis.

The financial support of Georgia Institute of Technology is gratefully acknowleged.

Finally I wish to thank my parents who gave me their whole-hearted encouragement and made all this possible.

TABLE OF CONTENTS

	Page
ACKNOWLEDGMENTS	ii
LIST OF ILLUSTRATIONS	iv
NOMENCLATURE	vii
SUMMARY	xi
Chapter	
I. INTRODUCTION	1
II. FINITE-BLADED FAN	5
Wake Model Analysis Of The Wake Model Estimation Of Thrust, Power, And Induced Efficiency Numerical Procedures	
III. INFINITE-BLADED FAN	79
Wake Model And Its Solution Estimation Of Thrust And Induced Power	
IV. RESULTS	92
V. DUCT/FAN DESIGN	125
Preliminary Discussion Design Outline	
VI. CONCLUDING REMARKS	138
INDEX TO DATA TABLES	141
BIBLIOGRAPHY	163

LIST OF ILLUSTRATIONS

Figure		Page
1.	Ultimate Wake Of A High By-Pass Ratio Ducted Fan; Paths Of Line Integrals	6
2.	Helical Coordinate System	9
3.	Velocity Diagram At A Vortex Filament On A B.T.E. Sheet	11
4.	Velocity Diagram With Respect To The Rotating Fan Blades Of The Outermost Filament Of The B.T.E. Sheet And At The Adjacent Point Of The Outer Boundary Sheet .	18
5.	Velocity Diagram With Respect To The Rotating Fan Blades At The Inner Boundary Sheet	21
6.	A Radial Section Of The Ultimate Wake	27
7.	Control Volume For The Determination Of Thrust And Induced Power	43
8.	A Path Of Line Integration In The Ultimate Wake	50
9.	Schematic Arrangement Of Control Points And Vortex Filaments In The Ultimate Wake	67
10.	A Typical zr-Surface Used In Computing The Volume Integrals	72
11.	Comparison Of Wright's Results For $K_0(X)$ With The Present Values	93
12.	Comparison Of Wright's Results For $K_0(X)$ With The Present Values	94
13.	Variation Of $K_0(X)$ With Number Of Blades	96
14.	Variation Of $K_0(X)$ With Number Of Blades	97
15.	Variation Of $K_0(X)$ With Number Of Blades	98
16.	Variation Of $K_0(X)$ With Number Of Blades	99

LIST OF ILLUSTRATIONS (Continued)

Figure		Page
17.	Variation Of Mass Coefficient, κ_0', With Number Of Blades	101
18.	Comparison Of Wright's Results For C_T With The Present Values	102
19.	Comparison Of Wright's Results For C_p With The Present Values	103
20.	Comparison Of Wright's Results For C_T With The Present Values	104
21.	Comparison Of Wright's Results For C_p With The Present Values	105
22.	Variation Of ϵ_z With Number Of Blades	107
23.	Variation Of ϵ_z With Number Of Blades	108
24.	Variation Of ϵ_ψ With Number Of Blades	110
25.	Variation Of ϵ_r With Number Of Blades	111
26.	Comparison Of Power Coefficients Computed Using Two Different Methods	112
27.	Variation Of Thrust Coefficient With Load For Fans With Varying Number Of Blades	114
28.	Variation Of Power Coefficient With Load For Fans With Varying Number Of Blades	115
29.	Variation Of Thrust Coefficient With Load For Fans With Varying Number Of Blades	116
30.	Variation Of Power Coefficient With Load For Fans With Varying Number Of Blades	117
31.	Variation Of Thrust Coefficient With Load For Fans With Varying Number Of Blades	118
32.	Variation Of Power Coefficient With Load For Fans With Varying Number Of Blades	119
33.	Variation Of Thrust Coefficient With Load For Fans With Varying Number Of Blades	120

LIST OF ILLUSTRATIONS (Continued)

Figure		Page
34.	Variation Of Power Coefficient With Load For Fans With Varying Number Of Blades	121
35.	Variation Of Induced Efficiency With Load For Fans With Varying Number Of Blades	122
36.	Variation Of C_{T_p}/C_T With Load	124
37.	Schematic Diagram Of A Fan Engine And Its Wake And Duct Contour After First Iteration	129

NOMENCLATURE

$B_{i,j}$	Elements of the coefficient matrix of a system of linear equations.
B.T.E.	Blade trailing edge.
b	Blade number.
C_p	Induced Power Coefficient, $C_p = P_D/[\rho(\Omega R_2)^3 \pi R_2^2]$.
C_T	Thrust coefficient, $C_T = T_D/(\rho(\Omega R_2)^2 \pi R_2^2)$.
C_{T_p}	Thrust coefficient due to fan or propeller alone.
e	Nondimenstional energy loss in the fan wake, $e = E_D/(\rho(\Omega R_2)^3 \pi R_2^2)$.
E_D	Total induced kinetic energy loss in the fan wake, $E_D = Q_D\Omega - T_D V_\infty$.
G	Scale factor, $G = 1 - U_{\xi_1}/W \sin\phi_1$.
K(X)	Goldstein coefficient, $K(X) = b\Gamma'(X)/2\pi R_2 W\lambda_2$.
$K_0(X)$	K(X) for $\overline{W} = 0$ case.
m	R_1/R_2.
P	Static pressure.
P_∞	Static pressure of the undisturbed fluid.
$\overline{P}$	Non-dimensional distance from a vortex filament to a control point.
P_D	Ideal induced power of the duct-fan system.
P_0	Stagnation pressure.
Q_D	Torque on the fan blades.
r,ψ,z	Cylindrical-polar coordinates.
r',ψ',z'	Cylindrical-polar coordinates of a vortex filament.

$\bar{r}$	Nondimensional radial coordinate, $\bar{r} = r/R_2$.
R_2	Outer radius of the ultimate wake of the fan.
R_2^-	Just inside of R_2.
R_2^+	Just outside of R_2.
R_1	Radius of the inner boundary sheet and hub trailing edge.
R_1^-	Just inside of R_1.
R_1^+	Just outside of R_1.
S'	A length of a vortex filament.
S	Surface area.
t	Time.
T_D	Total thrust of the duct-fan system.
T_p	Thrust due to fan alone.
U	Distrubance velocity component in the direction of the subscript.
U_{ξ_1}	Distrubance velocity in ξ direction at the innermost vortex filament of any B.T.E. sheet, $U_{\xi_1} = U_\xi$ at $r = R_1^+$.
U_{ψ_j}	Tangential velocity component on the jet wake boundary in the ultimate wake, $U_{\psi_j} = U_\psi$ at $r = R_1^-$.
$\bar{U}$	Nondimensional velocity, $\bar{U} = U/W$.
$U_{\zeta_{B_2}}$	Velocity describing the motion of vortex filaments on the outer uniform boundary sheet.
v	Total disturbance velocity.
V	Total velocity.
V_∞	Velocity of the undisturbed flow.
$\hat{V}_\infty$	Nondimensional velocity, $\hat{V}_\infty = V_\infty/W$.

V_j — Disturbance axial velocity on the jet boundary in the ultimate wake, $V_j = U_z$ at $r = R_1$.

W — Apparent axial disturbance velocity in the ultimate wake of the fan.

$\overline{W}$ — Dimensionless W, $\overline{W} = W/\Omega R_2$.

X — Nondimensional radial coordinate, $X = \overline{r} = r/R_2$.

$\overline{z}$ — Nondimensional axial distance, $\overline{z} = z/(2\pi R_2 \lambda_2/b)$.

$\hat{z}$ — Nondimensional axial coordinate, $\hat{z} = z/R_2$.

z_0' — Axial distance between the $z = 0$ plane and the point where the vortex filament intersects the rz-plane.

γ — Vortex filament strength.

$\overline{\gamma}$ — Nondimensional filament strength, $\overline{\gamma} = \gamma/4\pi R_2 WG$.

$\hat{\gamma}$ — Vortex sheet strength normal to the filaments.

γ' — Vorticity per unit area.

γ_{B_2} — Vortex sheet strength of the outer uniform boundary sheet.

γ_{B_1} — Vortex sheet strength of the inner uniform boundary sheet.

ε_ψ — Defined as $\varepsilon_\psi = \int_{R_1/R_2}^{1} \int_0^1 \int_0^{2\pi} \overline{U}_\psi^2 \, X dX \, d\overline{z} \, d\psi/2\pi$.

ε_r — Defined as $\varepsilon_r = \int_{R_1/R_2}^{1} \int_0^1 \int_0^{2\pi} \overline{U}_r^2 \, X dX \, d\overline{z} \, d\psi/2\pi$.

ε_z — Defined as $\varepsilon_z = \int_{R_1/R_2}^{1} \int_0^1 \int_0^{2\pi} \overline{U}_z^2 \, X dX \, d\overline{z} \, d\psi/2\pi$.

Γ — Vortex strength of an equivalent line vortex filament along the axis of the jet.

$\Gamma'(X)$ — Blade bound vortex strength at station X.

ξ Helical coordinate in the direction of the helix.

ζ Helical coordinate normal to the helical filaments.

κ' Mass coefficient, $\kappa' = 2 \int_m^1 K(X) X dx$

κ_0' κ' for $\bar{W} = 0$ case.

λ_2 Wake geometry parameter, $\lambda_2 = \frac{V_\infty + W}{\Omega R_2} = \tan\phi_2$.

λ_{B_2} Geometry parameter of outer uniform boundary sheet.

λ_1 Wake geometry parameter, $\lambda_1 = \frac{V_\infty + W}{\Omega R_1} = \tan\phi_1$.

μ' Defined as, $\mu' = 2 \int_m^1 \frac{K(X) X}{(X^2 + \lambda_2^2)} dX$.

μ_0' μ' for $\bar{W} = 0$ case.

ρ Density of the fluid.

Φ Disturbance velocity potential.

ϕ Pitch angle of any B.T.E. sheet at radius 'r'.

ϕ_2 ϕ at $r = R_2^-$.

ϕ_1 ϕ at $r = R_1^+$.

ϕ_{B_2} Pitch angle of the outer uniform boundary sheet.

ϕ_{B_1} Pitch angle of the inner uniform boundary sheet.

Ψ Total stream function.

Ω Rotational speed of the fan blades.

SUMMARY

Single-rotation high by-pass ratio ducted fans with a finite number of fan blades, zero tip clearance and no stator vanes and with the highest induced efficiency generate an ultimate wake vortex system whose apparent motion is that of rigid helical surfaces of constant geometric pitch. This helical wake vortex system is bounded on the inside by a constant diameter cylindrical vortex sheet shed from the trailing edge of the hub and on the outside by an another constant diameter cylindrical vortex sheet shed from the trailing edge of the duct. The outer cylindrical vortex sheet represents the continuation of blade bound vortex on to the duct where it is spread out on the duct surface and finally shed at the trailing edge of the duct. Concentric with the fan wake and inside of the inner boundary sheet is the jet wake which is assumed to be generated by an infinite-bladed turbine. The jet wake is assumed to be given.

A consistent mathematical potential wake model is presented for the fan wake and the boundary sheets and the compatibility relationships to be satisfied by each of the cylindrical boundary vortex sheets are obtained. It is shown that for the wake model to be consistent, the jet wake needs to satisfy certain conditions as far as the induced velocities in it are concerned. The compressibility and viscous effects are neglected in the analysis of the wake. Using the Biot-Savart law, the vortex strength distribution of the ultimate wake is found numerically and

then is related to the blade bound vortex strength distribution. The expressions for the thrust, induced power, and induced efficiency are developed using integral theorems and evaluated numerically.

The ultimate wake vortex model for a ducted fan with infinite number of blades is also developed. It is shown that this wake consists of a constant diameter cylinder of vorticity. The vortex strength distribution in the ultimate wake as well as the expressions for the thrust and induced power are obtained in closed form.

The bound vortex strength distribution, the thrust, and induced power are obtained numerically for heavily loaded ducted fans with a finite number of fan blades for different values of by-pass ratio, blade number, and wake geometric parameter. It is shown that with increasing blade number these values converge to that of the infinite-bladed fan.

A tentative procedure for the design of the duct which results in a compatible wake vortex system is suggested.

CHAPTER I

INTRODUCTION

Ducted fans are finding a wide application in modern aircraft either in the development of low-speed thrust as in the case of V/STOL aircraft or as high by-pass ratio ducted fan engines in the case of high-speed subsonic aircraft. In either case, these fans are the main propulsive units and are usually driven by jet-core engines housed in the hub of these fans. A review of ducted propellers or fans highlighting the theoretical as well as experimental investigations was given by Weetman and Cromack[1]. However, in the past most of these investigations are limited to fans without a finite hub and the emphasis was on the lightly loaded ducted fans. Optimum heavily loaded ducted fans without a hub but with a finite number of blades were analysed by Wright[2]. It is the purpose of this research to provide information regarding the design of optimum high by-pass ratio ducted fans which have a finite hub. The wakes of these ducted fans consist of two parts; one from the fan blades and the duct and the other from the turbine blades of the core engine. In this thesis, the wake of an optimum high by-pass ratio ducted fan with a finite as well as infinite number of blades is analyzed. The ducted fan is optimum in the sense that the induced efficiency of the duct-fan system excluding that of the core jet engine is maximum. High by-pass ratio ducted fans only are considered, so that the most of the thrust developed by the engine comes from the duct-

fan system. The primary emphasis of this thesis is on the wake of the duct-fan system. The classical analysis of an optimum free propeller due to Betz[3] was the basis of the work of Gray[4,5] and Wright[2]. It was shown by Betz that an isolated free propeller having the highest possible induced efficiency generates an ultimate wake vortex system which moves as if the vortex sheets of the wake formed a rigid helical structure of constant pitch. Application of this constraint to the motion of the vortex sheets provides a method for calculating the radial vorticity distribution of the shed wake. Wright[2] has shown that the same arguments are valid for the geometry and motion of the vortex sheets shed from the trailing edges of the blades of an optimum heavily loaded ducted fan. However, the presence of the duct results in a cylindrical vortex sheet shed from the trailing edge of the duct which represents the continuation of blade bound vortex from tips into the duct. Thus, the helicoidal vortex sheets shed from the trailing edges of the fan blades have at their outer edges the cylindrical vortex sheet shed from the trailing edge of the duct. Wright[2] developed the compatibility conditions required for the blade trailing edge sheets and the cylindrical boundary vortex sheet for a ducted fan without a finite hub and blade-tip clearance. With a straightforward application of Biot-Savart law to the mathematical model of the constant diameter ultimate wake, Wright[2] obtained the vorticity distribution in the ultimate wake. The blade bound vortex strength distribution and the thrust, induced power, and induced efficiency of the ducted fan were then obtained from a knowledge of wake vorticity.

In this thesis, Wright's[2] analysis has been extended to the case of an optimum heavily loaded high by-pass ratio ducted fan. In high by-pass ratio ducted fans, most of the thrust is developed by the fan which is driven by a core engine housed in a finite hub.

The mathematical model assumed for the ultimate wake of an optimum high by-pass ratio ducted fan with finite number of blades consists of helicoidal vortex sheets of constant pitch bounded on the inside by the jet wake and on the outside by the cylindrical vortex sheet shed from the trailing edge of the duct. The jet wake is of constant diameter and is assumed to be that generated by an infinite-bladed turbine. The axial velocity in the jet wake may vary radially. The jet wake consists of a distribution of ring and line vorticies and it is assumed that the net vorticity in the jet wake is zero. This implies that the jet wake as a whole does not affect the flow field outside of it. A cylindircal boundary vortex sheet equal in diameter to that of the trailing edge of the hub, referred to as the inner boundary sheet, accommodates the discontinuity in the velocities between the jet wake and the fan wake and cancels the effect of fan wake in the jet wake. Since the outer boundary sheet is similar to the one used in Wright's[2] model, the compatibility conditions developed by Wright are used at the outer boundary sheet. The necessary compatibility conditions required at the inner boundary sheet must be developed. It is shown that for the jet wake to be compatible with the fan wake, the vorticity in the jet wake boundary has to satisfy certain conditions.

A numerical scheme similar to the one proposed by Wright[2] has been employed to solve for the vorticity distribution in the fan wake.

The blade bound vortex strength distribution, the thrust, and induced power of the duct fan system, excluding the contribution due to the jet are computed. These results apply to the high by-pass ratio, single rotation, ducted fans without stator vanes and give an upper limit on the performance since compressibility and viscosity effects were neglected.

Based on unpublished work due to Gray[6], a wake model for the optimum high by-pass ratio ducted fan with infinite number of blades is developed and analyzed. Simple expressions for the bound vorticity distribution as well as the thrust and induced power are obtained. These are necessary in the development of a preliminary design procedure for the duct as well as that of the fan. A design outline of the duct and fan which result in the assumed ultimate fan wake is given.

CHAPTER II

FINITE-BLADED FAN

Wake Model

The wake vortex model developed for the optimum high by-pass ratio ducted fans is essentially an extension of the constant diameter wake vortex model used by Wright[2] for heavily loaded ducted fans. The ultimate wake of the optimum high by-pass ratio ducted fans consists of the following elements: the helical vortex sheets of constant pitch shed from the trailing edges of the fan blades, the cylindrical vortex sheet shed from the trailing edge of the duct, the cylindrical vortex sheet shed from the roots of the fan blades and subsequently from the trailing edge of the fan hub, and the jet wake from the turbine of the engine housed in the fan hub. The two cylindrical vortex sheets consist of helical vortex filaments and are of constant diameter. The vortex sheets shed from the trailing edges of the fan blades, hereafter referred to as B.T.E. sheets, are bounded by the two cylindrical sheets. Hence, these cylindrical sheets are referred to as boundary sheets. The outer boundary sheet separates the fan wake from the irrotational fluid outside of the wake. The inner boundary sheet separates the jet wake from the fan wake. (See Fig. 1).

The argument concerning the geometry and motion of the ultimate wake vortex system of an optimum single rotation, single-row, ducted fan or propeller is essentially the same as given by Theodorsen[7] for a free

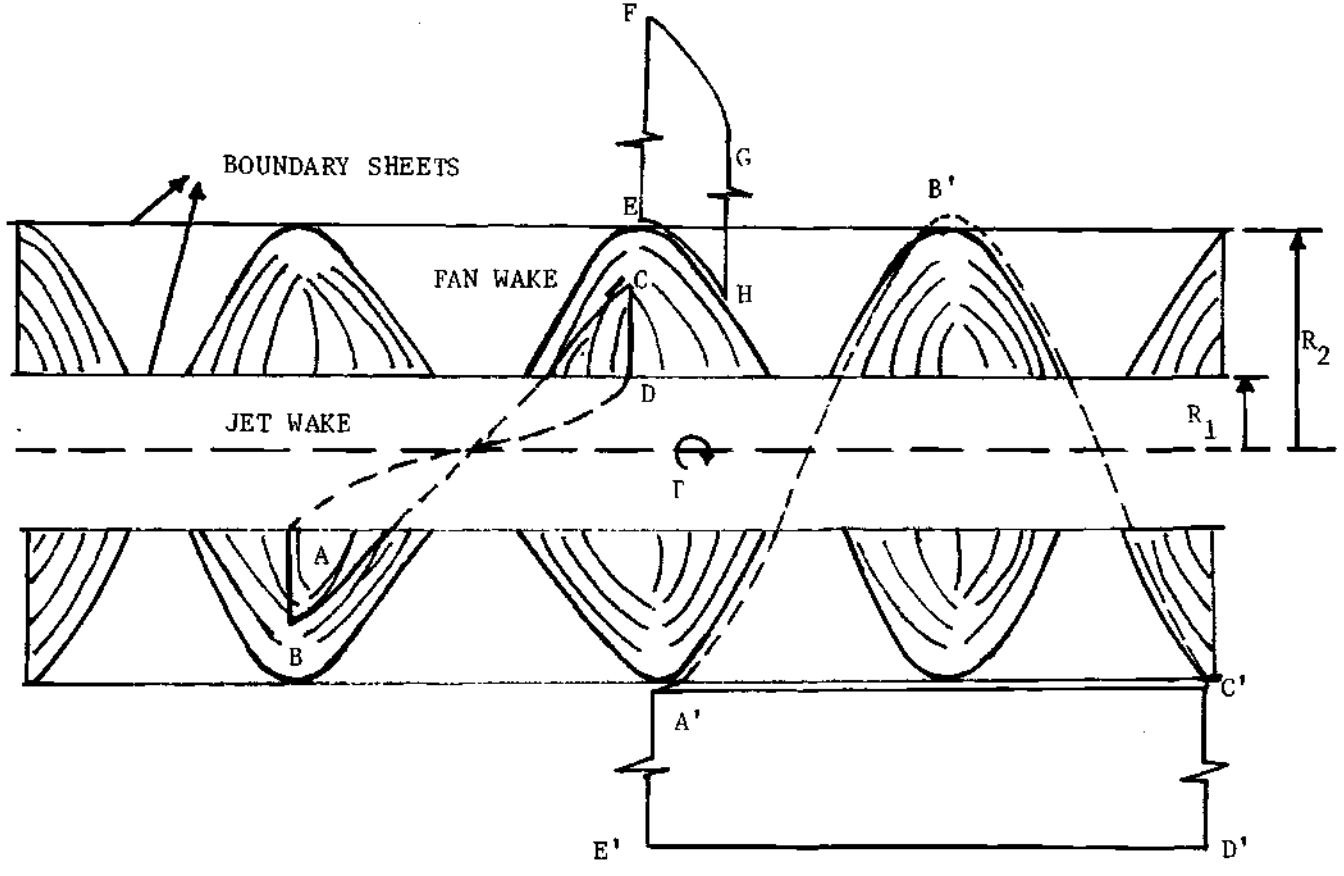

Figure 1. Ultimate Wake Of A High By-Pass Ratio Ducted Fan; Paths Of Line Integrals

propeller. In Ref. 3 it was shown that the optimum condition, that is, the one which results in the highest possible induced efficiency, is obtained for the ducted fan when the helical vortex sheets shed from the blades have a constant geometric pitch and appear to move as rigid screw surfaces of constant diameter in the ultimate wake. This wake model was used for an optimum ducted fan without a hub in Ref. 2. In the present case it is assumed that the same conditions hold for the ultimate wake of the fan of an optimum ducted fan with a finite hub. It is also assumed that the duct is designed such that there is no contraction or expansion of the wake downstream of the trailing edge of the duct. This is a feasible design problem and guarantees that the duct is compatible with the wake geometry and the analysis.

Wakes having an initial expansion or contraction can be treated if it is assumed for an incompressible flow, that a given vortex filament remains at the same nondimensional local radius as it moves down the wake. But in this case, the analysis gets involved since the continuity and force-free vortex must be maintained, while physical limitations such as flow separations must be avoided in the duct. Design of the fan blades also depends on the geometry of the expanding wake and proceeding from the ultimate wake to the fan blades is more involved. While the expanding wake might give a higher induced efficiency for a given thrust and duct diameter, it must be noted that the optimum condition referred to is for the assumed constant diameter wake downstream of the trailing edge of the duct.

In order to maintain the apparent rigid motion of the B.T.E.

sheets, certain compatibility conditions are to be satisfied by the jet wake as well as the two cylindrical boundary sheets. The compatibility conditions required at the outer boundary vortex sheet have been developed by Wright[2] and are rederived here in a slightly different fashion. The necessary compatibility conditions required at the inner boundary vortex sheet are developed here. Since the inner boundary sheet separates the B.T.E. sheets from the jet wake, a suitable model for the jet wake has been assumed.

The jet wake is assumed to be cylindrical with a volume distribution of ring and line vorticity. Essentially it is thought of as a wake generated by an infinite bladed turbine. The diameter of the jet wake is assumed to be equal to that of the trailing edge of the hub. It is assumed that the net vorticity in the jet wake is zero. This implies that in the ultimate wake, the jet wake does not influence the velocity field outside of it. The axial velocity in the jet wake may vary across the jet. This idealized jet wake model does not take into account any viscous interaction between the wakes.

Following the reasoning developed in Ref. 2, a description of the wake of the optimum high by-pass ratio ducted fan is given below.

Consider a helical co-ordinate system, r, ξ, ζ, defined in terms of the cylindrical coordinates, r, ψ, z, as shown in Fig. 2 such that at a given instant, a B.T.E. sheet in the ultimate wake coincides with $\zeta = 0$ surface. Then

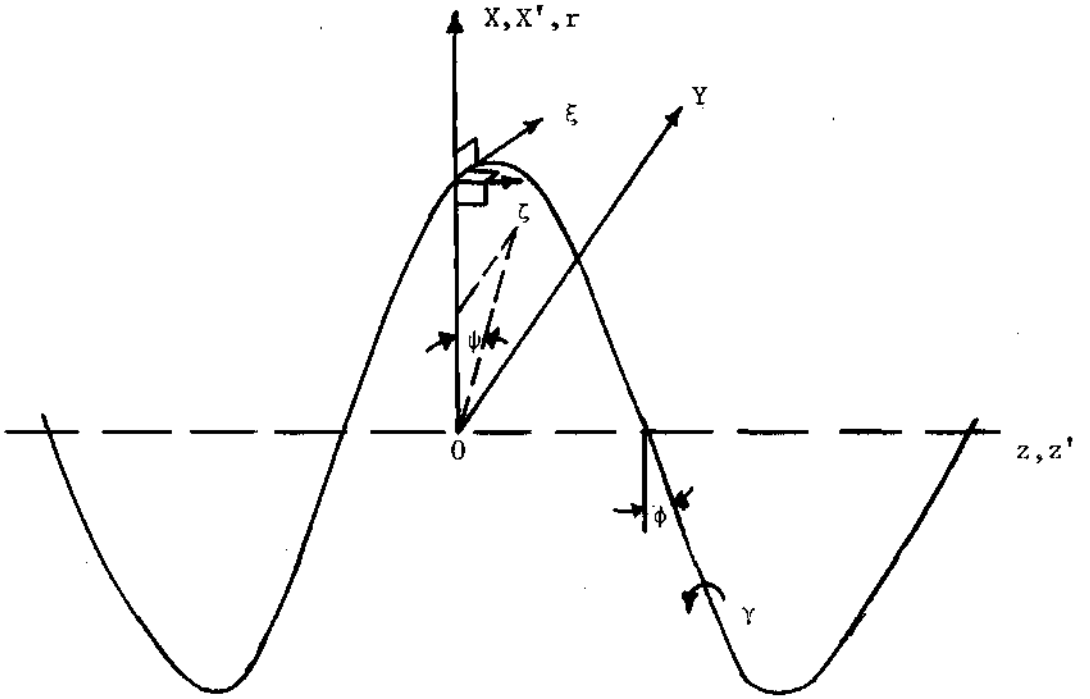

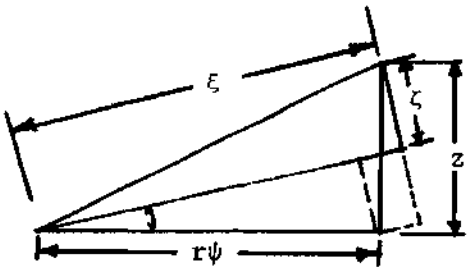

$$\xi = r\psi \cos\phi + z \sin\phi$$
$$\zeta = z \cos\phi - r\psi \sin\phi$$

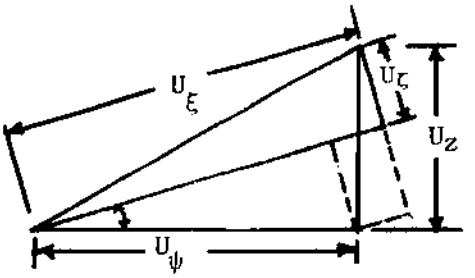

$$U_\xi = U_\psi \cos\phi + U_z \sin\phi$$
$$U_\zeta = U_z \cos\phi + U_\psi \sin\phi$$

Figure 2. Helical Coordinate System.

$$r = r,\ 0 \leq r \leq \infty. \tag{1}$$

$$\xi = r\psi \cos\phi + z \sin\phi,\ -\infty \leq \xi \leq \infty \tag{2}$$

$$\zeta = -r\psi \sin\phi + z \cos\phi,\ -\frac{(V_\infty + W)\cos\phi}{2b(\Omega/2\pi)} \leq \zeta \leq \frac{(V_\infty + W)\cos\phi}{2b(\Omega/2\pi)} \tag{3}$$

where Ω is the angular velocity of the blades and W is the apparent axial velocity in the ultimate wake. The apparent rigid structure of a B.T.E. sheet suggests that the apparent axial velocity, W, of a point on the B.T.E. sheet, that is, the velocity with which a point on the B.T.E. sheet appears to be moving relative to an observer fixed in space, be the same as that of any other point.

To maintain the apparent rigid structure of the B.T.E. sheets in the ultimate wake, a helical symmetry of the fan wake vortex system is necessary. This requires that the disturbance velocity vector is constant along the helical lines, r = constant and ζ = constant, both inside and outside the ultimate wake. Helical symmetry further requires that the boundary vortex sheet strength distribution be symmetric with respect to the lines of intersection of the B.T.E. sheets with the boundary vortex sheets for zero radial velocities at the B.T.E. sheets.

The region of interest is the fan wake between the two boundary vortex sheets. Consider a line integral of the velocity along the path $\overline{ABCDA}$ within the wake as shown in Fig. 1. The velocity diagram at a point on the B.T.E. sheet with respect to a rotating fan blade is shown in Fig. 3. Along $\overline{BC}$ and $\overline{DA}$ in Fig. 1, U_ξ is constant by virtue of helical symmetry. $\overline{AB}$ and $\overline{CD}$ are the radial lines intersecting the

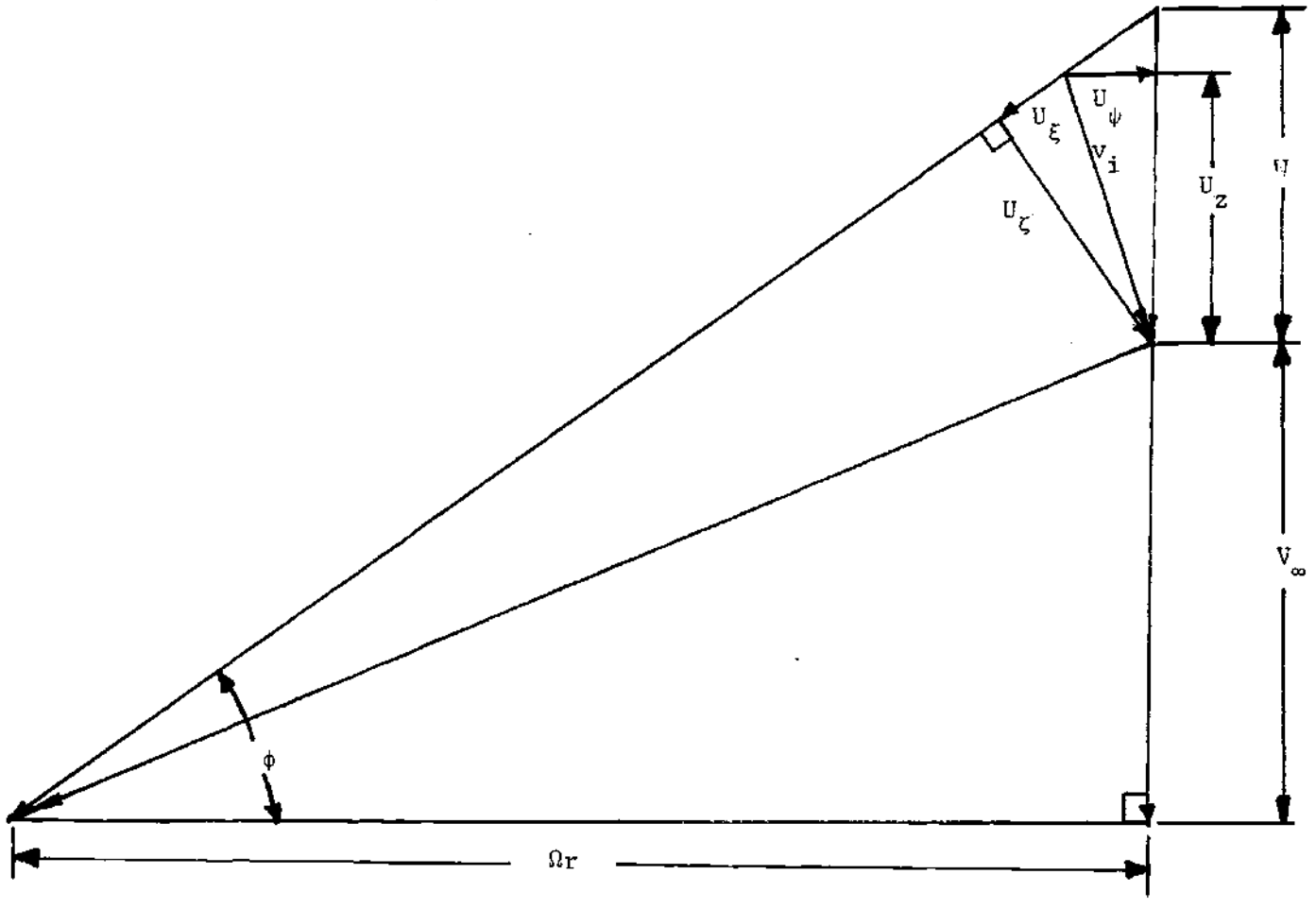

Figure 3. Velocity Diagram At A Vortex Filament On A B.T.E. Sheet.

helical lines $\overline{BC}$ and $\overline{DA}$. The points A and D are at R_1^+ on the B.T.E. sheet. The path so described lies entirely on the surface of the B.T.E. sheet and hence does not enclose any vorticity.

$$\int_A^B U_r \, dr + \int_B^C U_\xi \, d\xi + \int_C^D U_r \, dr + \int_D^A U_\xi \, d\xi = 0$$

since

$$U_r\big|_{\overline{AB}} = U_r\big|_{\overline{DC}},$$

$$U_\xi(\xi_C - \xi_B) + U_{\xi_1}(\xi_A - \xi_D) = 0,$$

where

$$U_{\xi_1} = U_{\xi_{r = R_1^+}}$$

After some simplification and using the fact that the B.T.E. sheets have a constant pitch, it can be shown that

$$U_\xi = U_{\xi_1} \sin\phi/\sin\phi_1, \; R_1 < r < R_2. \tag{4}$$

From the requirement of helical symmetry, it can be shown that the preceding relation holds along any arbitrary helical ine throughout the wake. A similar line integral along the path $\overline{EFGHE}$ establishes the same result outside of the ultimate wake. Further, for the helical coordinate ζ,

$$\tan \phi = (R_2/r)\tan \phi_2 \tag{5}$$

which is a consequence of the constant pitch condition. Thus since ϕ approaches zero as r approaches infinity, U_ξ from Eq. (4) becomes zero at infinite radial distances.

The wake is subject to the additional condition that the line integral of the velocity along a path enclosing all the wake must be zero to obtain a single-valued solution outside of the wake. Following the lines of reasoning given in Ref. 2, it can be shown by computing line integrals of the velocity along suitably chosen contours such as $\overline{A'B'C'A'}$ and $\overline{A'C'D'E'}$ (see Fig. 1) that for the flow to be irrotational outside of the wake U_{ξ_1} must be zero. This is true for a lightly loaded ducted fan. However, for a heavily loaded system, U_{ξ_1} is not zero. For this case, a geometry and motion similar to the one proposed by Wright[2] is necessary for the flow to be irrational outside of the wake.

In the heavily loaded case, the boundary vortex sheets will have an axial motion relative to the B.T.E. sheets and a symmetric strength distribution with respect to the lines of intersection between the B.T.E. sheets and boundary sheets. The relevant arguments given in Ref. 2 can be used here inspite of the presence of a coaxial jet wake, since the net vorticity in the jet wake is zero. Following the line of reasoning given in Ref. 2, it can be shown by taking line integrals of the velocity along suitably chosen contours that the only possible irrotational flow satisfying continuity outside of the constant diameter wake is the one in which all the distrubance velocities are zero.

In summary, the wake model for the high by-pass ratio heavily loaded optimum ducted fan consists of a constant diameter cylindrical jet wake and a coaxial fan wake. The fan wake comprises constant diameter helical B.T.E. sheets bounded on the inside by an inner boundary vortex sheet which separates the jet wake from the fan wake and on the outside by an outer boundary vortex sheet which separates the fan wake from the irrotational fluid outside of it. The fan wake system is helically symmetric to maintain the apparent rigid motion of the helical B.T.E. sheets. The boundary vortex sheets move axially relative to the B.T.E. sheets as a consequence of the heavily loaded condition. Irrotationality of the flow outside of the fan wake requires that the disturbance velocities be zero there. The necessary compatibility conditions required at the boundary vortex sheets are derived below.

Boundary Vortex Sheets

These sheets serve three purposes. First along the constant diameter boundaries, they must cancel the radial velocity field that is associated with the B.T.E. sheets. Second, they must accommodate the required discontinuities in the axial and tangential velocities as the boundary sheets are crossed. Third, they should not induce radial velocities at the B.T.E. sheets. The first and second conditions are satisfied by the boundary sheet strength distributions and geometries both as yet unknown. The third condition can automatically be satisfied by a strength distribution and geometry that is symmetrical with respect to the lines of intersection between the B.T.E. and boundary sheets.

The two boundary vortex sheets are considered separately.

Outer Boundary Sheet

This was the only boundary vortex sheet in the model developed by Wright[2]. The compatibility conditions for this sheet are derived in a similar fashion as in Ref. 2. At the outer edge of the B.T.E. sheet along the line of intersection with the outer boundary sheet,

$$U_\xi = U_{\xi_1} \sin\phi_2/\sin\phi_1, \tag{6}$$

$$U_\zeta = W \cos\phi_2. \tag{7}$$

Outside the wake at the line of intersection, that is, for

$$r = R_2^+, \qquad U_\xi = U_\zeta = 0.$$

Therefore, the filaments on the outer boundary sheet, at the line of intersection must have a velocity normal to their helical coordinate of (see Fig. 4)

$$U_{\zeta_{B_2}} = \frac{1}{2} \left(U_{\xi_1}^2 \sin^2\phi_2/\sin^2\phi_1 + W^2 \cos^2\phi_2\right)^{\frac{1}{2}}, \tag{8}$$

and the boundary sheet strength at the line of intersection must be

$$\gamma_{B_2} = (U_{\xi_1}^2 \sin^2\phi_2/\sin^2\phi_1 + W^2 \cos^2\phi_2)^{\frac{1}{2}}. \qquad (9)$$

The above relations are derived from the fact that the strength of a vortex sheet is equal to the discontinuity in the velocity components as the sheet is crossed and the velocity of the sheet is the mean of the velocities on either side of it.

Therefore, the helical vortex filaments on the outer boundary sheet must all cross the lines of intersection at a constant pitch angle, ϕ_{B_2}, not equal to ϕ_2, which is determined from the flight speed, the blade rotational velocity, and the total disturbance velocity as given in Eq. (8). The boundary vortex sheet strength must also be constant at the lines of intersection and is equal to γ_{B_2}. Thus, when relative motion exists between the B.T.E. sheets and the outer sheet, the two vortex systems are related by Eqs. (8) and (9) along the lines of intersection. These are the compatibility conditions for the outer boundary sheet. On this boundary sheet between the lines of intersection, the filament strengths and pitch angle vary with the helical coordinate ζ.

Wright[2] devised a clever scheme to obviate the difficulty of having to solve for both the strength and geometry of the outer boundary vortex sheet. In his wake model, the boundary sheet vortex system is replaced by two simpler systems of vortex sheets whose combined effect does not change the flow field inside the wake. The first of these is a uniform sheet of helical vortex filaments having a constant strength equal to γ_{B_2} and a constant helical pitch angle ϕ_{B_2}. The second is a

cylindrical sheet of helical filaments of varying and unknown strength but with a constant and known pitch angle Φ_2. The first sheet satisfies the required conditions at the lines of intersection as previously derived. The second sheet has zero strength at the line of intersection, has a symmetrical strength distribution about these lines and the mid point between the lines of intersection, and cancels the radial velocities on the boundary due to the B.T.E. sheets. Superposition of these two sheets must maintain the apparent rigid motion of the B.T.E. sheets.

The geometry and motion of the outer uniform sheet relative to the outermost filament of an adjacent B.T.E. sheet is discussed below. The velocity diagram with respect to the fan blades shown in Fig. 4 illustrates these relationships. From Fig. 4, it is seen, consistent with the compatibility conditions derived, that

$$\overline{PB} = \frac{1}{2}\overline{AB},$$

$$\hat{OPB} = 90°$$

and

$$\overline{OA} = \overline{OB}.$$

This means that the magnitude of the velocity just inside and outside of the outer boundary sheet at the line of intersection in a coordinate system fixed to the fan blades is the same. It is to be noted that the boundary vortex system is force-free and the static pressure should be continuous across it. From Fig. 4, considering the triangle ABC, it

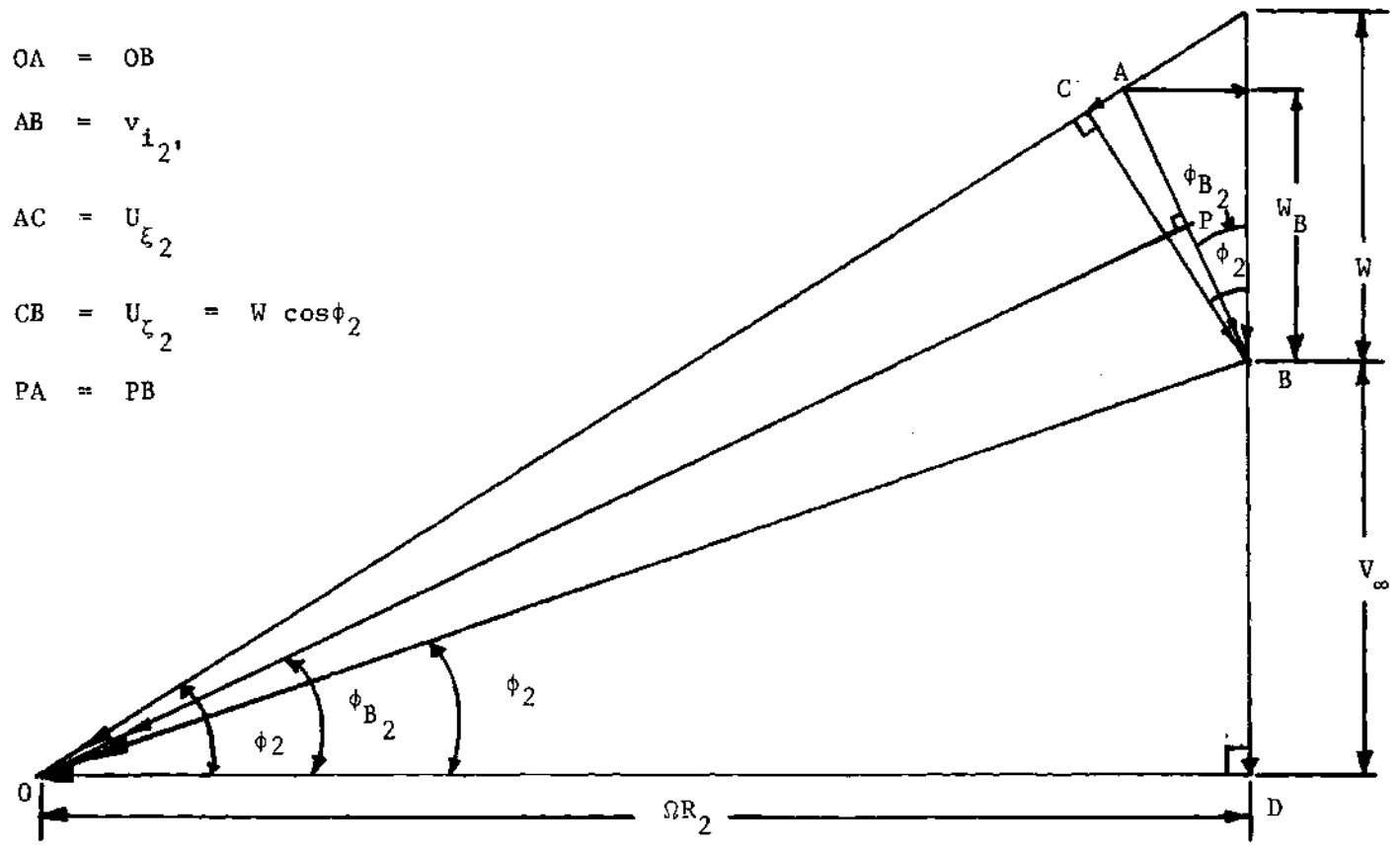

Figure 4. Velocity Diagram With Respect To The Rotating Fan Blades Of The Outermost Filament Of The B.T.E. Sheet And At The Adjacent Point Of The Outer Boundary Sheet.

can be shown that

$$\overline{AB} = \gamma_{B_2} = W \cos\phi_2 \sec(\phi_2 - \phi_{B_2}), \tag{10}$$

and,

$$\hat{POD} = \phi_{B_2} = \frac{\phi_2 + \hat{\phi}_2}{2}, \tag{11}$$

$$\text{where } \tan \hat{\phi}_2 = V_\infty/\Omega R_2,$$

and

$$\tan \phi_2 = (V_\infty + W)/\Omega R_2 = \lambda_2.$$

Thus γ_{B_2} and ϕ_{B_2}, the strength and the pitch angle of the outer uniform boundary sheet respectively are determined when $\overline{W}$, λ_2 and b are given.

The strength distribution of the nonuniform vortex sheet is determined later when the complete wake vortex system is solved.

Inner Boundary Sheet

As noted earlier, the inner boundary sheet like the outer one is cylindrical with helical vortex filaments wrapped on it. It accommodates the discontinuity of the velocity vector between the fan and the jet wake. It cancels the radial velocities associated with the B.T.E. sheets at the boundary sheets. It also cancels the velocities associated with the fan wake and the outer boundary sheet inside the jet wake. It must not induce radial velocities at the B.T.E. sheets. As was done in the case of the outer boundary sheet, the inner boundary

sheet vortex system is replaced by two simpler vortex systems. One is a uniform vortex sheet of helical filaments with a constant strength equal to that at its line of intersection with the B.T.E. sheets and a pitch angle, ϕ_{B_1}, to be determined. The other is a nonuniform vortex sheet of helical filaments with unknown strength distribution but a constant known pitch angle, ϕ_1, equal to the pitch angle of the innermost filament shed from the blade. The nonuniform sheet has a symmetric strength distribution about the line of intersection and has zero strength at the line of intersection. At a line of intersection with the B.T.E. sheets, for $r = R_1^+$,

$$U_\xi = U_{\xi_1},$$

$$U_\zeta = W \cos\phi_1.$$

At $r = R_1^-$, that is, just inside the boundary of the jet wake, the axial and tangential induced velocities are V_j and U_{ψ_j}. In the case of most turbofans, the turbine directly drives the fan and as such has the same rotational speed as that of the fan. As per the wake model assumed, the outer radius of the ultimate wake of the jet is the same as that of the trailing edge of the hub and the radius of the inner boundary sheet in the ultimate wake. Therefore, the velocity diagram at the line of intersection on the inner boundary sheet can be drawn with respect to a coordinate system fixed to the fan blades and is shown in Fig. 5. In this figure, $\overline{FO}$ represents the resultant velocity

$|\vec{EO}| = |\vec{FO}|$; GE = GF

$$\tan\phi_1 = \frac{V_\infty + W}{\Omega R_1} = \lambda_1$$

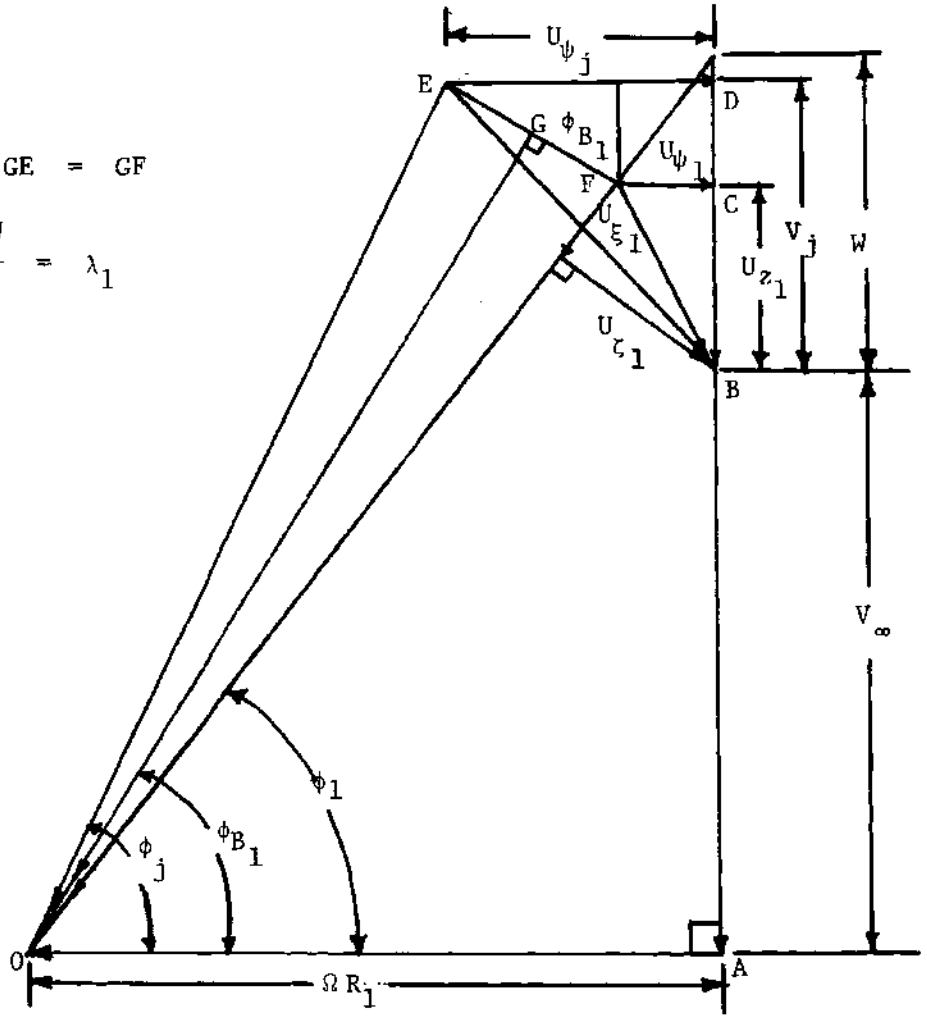

Figure 5. Velocity Diagram With Respect To The Rotating Fan Blades At The Inner Boundary Sheet.

of a vortex filament just outside the inner boundary sheet ($r = R_1^+$) at the line of intersection and $\overline{EO}$ represents the resultant velocity of a vortex filament just inside ($r = R_1^-$). The vector $\overline{EF}$ represents the discontinuity in velocity as the inner sheet is crossed at the line of intersection. The strength of the inner boundary sheet at the line of intersection is given by the magnitude of the vector $\overline{EF}$. The vortex sheet at the line of intersection moves with a velocity equal to the mean of the velocities on either side of it and is represented by the vector $\overline{GO}$. Since the direction of the vortex filament is perpendicular to the discontinuity velocity vector and since the pitch angle of these filaments is determined by their velocities, it follows from Fig. 5 that $|\overline{EO}| = |\overline{FO}|$ and $\hat{OGE} = \hat{OGF} = 90°$. Therefore, for the jet wake to be compatible, a particular combination of V_j and U_{ψ_j} as illustrated in Fig. 5 which satisfies the above two conditions is needed. However, there are several such combinations of V_j and U_{ψ_j} which can satisfy the above conditions, with each particular combination giving rise to a particular value of the pitch angle, ϕ_{B_1}, for the filaments on the inner boundary sheet at the line of intersection. If the parameters of the fan wake, λ_2 and $\bar{W}$, are fixed, the vector $\overline{FO}$ in Fig. 5 is fixed. Then several combinations of V_j and U_{ψ_j}, each of which satisfying the condition $|\overline{EO}| = |\overline{FO}|$, can be chosen with each one giving a different ϕ_{B_1}. A line vorticity distribution in the axial direction and a ring vorticity distribution in the jet wake can induce the required values of U_{ψ_j} and V_j just inside of the jet wake boundary at the line of intersection. As far as the tangential velocity U_{ψ_j} is concerned, the line vorticity distribution in the jet wake is equivalent to a

resultant line vortex filament along the axis of the jet with a strength equal to $\Gamma = U_{\psi_j} 2\pi R_1$. Since the net vorticity in the jet wake is zero, a line vorticity distribution of strength $-U_{\psi_j}$ per unit angular distance on the circular boundary of the jet wake is needed to cancel the line vorticity in the jet. At the line of intersection, for $r = R_1^+$, (see Fig. 5)

$$U_\psi = U_{\psi_1} = -W \cos\phi_1 \sin\phi_1 + U_\xi \cos\phi_1, \tag{12}$$

$$U_z = U_{z_1} = U_{\xi_1} \sin\phi_1 + W \cos^2\phi_1, \tag{13}$$

and for $r = R_1^-$

$$U_\psi = U_{\psi_j},$$

$$U_z = V_j.$$

The radial velocities on the boundary are zero. The magnitude of the vortex sheet strength at the line of intersection is given by,

$$\gamma_{B_1} = |\overline{EF}| = -[(V_j - U_{z_1})^2 + (U_{\psi_j} - U_{\psi_1})^2]^{\frac{1}{2}} \tag{14}$$

The negative sign has been chosen in accordance with the sign convention, that the strength of a vortex filament, γ, located on a wake cylindrical surface of radius, a, is considered to be positive if the axial component of the velocity induced by the vortex filament at point for which $r < a$ is in the direction of the positive z-axis. Bound vortex strengths are considered positive and vortex sheet strengths are considered negative. The pitch angle, ϕ_{B_1}, of these filaments is given by,

$$\tan \phi_{B_1} = -(U_{\psi_j} - U_{\psi_1})/(V_j - U_{z_1}), \tag{15}$$

the negative sign chosen in accordance with the sign convention. It can be seen from Fig. 5, that when $U_{\psi_j} = U_{\psi_1}$ and $V_j = U_{z_1}$, the inner boundary vortex sheet does not exist. In most of the turbofans in use, V_j is usually higher than U_{z_1}, and hence ϕ_{B_1} is always greater than ϕ_1. However, Eqs. (14) and (15) are valid even if ϕ_{B_1} is less than ϕ_1. For the jet wake to be compatible, the engine has to be designed such that $|U_{\psi_j}|$ is greater than $|U_{\psi_1}|$. This can be seen in Fig. 5. Substituting Eqs. (12) and (13) into Eqs. (14) and (15), it can be shown that

$$\gamma_{B_1} = -[(V_j - U_{\xi_1} \sin\phi_1 - W \cos^2\phi_1)^2 + (U_{\psi_j} - U_{\xi_1} \cos\phi_1 + W \cos\phi_1 \sin\phi_1)^2]^{\frac{1}{2}} \tag{16}$$

and

$$\tan \phi_{B_1} = -(U_{\psi_j} - U_{\psi_1})/(V_j - U_{\xi_1} \sin\phi_1 - W \cos^2\phi_1). \qquad (17)$$

Thus, the uniform sheet strength and pitch angle of the inner boundary sheet are determined, when λ_2, $\bar{W}$, V_j, and U_{ψ_j} are given. As discussed earlier, for each λ_2 and $\bar{W}$, several combinations of V_j and U_{ψ_j} with $|U_{\psi_j}| > |U_{\psi_1}|$ can satisfy the compatibility conditions. This uniform sheet induces rotational velocities in the fan wake. However, when the velocities induced due to the equivalent line vortex filament along the axis of the jet wake are taken into account, it is shown later that the velocity field in the fan wake is independent of the jet wake parameters V_j and U_{ψ_j}. This is consistent with the assumed mathematical model for the jet wake. However, for a given λ_2 and $\bar{W}$, only certain combinations of V_j and U_{ψ_j} are compatible with the fan wake. These can be determined once ϕ_{B_1} is chosen. Therefore, for a given λ_2, $\bar{W}$ and ϕ_{B_1}, V_j and U_{ψ_j} are fixed, as can be easily seen from Fig. 5. The nonuniform sheet strength distribution of the inner boundary sheet is determined later.

Analysis Of The Wake Model

Having established the geometry and motion of the ultimate wake vortex sheets, a procedure to solve for the vortex strengths and the associated velocity field can be developed. The procedure is similar to that proposed by Wright[2] but is more general in that the latter can be obtained as a special case.

It is noted that the assumed geometry and motion of the ultimate wake vortex sheets imply certain velocity boundary conditions. It is

the purpose of the discussion here to analyze the wake model and to develop a scheme that gives the vortex strength distribution which satisfies the required velocity boundary conditions. For the purpose of this analysis, it is sufficient to consider a unit length of ultimate wake, ABCDA, as shown in Fig. 6. The unit length is equal to the spacing between two adjacent B.T.E. sheets and is centered at a point on a line of intersection between a B.T.E. sheet and the boundary sheet. Each vortex sheet of this unit wake is divided into a finite number of strips of equal width. These strips are, for the purpose of numerical computation, replaced by vortex filaments of finite but unknown strengths lying on the centrelines of these strips. The strength of each filament must be equal to the integral of the sheet strength across the strip width. An adequate representation of the vortex sheet is achieved by placing each filament at the centreline of its corresponding strip, provided the strip width is sufficiently small compared to a characteristic sheet width.

The Biot-Savart law is used to provide a relation between the geometry, motion, and vortex strengths. The integral relations for the velocity components in cartesian coordinates are given by Lamb[8] and are reproduced here for a single vortex filament of finite strength. These are

$$\Delta U_x = (\gamma/4\pi) \int \left(\frac{dy'}{ds'} \frac{z - z'}{\bar{p}} - \frac{dz'}{ds} \frac{y - y'}{\bar{p}}\right) \frac{ds'}{\bar{p}^2},$$

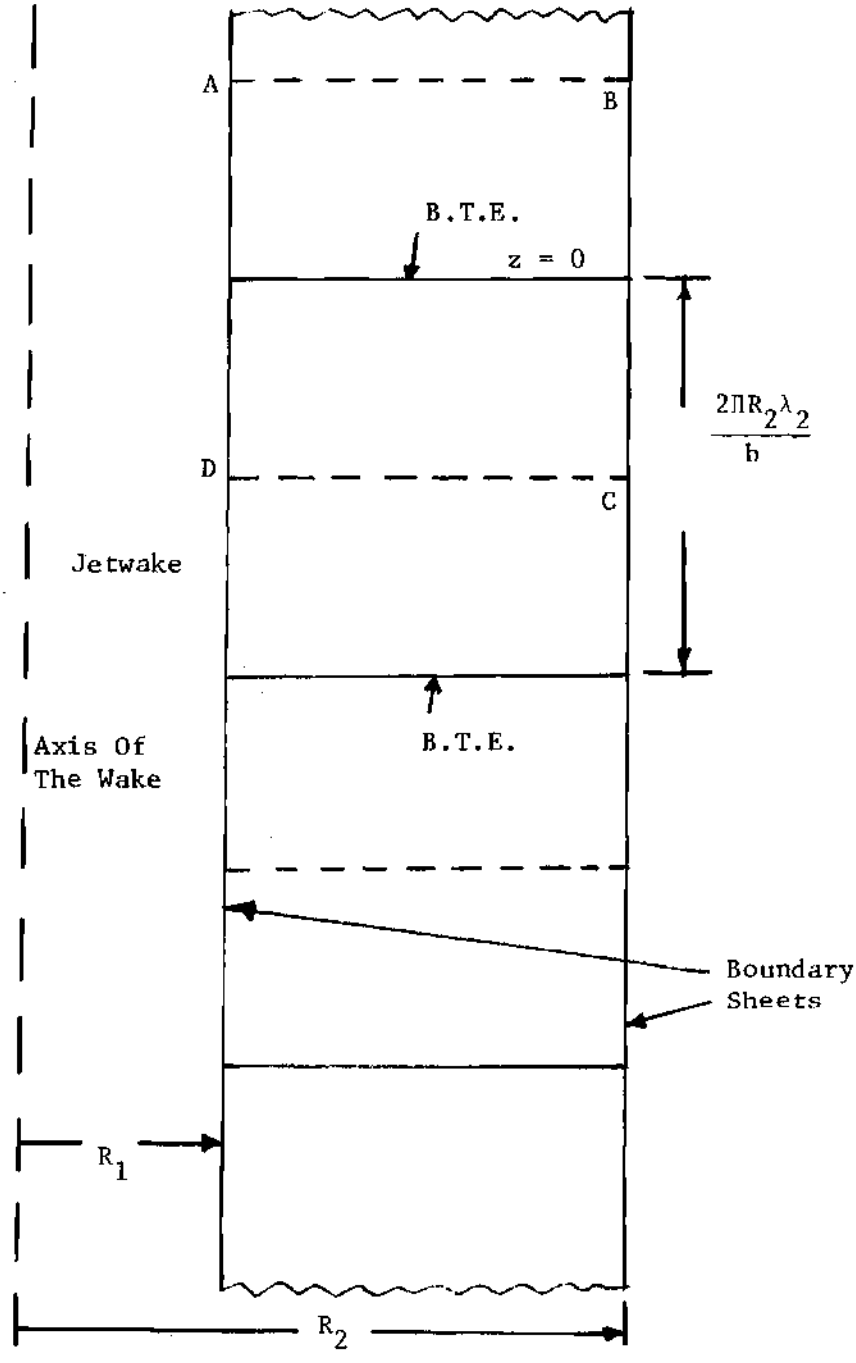

Figure 6. A Radial Section Of The Ultimate Wake.

$$\Delta U_y = (\gamma/4\pi) \int \left(\frac{dz'}{ds'} \frac{x - x'}{\bar{p}} - \frac{dx'}{ds'} \frac{z - z'}{\bar{p}}\right) ds'/\bar{p}^2,$$

and

$$\Delta U_z = (\gamma/4\pi) \int \left(\frac{dx'}{ds'} \frac{y - y'}{\bar{p}} - \frac{dy'}{ds'} \frac{x - x'}{\bar{p}}\right) ds'/\bar{p}^2.$$

It is more convenient to express these integral relations for a finite strength helical vortex filament in polar coordinates using the following transformation.

$$x' = r' \cos\psi, \qquad y' = r' \sin\psi,$$

$$x = r \cos\psi, \qquad y = r \sin\psi,$$

$$z' = z'_o + r'\psi' \tan\phi', \qquad z = z, \; s' = r'\psi' \sec\phi'.$$

The velocity boundary conditions are more conveniently expressed in terms of the velocity components along the vortex sheets and perpendicular to them. A helical coordinate system is then introduced, (see Fig. 2), where

$$U_r = U_x \cos\psi + U_y \sin\psi,$$

$$U_\xi = (U_y \cos\psi - U_x \sin\psi) \cos\phi + U_z \sin\phi$$

and

$$U_\zeta = U_z \cos\phi - (U_y \cos\psi - U_x \sin\psi) \sin\phi.$$

Using these transformations and employing the helical relation (due to the rigid motion of B.T.E. sheets)

$$r' \tan\phi' = R_1 \tan\phi_1 = R_2 \tan\phi_2, \tag{18}$$

the elemental velocities associated with a helical filament of infinite length are given by

$$\frac{\Delta U_r}{W} = \frac{\gamma}{(4\pi R_2 W)} \int_{-\infty}^{\infty} \left[\bar{r}' \tan\phi_2 \sin(\psi'-\psi) + \bar{r}'(\hat{z}-\hat{z}_o'-\psi' \tan\phi_2)\cos(\psi'-\psi) \right] \frac{d\psi'}{\bar{p}^3}, \tag{19}$$

$$\frac{\Delta U_\xi}{W} = \frac{\gamma}{4\pi R_2 W} \int_{-\infty}^{\infty} \left[\bar{r}' \tan\phi_2 \left(\frac{\bar{r}}{\bar{r}'} + \frac{\bar{r}'}{\bar{r}} - 2\cos(\psi'-\psi) \right) + (\hat{z}-\hat{z}_o'-\psi' \tan\phi_2)\sin(\psi'-\psi) \right] \frac{d\psi'}{\bar{p}^3} \tag{20}$$

and

$$\frac{\Delta U_\zeta}{W} = \frac{\gamma}{4\pi R_2 W} \int_{-\infty}^{\infty} \left[(\bar{r}'^2 - \bar{r}\,\bar{r}' \cos(\psi'-\psi)) - \tan^2\phi_2 \left(1 - \frac{\bar{r}}{\bar{r}'}\cos(\psi'-\psi)\right) - \frac{\bar{r}'}{\bar{r}} \sin(\psi'-\psi)\tan\phi_2(\hat{z}-\hat{z}_o'-\psi'\tan\phi_2) \right] \frac{d\psi'}{\bar{p}^3}, \tag{21}$$

where

$$\bar{p}^2 = \bar{r}^2 + \bar{r}'^2 - 2\bar{r}\,\bar{r}' \cos(\psi' - \psi) + (\hat{z} - \hat{z}'_o - \psi' \tan\phi_2)^2,$$

and all the length dimensions are nondimensionalized by R_2. The velocity boundary conditions on the ultimate wake vortex system can be written by summing up the contributions of every filament of the system. They are given by,

$$\sum(\Delta U_{\zeta/W}) = \cos\phi \tag{22}$$

and

$$\sum(\Delta U_{r/W}) = 0 \tag{23}$$

on the B.T.E. sheets,

$$\sum(\Delta U_{r/W}) = 0, \tag{24}$$

on the outer sheet, and

$$\sum\left(\frac{\Delta U r}{W}\right) = 0 \tag{25}$$

on the inner boundary sheet. The region of interest is the unit fan wake which is mathematically represented as, (see Fig. 6)

$$\left.\begin{aligned} R_1 \leq r \leq R_2, \\ -\pi R_2 \lambda_2/b \leq z \leq \pi R_2 \lambda_2/b. \end{aligned}\right\} \tag{26}$$

As far as the velocity field in the above region is concerned, the line

vorticity in the jet wake is equivalent to a resultant line vortex filament of strength $\Gamma = (U_{\psi_j})\ 2\pi R_1$ along the axis of the wake. This resultant line vortex filament can induce only tangential velocities in the ultimate wake. The uniform boundary sheets, ad described earlier, do not induce radial velocities anywhere in the ultimate wake. The non-uniform boundary sheets do not induce radial velocities on the B.T.E. sheets due to their symmetric strength distribution about the respective lines of intersection.

Examination of the integrand of Eq. (19) shows that no radial velocities are induced at a B.T.E. sheet by the evenly spaced B.T.E. sheets themselves. Thus, Eq. (23) is satisfied identically. There is another constraint on the wake vortex system which requires that the sum of the strengths of all the vortex filaments in the ultimate wake be equal to zero. The various constraints on the ultimate wake vortex system are then represented as:

On the B.T.E. sheets,

$$\sum_{\text{B.T.E.}} \left(\frac{\Delta U_\zeta}{W\cos\phi}\right) + \sum_{2U} \left(\frac{\Delta U_\zeta}{W\cos\phi}\right) + \sum_{2N} \left(\frac{\Delta U_\zeta}{W\cos\phi}\right) + \sum_{IU} \left(\frac{\Delta U_\zeta}{W\cos\phi}\right)$$

$$+ \sum_{1N} \left(\frac{\Delta U_\zeta}{W\cos\phi}\right) + \sum_{\text{jet}} \left(\frac{\Delta U_\zeta}{W\cos\phi}\right) = 1; \qquad (27)$$

On the outer boundary sheet,

$$\sum_{\text{B.T.E.}} \left(\frac{\Delta U_r}{W}\right) + \sum_{2N} \left(\frac{\Delta U_r}{W}\right) + \sum_{1N} \left(\frac{\Delta U_r}{W}\right) = 0; \qquad (28)$$

On the inner boundary sheet,

$$\sum_{B.T.E.} \left(\frac{\Delta U_r}{W}\right) + \sum_{2N} \left(\frac{\Delta U_r}{W}\right) + \sum_{1N} \left(\frac{\Delta U_r}{W}\right) = 0; \tag{29}$$

and

$$\sum_{B.T.E.} \left(\frac{\gamma}{4\pi R_2 W}\right) + \sum_{1U} \left(\frac{\gamma}{4\pi R_2 W}\right) + \sum_{1N} \left(\frac{\gamma}{4\pi R_2 W}\right)$$

$$+ \sum_{2U} \left(\frac{\gamma}{4\pi R_2 W}\right) + \sum_{2N} \left(\frac{\gamma}{4\pi R_2 W}\right) + \sum_{jet} \left(\frac{\gamma}{4\pi R_2 W}\right) = 0; \tag{30}$$

where $\sum_{B.T.E.}$ refers to the summation over the blade trailing edge sheets. $\sum_{1U}$ refers to the summation over the inner uniform boundary sheet, $\sum_{2U}$ refers to that over the outer uniform boundary sheet, $\sum_{2N}$ refers to the outer nonuniform sheet, $\sum_{1N}$ refers to the inner nonuniform sheet, and $\sum_{jet}$ refers to that over the jet wake.

Since the geometry and strengths of the uniform boudary sheets and jet wake are known, their contributions can be derived explicitly. First, consider the outer uniform boundary sheet. The velocity field associated with this sheet is (see Ref. 2)

$$U_{z_{2U}} = \gamma_{B_2} \cos\phi_{B_2}, \qquad r < R_2,$$

$$U_{r_{2U}} = U_{\psi_{2U}} = 0, \qquad \text{everywhere.}$$

Using Eqs. (10) and (11), it can be shown that

$$\left(\frac{U_z}{W}\right)_{2U} = \cos\phi_2 \sec(\phi_2 - \phi_{B_2}) \cos(\phi_{B_2})$$

or,

$$\left(\frac{U_z}{W}\right)_{2U} = 1/(1 + \lambda_2\lambda_{B_2}).$$

It is to be noted that on the outer B.T.E. sheet,

$$(U_z/W)_{2U} = (U_\zeta/W \cos\phi)_{2U} = 1/(1 + \lambda_2\lambda_{B_2}).$$

From Fig. 4 and Eq. (4), it can be shown that

$$\tan(\phi_2 - \phi_{B_2}) = U_{\xi_2}/W \cos\phi_2 = U_{\xi_1} \tan\phi_2/W \sin\phi_1.$$

Define

$$G = 1 - U_{\xi_1}/W \sin\phi_1 \tag{31}$$

Using Eq. (11) and the above relations, it can be shown that

$$G = 1 - \tan((\phi_2 - \hat{\phi}_2)/2) \quad / \tan\phi_2 . \tag{32}$$

G is therefore determined once λ_2 and either $\overline{W}$ or $V_\infty/\Omega R_2$ are known. It can also be shown that

$$1 - 1/(1 + \lambda_2\lambda_{B_2}) = (\lambda_2/(1 + \lambda_2^2) \quad \left(1 - \frac{1}{\lambda_2}\left(\frac{\lambda_2 - \lambda_{B_2}}{1 + \lambda_2\lambda_{B_2}}\right)\right)$$

and then

$$(U_z/W)_{2U} = 1 - \frac{G\lambda_2^2}{(1 + \lambda_2^2)} . \tag{33}$$

since the length of the uniform boundary sheet considered corresponds to that of the unit wake,

$$\sum_{2U} (\gamma/4\pi R_2 W) = (\gamma_{B_2}/4\pi R_2 W)(2\pi R_2 \lambda_{B_2} \cos\phi_{B_2}/b) .$$

which can be simplified as

$$\sum_{2U} (\gamma/4\pi R_2 W) = (G/2b)(\lambda_2/(1 + \lambda_2^2)) . \tag{34}$$

It will be shown that when the contributions due to the jet wake are added to those of the inner uniform boundary sheet, the resulting

expression do not contain any of the jet wake parameters, U_{ψ_j}, and V_j. These expressions depend only on the fan wake parameters, λ_2, $\bar{W}$, b and G. This can be expected due to the fact that the jet wake model is such that it does not affect the velocity field in the fan wake.

In the region of interest as described by Eq. (26), the uniform vortex sheet of the inner boundary induces only tangential velocities. It can be shown that

$$(U_\psi/W)_{1U} = -\gamma_{B_1} \sin\phi_{B_1} R_1/(Wr), \qquad r > R_1$$

From Fig. 5 and using the sign convention described earlier

$$\gamma_{B_1} \sin\phi_{B_1} = (U_{\psi_j} - U_{\psi_1})$$

and

$$(U_\psi/W)_{1U} = (\bar{U}_{\psi_1} - \bar{U}_{\psi_j})R_1/r. \tag{35}$$

The jet wake induces tangential velocities in the fan wake and is equivalent to a resultant line vortex filament along the wake axis of strength equal to $\Gamma = (U_{\psi_j})2\pi R_1$ so that

$$(U_\psi/W)_{jet} = \Gamma/2\pi rW = (\bar{U}_{\psi_j})R_1/r. \tag{36}$$

The inner boundary sheet is made up of the filaments on the boundary of the jet wake and the filaments that are shed from the roots of the fan blades. The jet wake, hereafter when it is referred to, does not include its boundary since its boundary is already included in the inner boundary sheet. Combining Eqs. (35) and (36)

$$(U_\psi/W)_{1U} + (U_\psi/W)_{jet} = \bar{U}_{\psi_1} R_1/r. \tag{37}$$

Since $U_{z_{1U}} = U_{z_{jet}} = 0$, $U_\zeta = -U_\psi \sin\phi$, and therefore

$$(U_\zeta/W \cos\phi)_{1U} + (U_\zeta/W \cos\phi)_{jet} = -\bar{U}_{\psi_1} R_1 \tan\phi/r,$$

Using Eq. (18) and the fact that $\bar{U}_{\psi_1} = -G \sin\phi_1 \cos\phi_1$, it can be shown that

$$(U_\zeta/W \cos\phi)_{1U} + (U_\zeta/W \cos\phi)_{jet} = \frac{G \lambda_1\lambda_2}{(1 + \lambda_1^2)x^2} \left(\frac{R_1}{R_2}\right). \tag{38}$$

since the characteristic length of the fan wake need not correspond to that of the jet wake, the vorticity due to all the blades of the fan is considered while computing the total vorticity in the ultimate wake so that

$$\sum_{1U} (\gamma/4\pi R_2 W) = (\gamma_{B_1}/4\pi R_2 W) 2\pi R_1 \lambda_{B_1} \cos\phi_{B_1}$$

or from Fig. 5, it can be shown that

$$\sum_{1U} (\gamma/4\pi R_2 W) = \frac{(\bar{U}_{\psi_1} - \bar{U}_{\psi_j})}{2} \left(\frac{R_1}{R_2}\right).$$

When computing the total vorticity in the jet wake, all the line vortex filaments excluding the ones on its boundary are taken into account since the latter are already included in the contribution from the inner boundary sheet. As noted earlier, all of the line vortex filaments inside the jet wake are equivalent to a line filament along its axis so that

$$\sum_{jet} (\gamma/4\pi R_2 W) = \Gamma/4\pi R_2 W = U_{\psi_j} R_1/2WR_2.$$

Combining the contributions due to the jet and the inner uniform boundary sheet, it can be shown that

$$\sum_{1U} (\gamma/4\pi R_2 W) + \sum_{jet} (\gamma/4\pi R_2 W) = \frac{\bar{U}_{\psi_1} R_1}{2 R_2} = -\frac{G}{2} \frac{\lambda_1}{1 + \lambda_1^2} \left(\frac{R_1}{R_2}\right). \qquad (39)$$

While computing $\sum_{2U} (\gamma/4\pi R_2 W)$, only a unit length of the wake has been considered. The contribution to $\sum_{2U} (\gamma/4\pi R_2 W)$ from all of the fan blades will be 'b' times the value given by Eq. (34). However, after summing up all the contributions, the resulting expression can be divided by

the number of blades, b, as is done in Eq. (43) below. Equations (27), (28), (29) and (30) can now be written as:

On the B.T.E. sheets,

$$\sum_{\text{B.T.E.}} \frac{\Delta U_\zeta}{W \cos\phi} + \sum_{2N} \frac{\Delta U_\zeta}{W \cos\phi} + \sum_{1N} \frac{\Delta U_\zeta}{W \cos\phi} = \frac{G\lambda_2^2}{1 + \lambda_2^2} - \frac{G\lambda_1}{(1 + \lambda_1^2)} \left(\frac{R_1}{R_2}\right) \frac{\lambda_2}{X^2}; \tag{40}$$

On the outer boundary sheet,

$$\sum_{\text{B.T.E.}} (\Delta U_r/W) + \sum_{2N} (\Delta U_r/W) + \sum_{1N} (\Delta U_r/W) = 0; \tag{41}$$

On the inner boundary sheet,

$$\sum_{\text{B.T.E.}} (\Delta U_r/W) + \sum_{2N} (\Delta U_r/W) + \sum_{1N} (\Delta U_r/W) = 0; \tag{42}$$

and

$$\sum_{\text{B.T.E.}} \left(\frac{\gamma}{4\pi R_2 W}\right) + \sum_{2N} \left(\frac{\gamma}{4\pi R_2 W}\right) + \sum_{1N} \left(\frac{\gamma}{4\pi R_2 W}\right) = \frac{G}{2b} \left(\frac{R_1}{R_2}\right) \frac{\lambda_1}{1 + \lambda_1^2} - \frac{G}{2b} \frac{\lambda_2}{(1 + \lambda_2^2)} . \tag{43}$$

Eq. (40) is evaluated at a number of control points on the

B.T.E. sheet. These points are placed between the adjacent filaments and at the two end points ($r = R_1^+$ and $r = R_2^-$) of the sheet. Thus, the number of control points is one higher than that of the filaments. Equations (41) and (42) are evaluated at control points on the portions of the cylindrical boundary sheets which lie between a line of intersection and the point midway between the adjacent lines of intersection. When the nonuniform strength boundary sheets are replaced by a set of vortex filaments of finite but unknown strength, the fact that the vortex strength distribution is symmetric with respect to any line of intersection and the midpoint between any two adjacent lines of intersection is taken into account. Consequently only the vortex filaments that lie between a line of intersection and the midpoint between adjacent lines of intersection enter into the problem as those of unknown strength. The control points are placed between the adjacent vortex filaments. The end points of this portion of the boundary sheets ($z = 0$, $z = \pi R_2 \lambda_2 / b$) are excluded since the Eqs. (41) and (42) are satisfied identically at these points. While evaluating Eq. (43), all the vortex filaments of the characteristic unit length of the wake are taken into account.

Now the integrals in Eqs. (19) and (21) are defined respectively as

$$I_r = (\Delta U_r / W) / (\gamma / 4\pi R_2 W). \tag{44}$$

and

$$I_\zeta = (\Delta U_\zeta / W)/(\gamma/4\pi R_2 W). \tag{45}$$

The system of Eqs. (40) through (42) can then be expressed in terms of I_r and I_ζ. It is also seen from Eqs. (19) and (21) that I_r and I_ζ depend only on the choice of λ_2 and b. Since the right hand side of Eqs. (40) through (43) is multiplied by G, this system of equations is written in terms of a new vortex filament strength, $\bar{\gamma} = (\gamma/4\pi R_2 WG)$. Using Eqs. (44) and (45) and the definition of $\bar{\gamma}$, the system of Eqs. (40) through (43) is written as:

At the control points on the B.T.E. sheet,

$$\sum_{\text{B.T.E.}} I_\zeta \bar{\gamma} + \sum_{1N} I_\zeta \bar{\gamma} + \sum_{2N} I_\zeta \bar{\gamma} = \frac{\lambda_2^2}{1+\lambda_2^2} - \frac{\lambda_1 \lambda_2}{(1+\lambda_1^2)} \left(\frac{R_1}{R_2}\right) \frac{1}{x^2}; \tag{46}$$

At the control points on the outer boundary sheet,

$$\sum_{\text{B.T.E.}} I_r \bar{\gamma} + \sum_{1N} I_r \bar{\gamma} + \sum_{2N} I_r \bar{\gamma} = 0; \tag{47}$$

At the control points on the inner boundary sheet,

$$\sum_{\text{B.T.E.}} I_r \bar{\gamma} + \sum_{1N} I_r \bar{\gamma} + \sum_{2N} I_r \bar{\gamma} = 0; \tag{48}$$

and

$$\sum_{B.T.E.} \bar{\gamma} + \sum_{1N} \bar{\gamma} + \sum_{2N} \bar{\gamma} = \frac{1}{2b} \left[\frac{R_1}{R_2} \frac{\lambda_1}{1 + \lambda_1^2} - \frac{\lambda_2}{1 + \lambda_2^2} \right]. \qquad (49)$$

This system of equations does not contain the parameter $\bar{W}$, so that a solution may be obtained which may be scaled directly for any value of $\bar{W}$. This means that the equations are solved only once for the $\bar{W} = 0$ case ($G = 1$) to get the values of $\bar{\gamma}$. The wake vorticity distribution for any value of $\bar{W}$ is easily obtained by multiplying the values of $\bar{\gamma}$ for the $\bar{W} = 0$ case by the appropriate value of G. This scheme was originally used by Wright.[2]

The blade bound vortex strength at any radial station is found by summing up the strengths of all the filaments of the B.T.E. sheet inboard of the radial station in question and then adding to it the strength of the vortex filament shed from the root of the blade. The strengths of the nonuniform sheet filaments are also obtained as part of the solution of Eqs. (46) through (49) and are used along with the vortex filaments on B.T.E. sheet to obtain the velocity field in the ultimate fan wake. The detailed numerical evaluation of the integrals of I_r and I_ζ, the positioning of the filaments, and the simultaneous solution of the system of linear equations that results from Eqs. (46) through (49) are considered in a forthcoming section of this chapter.

Estimation Of Thrust, Power And Induced Efficiency

The solution of the vorticity distribution in the ultimate wake allows a calculation of the velocity field in the wake. The knowledge of the velocity field in the wake, and hence the momentum and kinetic

energy in the wake leads to the determination of thrust, induced power, and induced efficiency of the high by-pass ratio ducted fan.

Thrust

It is the main interest of this analysis to develop an expression for the thrust of the ducted fan in terms of the known velocity field of its ultimate wake. The thrust that may be developed due to the jet exhaust is not considered. Along the lines of Theodorsen's[7] analysis a control volume enclosing the high by-pass ratio ducted fan and its wake is considered. (See Fig. 7.) Using the momentum theorem, the thrust of the ducted fan can be found by considering the average pressure forces acting on the control surface and the average flux of momentum through the surface. The thrust thus obtained is the total thrust developed by the ducted fan and as such includes the thrust due to the jet exhaust. In the absence of the fan and the duct, with the jet wake parameters the same as those in the ultimate jet wake of the ducted fan with jet, the thrust due to the jet exhaust can be determined using a control volume approach similar to the one suggested earlier. Subtracting the expression for the thrust due to the jet exhaust from the expression for the total thrust gives an expression for the thrust developed by the fan with a finite hub and the duct. Implicit in this procedure is the assumption that there is no interaction between the jet wake and the fan wake.

As noted earlier, the thrust of the ducted fan is found by considering the average pressure forces acting on the control surface and the average flux of momentum through the surface. These averages are taken over a time $\Delta t = 2\pi/b\Omega$ and the integration is performed with

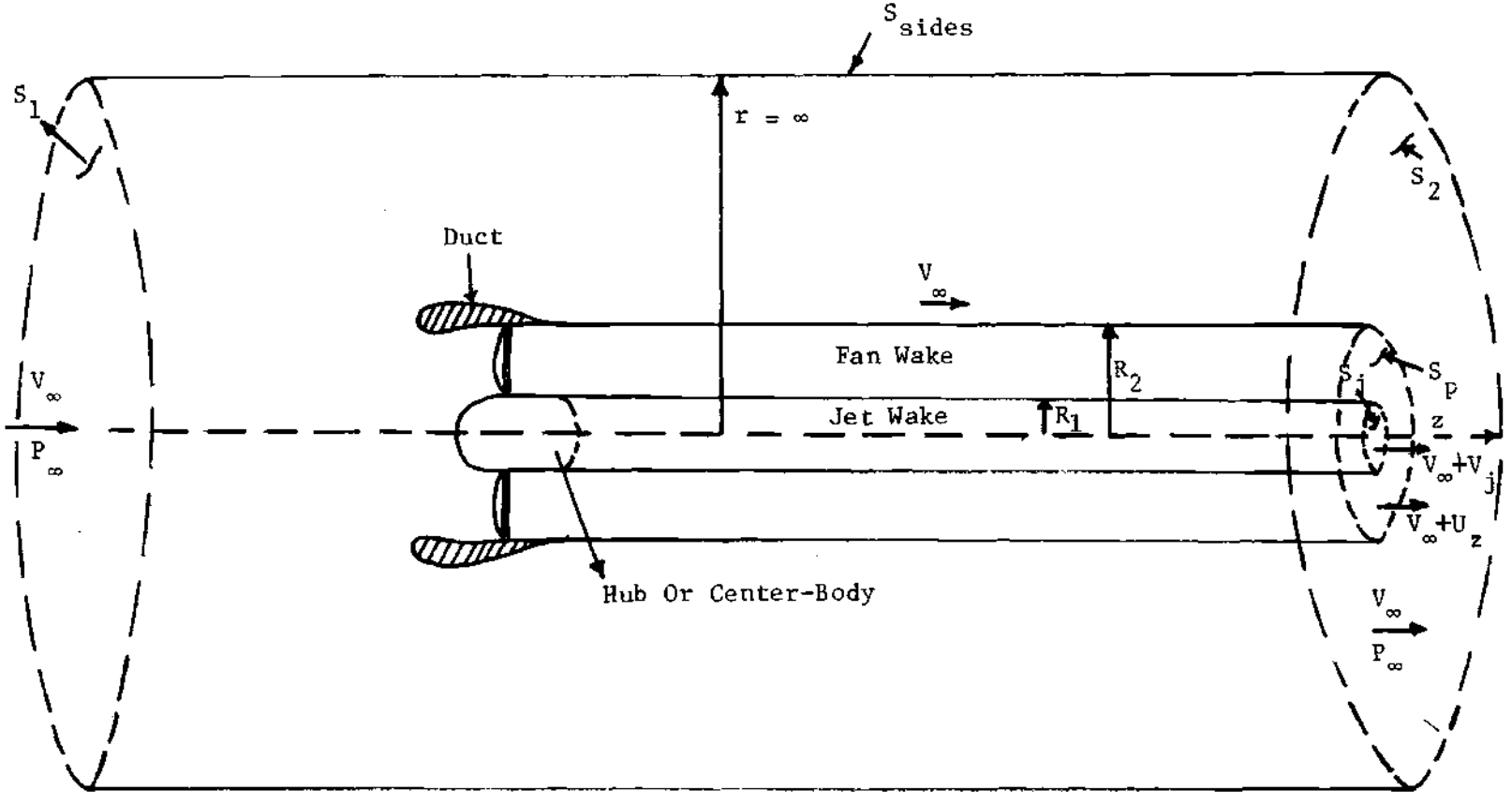

Figure 7. Control Volume For The Determination Of Thrust And Induced Power.

respect to time $dt = dz/(V_\infty + W)$. From Fig. 7 and using the momentum theorem, it can be shown that

$$T_t + \frac{1}{\Delta t} \int_{S_1,S_2} p \, dt \, ds = \frac{1}{\Delta t} \int_{S_2,S_1,S_{sides}} \rho(\vec{V}\cdot\vec{k})(\vec{V}\cdot\vec{k}) ds \, dt \qquad (50)$$

where $\vec{k}$ is the unit vector in the axial direction away from the fan. The wakes are cylindrical with constant radii and, as such, the wake surfaces are connected by the relation $S_2 = S_{jet} + (S_p - S_{jet}) + (S_2 - S_p)$, where S_{jet} refers to the area of intersection of the jet wake with the control surface S_2, $(S_p - S_j)$ refers to the area of the intersection of the fan wake with S_2, and $(S_2 - S_p)$ is the remaining area of S_2. The fluid is assumed to be incompressible as far as the fan wake is concerned. Using the continuity equation for the system, Eq. (50) can be written as

$$T_t + \frac{1}{\Delta t}\left[\int_{S_1} p \, ds \, dt - \int_{S_2} p \, ds \, dt \right] = \frac{1}{\Delta t} \int_{S_{jet}} \rho_j (V_j V_\infty + V_j^2) ds \, dt$$

$$+ \frac{1}{\Delta t} \int_{(S_p - S_{jet})} \rho(V_\infty U_z + U_z^2) ds \, dt + m_f \, V_\infty \qquad (51)$$

where m_f is the mass rate of fuel injected. Considering a similar control volume approach with an isolated jet wake with the same jet wake parameters as those of the above, it can be shown that the thrust, T_j, due to jet wake alone is given by

$$T_j + \frac{1}{\Delta t}\int_{S_{jet}} (p_\infty - p)ds\ dt = \frac{1}{\Delta t}\int_{S_{jet}} \rho_j(V_j V_\infty + V_j^2)ds\ dt + m_f V_\infty \tag{52}$$

Subtracting Eq. (52) from Eq. (51), the following expression for the thrust developed by the fan-duct system is obtained.

$$T_D = \frac{1}{\Delta t}\int_{(S_p - S_{jet})} (p - p_\infty)ds\ dt + \frac{1}{\Delta t}\int_{(S_p - S_{jet})} \rho(V_\infty U_z + U_z^2)ds\ dt$$

In the ultimate fan wake for

$dt = dz/(V_\infty + W)$ and a characteristic time, $\Delta t = 2\Pi/b\Omega$,

$$T_D = \frac{b\Omega}{2\Pi(V_\infty + W)}\int_{\text{fan wake}} (p - p_\infty)ds\ dz + \frac{b\Omega\rho}{2\Pi(V_\infty + W)} \left(\int_{\substack{\text{fan}\\\text{wake}}} (V_\infty U_z + U_z^2)ds\ dz\right). \tag{53}$$

In order to evaluate the above integral, the pressure term must be evaluated in terms of the velocity field by employing the equation of motion for an unsteady, incompressible, potential flow. Bernoulli s equation for such a type of flow is given by

$$\partial\Phi/\partial t + p/\rho + V^2/2 = f(t)$$

The unsteady term is eliminated by considering the potential flow field in a steady coordinate system, the one fixed to the blade, such that,

$$\Phi(r, \psi, z, t) = \Phi(r, \psi_o + \Omega r t, z),$$

$$\partial\Phi/\partial t = (\partial\Phi/\partial\psi)(\partial\psi/\partial t) = U_\psi(\Omega r) = X\ U_\psi\ \Omega R_2.$$

It is to be noted that the flow field is potential in the fan wake except at points on the B.T.E. sheets and the cylindrical boundary sheets. In the fan wake, for an arbitrary helical filament of pitch angle ϕ at radius r,

$$U_\xi = U_{\xi_1} \sin\phi/\sin\phi_1,$$

where U_{ξ_1} is the velocity along the helical filament at radius $r = R_1^+$. It can be shown that U_{ξ_1} at any point on $r = R_1^+$ is the same as U_{ξ_1} of the B.T.E. sheets. Thus at any point in the fan wake,

$$U_\xi = U_\psi \cos\phi + U_z \sin\phi = U_{\xi_1} \sin\ /\sin\phi_1,$$

$$U_\psi = (1 - G)W \tan\phi - U_z \tan\phi,$$

and

$$\partial\Phi/\partial t = (V_\infty + W)\ W(1 - G) - (V_\infty + W)\ U_z. \qquad (54)$$

In the fan wake,

$$P/\rho + V^2/2 - (V_\infty + W)U_z + (V_\infty + W)\, W(1 - G) = P_o/\rho .$$

Since the flow is irrotational inside the wake except at points on B.T.E. sheets,

$$P/\rho + V^2/2 - (V_\infty + W)U_z + (V_\infty + W)\, W(1 - G) = P_{o_{R_2^-}}/\rho . \qquad (55)$$

The outer boundary of the vortex system is force-free and therefore the static pressure is continuous across it, that is,

$$P_{R_2^-} = P_{R_2^-} .$$

As discussed earlier, there are no disturbance velocities outside of the ultimate wake. Therefore,

$$P_{R_2^-} = P_\infty \quad \text{and} \quad V^2 = V_\infty^2 \quad \text{for } r > R_2$$

and

$$P_\infty = P_{o_{R_2^-}} - V_{R_2^-}^2/2 + (V_\infty + W)U_{z_{R_2^-}} - W(V_\infty + W)(1 - G)$$

substituting Eq. (55) into the above expression,

$$(P_\infty - P) = \frac{1}{2}\rho(V^2 - V_{R_2^-}^2) - \rho(V_\infty + W)(U_z - U_{z_{R_2^-}}). \tag{56}$$

Substitution Eq. (56) into Eq. (53), it is shown that

$$T_D = \frac{\rho b\Omega}{2\Pi(V_\infty + W)} \int_{\substack{\text{vol. of the} \\ \text{fan wake}}} \left[\frac{1}{2}(V_{R_2^-}^2 - V_\infty^2) + (V_\infty + W)(U_z - U_{z_{R_2^-}}) + (V_\infty U_z + U_z^2)\right] dVol \tag{57}$$

where,

$$V^2 = (V_\infty + U_z)^2 + U_r^2 + U_\psi^2,$$

$$V_{R_2^-}^2 = (V_\infty + U_{z_{R_2^-}})^2 + U_{\psi_{R_2^-}}^2.$$

the limites of integration are taken over a characteristic volume of the fan wake, that is,

$$0 \le z \le 2\Pi R_2\lambda_2/b,\ 0 \le \psi \le 2\Pi, \text{ and, } R_1 \le r \le R_2.$$

Defining a thrust coefficient $C_T = T_D/\rho(\Omega R_2)^2\Pi R_2^2$. Eq. (57) can be written as

$$C_T = 2\bar{W}^2 \int_{R_1/R_2}^{1} \int_{0}^{1} \int_{0}^{2\pi} \Big[\frac{1}{2}(\bar{U}^2_{z_{R_2^-}} + \bar{U}^2_{\psi_{R_2}}) + \bar{U}^2_z - \frac{1}{2}(U^2_z + \bar{U}^2_r + \bar{U}^2_\psi) + (\lambda_2/\bar{W})\ \bar{U}_z - \bar{U}_{z_{R_2^-}} \Big] x\,dx\ d\bar{z}\ d\psi/2\pi. \quad (58)$$

where, $\bar{z} = z/(2\pi R_2 \lambda_2/b)$, $x = r/R_2$, and all the disturbance velocities are non-dimensionalized with respect to W except that $\bar{W} = W/R_2$. Some of the terms in Eq. (58) can be evaluated explicitly through a consideration of a line integral $\overline{ABCDA}$ as shown in Fig. 8. Note that $\overline{CB}$ is a helical line on the B.T.E. sheet at $r = R_1$. The line integral about the path $\overline{ABCDA}$ encloses the vortex filaments shed by 'b' blades between $r = R_1$ and $r = r$ so that the line integral is evaluated as

$$\int_A^B U_r\ d_r + \int_B^C U_\xi\ d_\xi + \int_C^D U_r\ d_r + \int_D^A U_z\ d_z = b\Gamma'(r).$$

where $\Gamma'(r)$ is the blade bound vorticity at radius 'r'.

But
$$\int_A^B U_r\ dr = -\int_C^D U_r\ dr,$$

$$\int_B^C U_\xi\ d\xi = U_{\xi_1}\ 2\pi R_1 \sec(\phi_1).$$

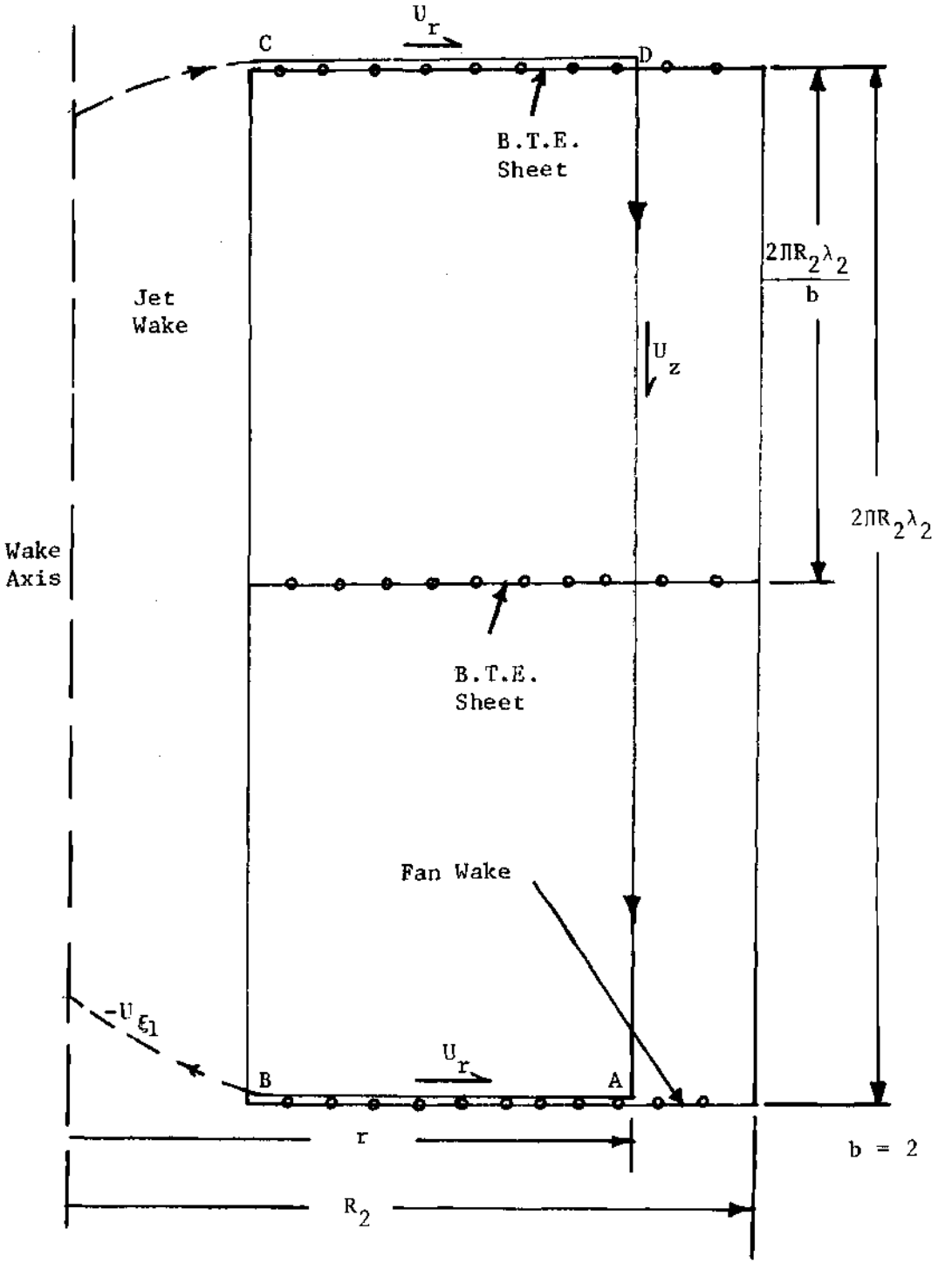

Figure 8. A Path Of Line Integration
In The Ultimate Wake.

$$\int_D^A U_z \, dz = b \int_D^E U_z \, dz = b\,\Gamma'(r) + U_{\xi_1} 2\pi R_1 (1 + \lambda_1^2)^{1/2}$$

so that

$$\int_0^1 \bar{U}_z \, d\bar{z} = \frac{b\,\Gamma'(X)}{2\pi R_2 W \lambda_2} + \bar{U}_{\xi_1} (1 + \lambda_1^2)^{1/2}/\lambda_1 .$$

Defining the Goldstein coefficient, $K(X) = b\,\Gamma'(X)/2\pi R_2 W \lambda_2$ it can be shown that,

$$\int_0^1 \bar{U}_z \, dz = K(X) + (1 - G) \tag{59}$$

Defining a mass coefficient κ' as

$$\kappa' = 2 \int_{R_1/R_2}^1 K(X) X dX,$$

it can be shown that

$$\int_{R_1/R_2}^1 \int_0^1 \int_0^{2\pi} \bar{U}_z \, X dX \, d\bar{z} \, d\psi/2\pi = \frac{1}{2}[\kappa' + (1 - G)(1 - R_1^2/R_2^2)]. \tag{60}$$

and

$$\int_{R_1/R_2}^{1} \int_{0}^{1} \int_{0}^{2\pi} \bar{U}_{z_{R_2^-}} X dX \, d\bar{z} \, d\psi/2\pi = \frac{1}{2}[K(1)+(1 - G)](1 - R_1^2/R_2^2). \quad (61)$$

It was shown earlier that the flow fields of the uniform boundary sheets are known and that the flow fields of sheets of varying strength, namely, the inner and outer nonuniform boundary sheets and the B.T.E. sheet, need only be computed for the case, $\bar{W} = 0$. It is therefore possible to compute C_T in terms of the $\bar{W} = 0$ wake solution and the scale factor G. The integrands of Eq. (58) are therefore modified as follows. The velocities are separated into those associated with the nonuniform boundary sheets and the B.T.E. sheets and those associated with the uniform boundary sheets and the jet wake. Denoting the velocity field due to the B.T.E. sheets and nonuniform boundary sheets by the subscript, 'vs', it is seen that

$$\bar{U}_{VS_{\bar{W}}} = G \, \bar{U}_{VS_{\bar{W}=0}} = G \, \bar{U}_{VS},$$

$$K(X) = G \, K(X)_{\bar{W}=0} = G \, K_o(X)$$

and

$$\kappa' = 2G \int_{R_1/R_2}^{1} K_o(X) X dX = G \, \kappa'_o. \quad (62)$$

It was shown earlier that the velocity field associated with the outer uniform boundary sheet is

$$(\bar{U}_z)_{2U} = 1 - \frac{G\lambda_2^2}{(1 + \lambda_2^2)}, \qquad X < 1$$

and the velocity associated with the inner uniform sheet and the jet wake is,

$$(\bar{U}_\psi)_{1U} + (\bar{U}_\psi)_{jet} = -(G\lambda_1/(1 + \lambda_1^2))(R_1/R_2)1/X \qquad \text{for } X > R_1/R_2.$$

In the following discussion, let

$$\int dvol' = \int_{R_1/R_2}^{1}\int_0^1\int_0^{2\pi} X dX\, d\bar{z}\, d\psi/2\pi = \frac{1}{2}(1 - R_1^2/R_2^2)$$

The integrals in Eq. (58) can be written as

$$\int \bar{U}_z^2\, dvol' = \int [G\, \bar{U}_{z_{VS}} + (1 - G\lambda_2^2/(1 + \lambda_2^2))]^2\, dvol'.$$

which can be simplified as,

$$\int \bar{U}_z^2\, dvol' = G^2 \int \bar{U}_{z_{VS}}^2\, dvol' + 2G(1 - G\lambda_2^2/(1 + \lambda_2^2)) \int \bar{U}_{z_{VS}}\, dvol'$$

$$+ (1 - G\lambda_2^2/(1 + \lambda_2^2))^2\, (1 - R_1^2/R_2^2)/2$$

Similarly, it can be shown that

$$\int \bar{U}_{\psi}^2 \, dvol' = G^2 \int \bar{U}_{\psi_{VS}}^2 \, dvol' - (2G^2\lambda_1/(1 + \lambda_1^2))(R_1/R_2)$$

$$\left(\int (\bar{U}_{\psi_{VS}}/X) dvol'\right) + (G^2\lambda_1^2/(1 + \lambda_1^2)^2)(R_1^2/R_2^2)Ln(R_2/R_1),$$

$$\int \bar{U}_r^2 \, dvol' = G^2 \int \bar{U}_{r_{VS}}^2 \, dvol',$$

$$\int \bar{U}_{z_{R_2^-}}^2 \, dvol' = G^2 \int \bar{U}_{z_{R_2^-_{VS}}}^2 \, dvol' + 2G(1 - G\lambda_2^2/(1 + \lambda_2^2))$$

$$\left(\int \bar{U}_{z_{R_2^-_{VS}}} \, dvol'\right) + (1 - G\lambda_2^2/(1 + \lambda_2^2))^2(1 - R_1^2/R_2^2)/2,$$

and

$$\int \bar{U}_{\psi_{R_2^-}}^2 \, dvol' = G^2 \int \bar{U}_{\psi_{R_2^-_{VS}}}^2 \, dvol' - \frac{2G^2\lambda_1}{(1 + \lambda_1^2)} \frac{R_1}{R_2} \int \bar{U}_{\psi_{R_2^-_{VS}}} \, dvol'$$

$$+ \frac{1}{2} \frac{G^2\lambda_1^2}{(1 + \lambda_1^2)^2} \left(\frac{R_1^2}{R_2^2}\right) \left(1 - \frac{R_1^2}{R_2^2}\right).$$

Using Eq. (60) and Eq. (61), it can be shown that

$$\int \bar{U}_{z_{VS}} \, dvol' = \frac{1}{2} \left[\kappa'_o - (1 - R_1^2/R_2^2)/(1 + \lambda_2^2)\right]$$

and

$$\int \bar{U}_{z_{R_2^-VS}} \, dvol' = \frac{1}{2} \left[K_o(1) - \frac{1}{(1 + \lambda_2^2)}\right] \left[1 - \frac{R_1^2}{R_2^2}\right].$$

Substituting these integrals in Eq. (58) and defining

$$\epsilon_o = \int [\bar{U}^2_{\psi_{R_2^-VS}} + \bar{U}^2_{z_{R_2^-VS}} + \bar{U}^2_{z_{VS}} - \bar{U}^2_{\psi_{VS}} - \bar{U}^2_{r_{VS}}] \, dvol'$$

and $m = R_1/R_2$, the thrust coefficient is written as,

$$C_T = \bar{W}^2 \left\{ G \kappa'_o(\lambda_2/\bar{W} + 1 - G\lambda_2^2/(1 + \lambda_2^2)) - (1 - m^2)K_o(1)G^2\lambda_2^2/(1 + \lambda_2^2) \right.$$

$$+ G^2\epsilon_o + (1 - G)(1 - m^2)(1 - 2G\lambda_2^2/(1 + \lambda_2^2) + \lambda_2/\bar{W})$$

$$- (1 - m^2)(1 - G\lambda_2^2/(1 + \lambda_2^2))^2 + (G^2\lambda_1^2 m^2/(1 + \lambda_1^2))$$

$$(\mathrm{Ln}\, m + (1 - m^2)/2) + (2G^2\lambda_1 m/(1 + \lambda_1^2)) \left[\int [\bar{U}_{\psi_{VS}}/X - \bar{U}_{\psi_{R_2^-VS}}] \right.$$

$$\left. \left. dvol' \right] \right\} \qquad (63)$$

For a given λ_2 and 'b', κ_0', $K_0(1)$, and ϵ_0 are evaluated from the solution corresponding to $\bar{W} = 0$. The scale factor G can be computed algebraically for a given λ_2 and W. Therefore Eq. (63) provides an entire family of values of C_T for different values of $\bar{W}$.

Induced Power

The ideal power required by the optimum high by-pass ratio ducted fan, excluding the jet, can be obtained through a consideration of the induced energy loss in the fan wake. An analysis similar to the one used for the thrust is used to compute the induced energy loss in the ultimate wake. Considering a control volume as shown in Fig. 7, the induced energy loss can be obtained by considering the average of the work done by pressure forces acting on the control surfaces and the average kinetic energy flux through the surfaces. These averages are once again taken over a time, $\Delta t = 2\pi/b\Omega$, and the integration is with respect to time, $dt = dz/(V_\infty + W)$. As done earlier, subtracting the contribution due to the jet wake, the energy loss in the ultimate wake of the fan is obtained as

$$E_D = \frac{b\Omega}{2\,(V_\infty + W)} \int_{\substack{\text{vol. of the} \\ \text{fan wake}}} \left[\frac{1}{2}\rho v^2 V_\infty + \frac{1}{2}\rho v^2 U_z + \rho(V_\infty + W)\right.$$

$$\left.(U_z - U_{z_{R_2}})U_z - \frac{1}{2}\rho(V^2 - V_{R_2}^2)U_z\right] d\text{vol}', \quad (64)$$

where $$v^2 = U_z^2 + U_r^2 + U_\psi^2.$$

Nondimensionalizing the lengths and velocities and defining $e = E_D/\rho(\Omega R_2)^3 \pi R_2^2$, Eq. (64) is written as

$$e = 2\bar{W}^3 \int_m^1 \int_0^1 \int_0^{2\pi} [\bar{U}_z^2 + \tfrac{1}{2}(\lambda_2/\bar{W} - 1)\bar{v}^2 + \bar{U}_z(\tfrac{1}{2}\bar{v}_{R_2}^2 - \bar{U}_{z_{R_2}})]X dX\, d\bar{z}\, d\psi/2\pi \cdot (65)$$

Once again the induced velocities in the above integral are divided into those associated with the uniform boundary sheets and the jet wake and those associated with the sheets of varying strength, namely the nonuniform boundary sheets and the B.T.E. sheets. Using the expressions developed earlier for $\bar{U}_{z_{VS}}$ and $\bar{U}_{\psi_{VS}}$, the expression for 'e' can be obtained in terms of the $\bar{W} = 0$ wake solution and G. It can be shown that

$$e = \bar{W}^3 \left\{ [G\kappa_0' - G(1 - m^2)/(1 + \lambda_2^2)]\, [(1 - G\lambda_2^2/(1 + \lambda_2^2)) \left(\lambda_2/\bar{W} + \tfrac{1}{2}(1 - \frac{G\lambda_2^2}{1 + \lambda_2^2})\right) + \tfrac{1}{2} G^2 m^2 \lambda_1^2/(1 + \lambda_1^2)] - \frac{G\lambda_2^2(1 - m^2)}{(1 + \lambda_2^2)} \right.$$

$$\left. (1 - \frac{G\lambda_2^2}{1 + \lambda_2^2})\, [G\, K_0(1) - \frac{G}{1 + \lambda_2^2}] + \tfrac{1}{2}\,(1 - m^2)(\frac{\lambda_2}{\bar{W}} - 1) \left(1 - \frac{G\lambda_2^2}{1 + \lambda_2^2}\right)^2 \right.$$

$$+\frac{1}{2}(1-m^2)\left(1-\frac{G\lambda_2^2}{1+\lambda_2^2}\right)^3+\frac{1}{2}m(1-m^2)\frac{G^2\lambda_1^2}{(1+\lambda_1^2)^2}\left(1-\frac{G\lambda_2^2}{1+\lambda_2^2}\right)$$

$$+G^2(\lambda_2/\overline{W}+1)\int \overline{U}^2_{z_{VS}}\,dvol'+G^2(\lambda_2/\overline{W}-1)\int(\overline{U}^2_{\psi_{VS}}+\overline{U}^2_{r_{VS}})$$

$$dvol'+G^2(1-G\lambda_2^2/(1+\lambda_2^2))\int[\overline{U}^2_{z_{R_2^-VS}}+\overline{U}^2_{\psi_{R_2^-VS}}]\,dvol'-2G^3\lambda_2^2/$$

$$(1+\lambda_2^2)\int \overline{U}_{z_{VS}}\,\overline{U}_{z_{R_2^-VS}}\,dvol'+G^3\int \overline{U}^2_{z_{VS}}[\overline{U}^2_{z_{R_2^-VS}}+\overline{U}^2_{\psi_{R_2^-VS}}]\,dvol'$$

$$-2G^3m\lambda_1/(1+\lambda_1^2)\int \overline{U}_{z_{VS}}\,\overline{U}_{\psi_{R_2^-VS}}\,dvol'-(2G^2m\lambda_1/(1+\lambda_1^2))$$

$$(1-G\lambda_2^2/(1+\lambda_2^2))\int \overline{U}_{\psi_{R_2^-VS}}\,dvol'-(\lambda_2/\overline{W}-1)(2G^2m\lambda_1/(1+\lambda_2^2))$$

$$\left(\int \overline{U}_{\psi_{VS}}/X\,dvol'\right)-(\lambda_2/\overline{W}-1)G^2m^2\lambda_1^2\,Ln(R_1/R_2)/(1+\lambda_1^2)^2\Bigg\}. \quad (66)$$

Then,

$$E_D = Q_D\Omega - T_D V_\infty$$

where Q_D is the induced torque on the fan blades. The induced power can be written as

$$P_{D_{in}} = Q_D \Omega = T_D V_\infty + E_D.$$

Defining the induced power coefficient, $C_p = P_{D_{in}} / \rho (\Omega R_2)^3 \pi R_2^2$, it is shown that

$$C_p = (\lambda_2 - \bar{W}) C_T + e.$$

The power requirement for the constant diameter wake of the ducted fan can also be obtained using Kutta-Joukowski theorem provided it is assumed that due to the non-contracting wake and compatible shroud, velocities at the fan are the same as those in the wake. It is to be noted that this need not be a physically possible configuration. According to the Kutta-Jourkowski theorem, the incremental torque dQ_D of the fan blades is given by

$$dQ_D = \rho b \Gamma'(r) V_{axial} \, r \, dr$$

where

$$V_{axial} = V_\infty + W \left(1 - G\lambda_2^2 / (X^2 + \lambda_2^2)\right).$$

Blades must be designed to give the distribution, $\Gamma'(r)$.

Therefore,

$$dQ_D = \rho b K(X) 2\pi R_2 W \lambda_2 V_{axial},$$

so that,

$$Q_D = \rho \pi R_2^2 \lambda_2 R_2 W \left[(V_\infty + W) 2 \int_m^1 K(X) X dX \right.$$

$$\left. - 2GW\lambda_2^2 \int_m^1 XK(X)/(X^2 + \lambda_2^2) dX \right]$$

Defining $\mu_0' = 2 \int_m^1 K_0(X) X/(X^2 + \lambda_2^2) dX$, and $\mu' = G\mu_0'$, it can be shown that

$$P_{Din} = Q_D \Omega = \rho \pi R_2^2 (\Omega R_2)^3 \bar{W} \lambda_2^2 [G\kappa_0' - G^2 \bar{W} \lambda_2 \mu_0']$$

and

$$C_{P_{KJ}} = G \bar{W} \lambda_2^2 [\kappa_0' - G \bar{W} \lambda_2 \mu_0'] \qquad (67)$$

Induced Efficiency

The induced efficiency, η_i, of the fan-duct system can be defined as,

$$\eta_i = T_D V_\infty / P_{D_{in}}.$$

The above expression can also be written as

$$\eta_i = (\lambda_2 - \bar{W}) C_T / (C_T(\lambda_2 - \bar{W}) + e) \tag{68}$$

or

$$\eta_i = (\lambda_2 - \bar{W}) C_T / C_p.$$

For a constant diameter wake from the fan blades, the Kutta-Jourkowski theorem can be used to compute the thrust developed by the fan blades alone. The incremental thrust developed by the fan blades is given by

$$d T_p = \rho b V_{tan} \Gamma'(r)\, dr$$

where $V_{tan} = (\Omega r - U_\psi/2) = \Omega r - GWX\lambda_2/2(X^2 + \lambda_2^2)$.

$U_\psi/2$ was chosen since the tangential velocity ahead of the fan is zero and behind it is U_ψ.

Following a procedure as adopted earlier,

$$T_p = \int_m^1 \rho \left(\Omega r - GWX\lambda_2/2(X^2 + \lambda_2^2)\right) K(X) 2\pi R_2^2 W\lambda_2\, dX.$$

Defining $C_{T_P} = T_p/\rho\Omega^2 R_2^2 \pi R_2^2$, it can be shown that

$$C_{T_P} = G\,\bar{W}\,\lambda_2\,[\kappa_0' - G\,\bar{W}\,\mu_0'\,\lambda_2/2] \tag{69}$$

Thus the expressions for C_T, C_{T_P}, C_P, and η_i have been obtained in terms of the wake solution for the $\bar{W} = 0$ case. In the following section, a discussion of the computational procedure is given.

Numerical Procedures

The wake model and its mathematical solution have been discussed in terms of the basic procedures and developments. To obtain a solution it is necessary to evaluate the velocities due to a helical vortex filament of finite but unknown strength at any arbitrary location in its flow field. A system of linear equations is developed by equating the sums of velocities due to all the filaments in the wake at the control points to the required normal velocities at these points. The velocity influence coefficients are evaluated by numerical integration procedures and the system of linear equations is solved by a suitable numerical technique. After obtaining the solutions for the vortex strengths in the ultimate wake, the velocity field in the wake can be computed. Then, Eqs. (63) and (66) are evaluated numerically to obtain the thrust and induced energy loss in the wake. In addition to these, the values of $K_0(X)$, κ_0', and μ_0' are also obtained.

The velocity components associated with a single helical vortex filamanet of finite but unknown strength at any arbitrary location are obtained by numerically evaluating the integrals of Eqs. (19) through

(21). It is seen from these equations that the integrands are solely functions of the geometry of the filament and the location of the point at which the velocity components are evaluated. Since the integrals are evaluated for points in the ultimate wake, the limits of integrations range from $-\infty$ to ∞. The numerical integrations are simplified by converting the limits from $-\infty \leq \psi' \leq \infty$ to $0 \leq \psi' \leq \infty$ with the appropriate changes in the integrands. Equations (19), (20) and (21) are then written as

$$(\Delta U_r/W) = (\gamma/4\pi R_2 W) \int_0^\infty f_r(\psi'; \bar{r}, \bar{r}', \hat{z}, \hat{z}_0', \psi, \lambda_2) d\psi', \tag{70}$$

$$(\Delta U_\zeta/W) = (\gamma \cos\phi/4\pi R_2 W) \int_0^\infty f_\zeta(\psi'; \bar{r}, \bar{r}', \hat{z}, \hat{z}_0', \psi, \lambda_2) d\psi', \tag{71}$$

and

$$(\Delta U_\xi/W) = (\gamma \cos\phi/4\pi R_2 W) \int_0^\infty f_\xi(\psi'; \bar{r}', \bar{r}', \hat{z}_0', \hat{z}, \psi, \lambda_2) d\psi', \tag{72}$$

where the primed quantities refer to the location of an elemental length of the vortex filament and the unprimed quantities refer to the location of the point at which the velocity components are evaluated.

The Romberg Integration technique was used to numerically evaluate the integrals of Eqs. (70) through (72). Since the limits of integration range from 0 to ∞, a stepwise integration procedures is adopted. The integration is first performed between the limits 0 and 2Π and the resulting value is denoted by δ_1, which actually is the contribution to the integral of the first turn of the helical filament and its reflection ($-2\Pi \leq \psi' \leq 0$). The contribution to the integral from the second turn of the filament ($2\Pi \leq \psi' \leq 4\Pi$) and its reflection ($-4\Pi \leq \psi' \leq 4\Pi$) is then evaluated using the Romberg Integration technique and is denoted by δ_2. Then δ_2 is compared with the sum of δ_1 and δ_2. A percentage change is then defined as $(100)\left|(\delta_2/(\delta_1 + \delta_2)\right|$. If this change is not acceptably small, contribution to the integral from the following turn of the helical filament is evaluated and the percentage change is again determined according to the formula, $(100)\left|\delta_j/\left(\sum_{i=1}^{j} \delta_i\right)\right|$, where δ_j is the contribution of the integral from the j^{th} turn and its reflection of the helical filament and $\sum_{i=1}^{j} \delta_i$ is the sum of all the δ_j. The process is continued until the percentage change is less than some specified tolerance level. The value of the integral is then set equal to the sum of all the δ_j.

An investigation of the permissible tolerances for each integral has been made. It was found that the tolerances suggested by Wright[2] are satisfactory in the sense that significant changes in the tolerance levels from those suggested by Wright[2] did not significantly change the end result of the integrations. A value of 0.5 has been chosen as the permissible tolerance for the integrations involved in the

computation of the velocity component ΔU_ζ. A range of values from 0.25 to 1.5 has been chosen (depending on the value of λ_2/b) for the computation of the integrals for ΔU_r. When the tolerance levels are changed to 10^{-6}, an enormous amount of computational time was required to evaluate the above integrals. However, the values of the integral did not differ significantly from those having the higher tolerances.

It can be seen from Eqs. (19) through (21) that the velocity components associated with a single helical vortex filament at any arbitrary location in its flow field are linear functions of its strength. For example, if the contributions of n filaments to a velocity component, $\Delta U_r/W$, at a given point are summed, then the result is of the form $\sum_{i=1}^{n} h_i \bar{\gamma}_i = \bar{U}_r$, where h_i is the influence coefficient of the helical filament $\bar{\gamma}_i$. If the filament strengths are unknown and their geometry is known, as in the case of the mathematical model of the ultimate wake developed earlier, specifying the value of $\bar{U}_r$ at a calculation point yields a linear equation in $\bar{\gamma}_i$. If n such calculation points hereafter referred to as control points are chosen and if the appropriate velocity components is specified at each one of these points, the end result is a system of n linear algebraic equations in n unknowns $\bar{\gamma}_i$. Such a system of equations is developed and solved for the strengths of the unknown vorticies in the ultimate wake.

As discussed earlier, the vortex sheets of the ultimate wake are divided into strips and the strips are replaced by vortex filaments of finite strength. Since the strengths of the B.T.E. sheets and the nonuniform boundary vortex sheets in the ultimate wake are not known,

these sheets are replaced by a number of vortex filaments of finite strength. The portions of the nonuniform boundary sheets and the B.T.E. sheets that are replaced by the filaments correspond to the unit wake as shown in Fig. 9. In order to arrive at the optimum number of filaments which replace these vortex sheets, an investigation has been made to determine the effect of the number of filaments on the end result as well as on the computational time. It has been found that ten filaments replacing the B.T.E. sheet and eight filaments replacing each of the nonuniform sheets were sufficient from the standpoint of computation time and accuracy of the result. A lower number of filaments tend to overestimate the influence and a higher number of filaments tend to increase the computation time without any significant change in the value. In fact, doubling the number of filaments almost quadruples the computation time with the values being less than 1% different from those of the former.

It is to be noted that the nonuniform vortex sheet strengths are symmetric about the lines of intersection. Because of this symmetry, the eight filaments that replace each of the non-uniform sheets introduce only four unknowns for each sheet. However, it is to be noted that all of the vortex filaments in the ultimate wake are to be taken into account in the computation of velocities at the control points. For example, in the case of a fan with b number of blades, all the vortex filaments corresponding to these b blades are used in the computation of velocity components.

It was shown earlier that the number of control points at which

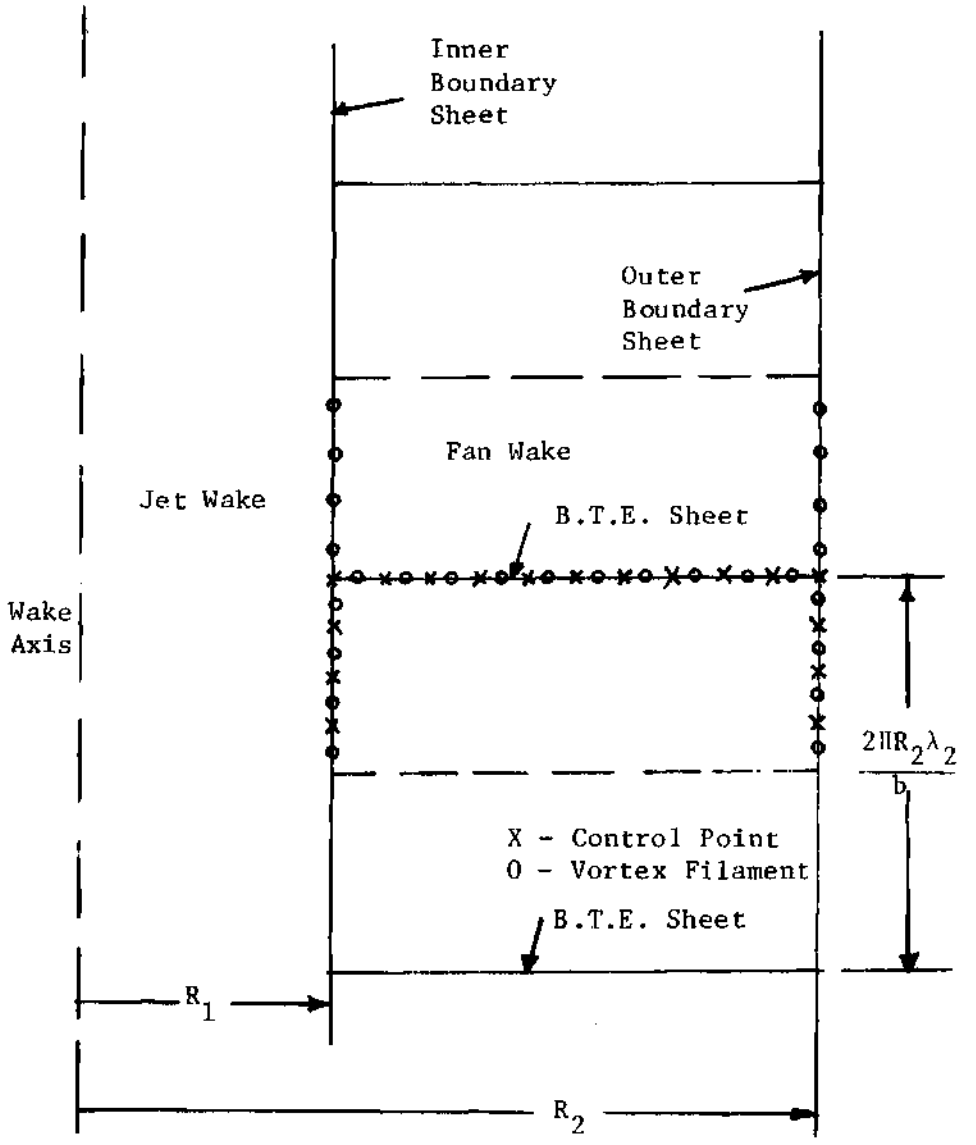

Figure 9. Schematic Arrangement Of Control Points And Vortex Filaments In The Ultimate Wake.

the velocity components are computed is one less than the total number of vortex filaments of unknown strength. The arrangement of vortex filaments and the control points in the ultimate wake is shown in Fig. 9. There are eleven control points on the B.T.E. sheet and three each on the inner and outer boundary sheets. There are eighteen vortex filaments of unknown strength. At the control points on the B.T.E. sheet, the contributions to $\bar{U}_\zeta / \cos\phi = 1$ from all of the vortex filaments in the ultimate wake are computed and summed to yield eleven algebraic equations. At the three control points on each of the boundary sheets, the contributions to $\bar{U}_r = 0$ from all of the vortex filaments are evaluated and summed to yield six equations. A final eighteenth equation is obtained by equating the net vorticity in the ultimate wake to zero. All of the control points are assumed to lie in the $\psi = 0$ plane. The computation of the velocity components due to the vortex filaments lying on the B.T.E. sheets of all of the blades is facilitated in the integrands of Eqs. (19) through (21) by increasing the value of ψ from 0 to $2\pi(1 - \frac{1}{b})$ in steps of $2\pi/b$. The system of linear equations thus obtained is given below. As discussed earlier, the righthand sides of these equations are modified to take into account the contributions due to the uniform boundary sheets and the jet wake.

$$\sum_{j=1}^{18} B_{i,j} \bar{\gamma}_j = 0, \quad i = 1 - 3.$$

$$\sum_{j=1}^{18} B_{i,j} \bar{\gamma}_j = \lambda_2^2 \left[\frac{1}{(1 + \lambda_2^2)} - \frac{1}{(1 + \lambda_1^2) X_i^2}\right], \quad i = 4 - 14.$$

$$\sum_{j=1}^{18} B_{i,j}\,\bar{\gamma}_j = 0, \qquad i = 15 - 17.$$

and

$$\sum_{j=1}^{18} B_{18,j}\,\bar{\gamma}_j = \frac{1}{2b}\left[\frac{\lambda_2}{1+\lambda_1^2} - \frac{\lambda_2}{1+\lambda_2^2}\right].$$

In the above equations, $X_i = r_i/R_2$, $B_{i,j}$ is the appropriate velocity influence coefficient and γ_j is the vortex strength of the filament j. In the last equation, $B_{18,5}$ through $B_{18,14}$ are each equal to 1.0 and the rest of the coefficients are equal to 2.0. $\bar{\gamma}_5$ through $\bar{\gamma}_{14}$ are the nondimensional vortex strengths of the filaments on the B.T.E. sheet, $\bar{\gamma}_1$ through $\bar{\gamma}_4$ are the strengths of the filaments on the outer boundary sheet and $\bar{\gamma}_{15}$ through $\bar{\gamma}_{18}$ are the strengths of those on the inner boundary sheet. The set of the linera algebraic equations thus obtained was solved numerically using the Gauss-Jordan Reduction Method (Ref. 9) for particular values of λ_2, b and R_1/R_2. $K_0(X)$, κ_0', and μ_0' are then obtained from a knowledge of the vortex strength distribtuions in the wake.

Thrust And Power Integrations

As was shown earlier, certain volume integrals of velocity components need to be evaluated to obtain the thrust and power coefficients. These volume integrals are

$$\epsilon_0 = \int_{R_1/R_2}^{1} \int_0^1 \int_0^{2\pi} [\bar{U}^2_{\psi_{R_2^-}VS} + \bar{U}^2_{z_{R_2^-}VS} + \bar{U}^2_{z_{VS}} - \bar{U}^2_{\psi_{VS}} - \bar{U}^2_{r_{VS}}] X dX \, d\bar{z} \, \frac{d\psi}{2\pi} ,$$

(73)

$$\int_m^1 \int_0^1 \int_0^{2\pi} [\bar{U}_{\psi_{VS}}(\tfrac{1}{X}) - \bar{U}_{\psi_{R_2^-}VS}] X dX \, d\bar{z} \, d\psi/2\pi,$$

$$\int_m^1 \int_0^1 \int_0^{2\pi} \bar{U}_{z_{VS}} \bar{U}_{z_{R_2^-}VS} \, X dX \, d\bar{z} \, d\psi/2\pi,$$

$$\int_m^1 \int_0^1 \int_0^{2\pi} \bar{U}_{z_{VS}} [\bar{U}^2_{z_{R_2^-}VS} + \bar{U}^2_{\psi_{R_2^-}VS}] X dX \, d\bar{z} \, d\psi/2\pi,$$

and

$$\int_m^1 \int_0^1 \int_0^{2\pi} \bar{U}_{z_{R_2^-}VS} \bar{U}_{\psi_{R_2^-}VS} \, X dX \, d\bar{z} \, d\psi/2\pi.$$

The velocity components at the specified points in the unit wake are found by numerical integration techniques discussed earlier in setting up the system of linear equations. Due to the helical symmetry of the vorticity and velocity distributions in the ultimate wake, the volume integrations may be performed by obtaining a detailed knowledge of the

flow field on a $\overline{zr}$-surface. This idea, originally due to Wright[2], has been extended to this system. The $\overline{zr}$-surface chosen is bounded by the inner and outer cylindrical boundaries, a B.T.E. sheet, and a radial line midway between the chosen B.T.E. sheet and an adjacent B.T.E. sheet. This surface is divided into a network or grid as shown in Fig. 10. The velocity components are evaluated at the intersection points of the grid. A two dimensional array of the values of the velocity components and their squares is thus obtained. Using a strip method, a formula has been developed for the evaluation of the volume integral using these two dimensional arrays of velocity components. It can be shown that

$$\int_{m}^{1}\int_{0}^{1}\int_{0}^{2\pi} f\, X dX\, d\bar{z}\, d\psi/2\pi = \frac{(1-m^2)}{8I^2J}\sum_{i=2}^{I+1}\sum_{j=2}^{J+1}(2i-3)$$

$$(f_{i,j} + f_{i-1,j} + f_{i-1,j-1} + f_{i,j-1}) + \frac{m(1-m)}{4IJ}\sum_{i=2}^{I+1}\sum_{j=2}^{J+1}$$

$$(f_{i,j} + f_{i-1,j} + f_{i-1,j-1} + f_{i,j-1}). \quad (74)$$

Where i,j refers to the location of a grid point as shown in Fig. 10, I+1 refers to the number of grid points in the radial direction and J+1 refers to the number of grid points in the axial direction. For the network illustrated in Fig. 10, I=10, J=4 and 'f' can be the 2-D array

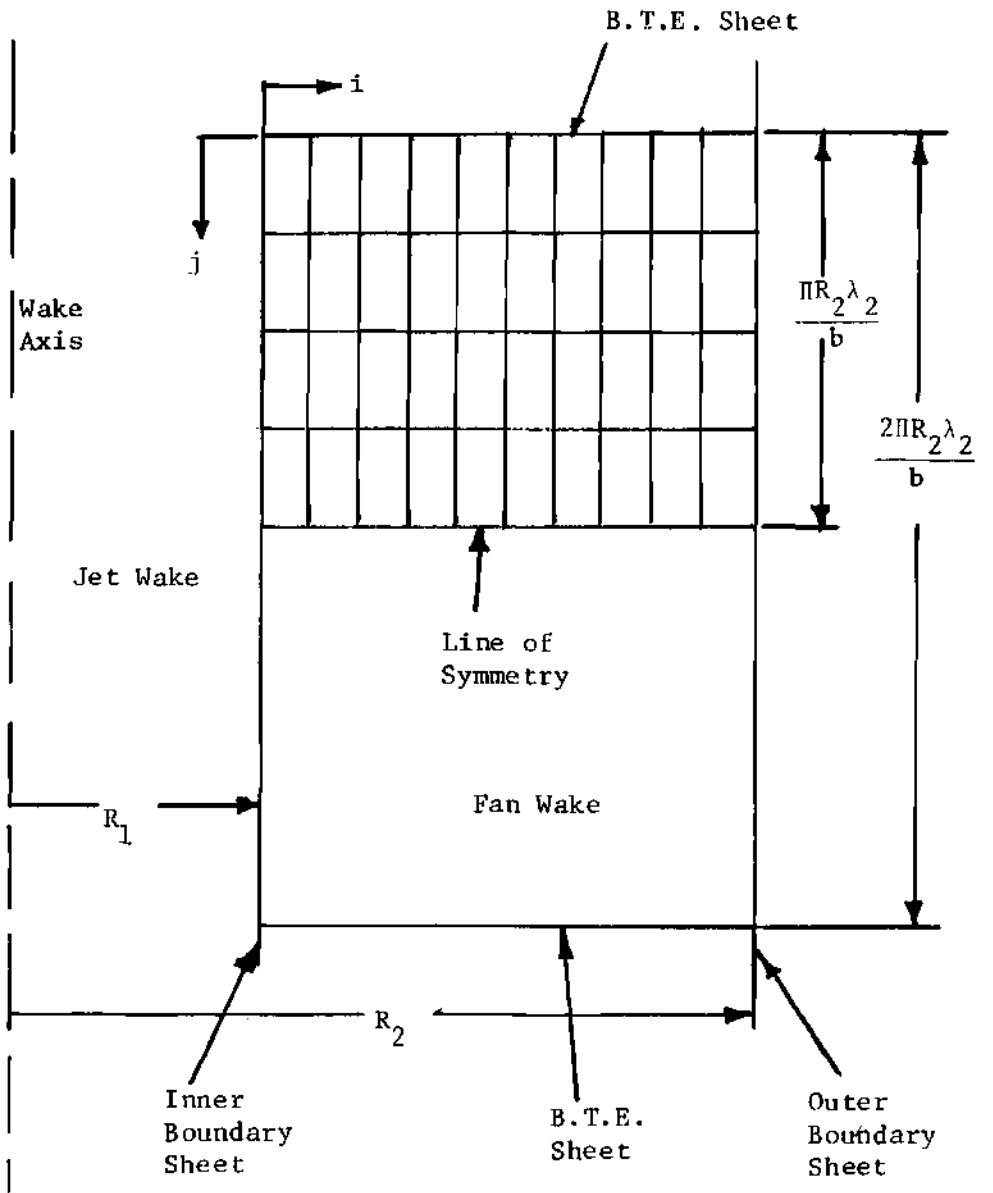

Figure 10. A Typical zr-Surface Used In Computing The Volume Integrals.

of any velocity component or its square.

Since the motion and vorticity of the wake are known, the numerical computation of the velocity components on the edges of the $\overline{zr}$-surface at the vortex sheets is not required. It is to be noted that the edges of the grid do not exactly lie on the vortex sheets. Mathematically the network is represented as $R_1 < r < R_2$, $0 < z \leq \pi R_2 \lambda_2 / b$. As discussed earlier, velocity components only due to B.T.E. sheets and the nonuniform boundary sheets need to be evaluated.

The velocity components at the grid points on all but one edge of the network are obtained from a knowledge of geometry and the strength of the appropriate adjoining vortex sheet. Consider first the edge of the network at the B.T.E. sheet. This edge is represented mathematically as, $z = 0^+$ and $R_1 < r < R_2$. The velocity components U_z and U_ψ are continuous across the B.T.E. sheet and hence the values of U_z and U_ψ at this edge are the same as those at the corresponding points on the B.T.E. sheet. It can be shown that

$$\bar{U}_{z_{VS}}(X, 0^+) = \bar{U}_{z_{VS}}(X, 0) = G\lambda_2^2\left[\frac{1}{1 + \lambda_2^2} - \frac{1}{X^2 + \lambda_2^2}\right] \qquad (75)$$

and

$$\bar{U}_{\psi_{VS}}(X, 0^+) = \bar{U}_{\psi_{VS}}(X, 0) = G\left[\frac{\lambda_2}{x(1 + \lambda_1^2)} \frac{X\lambda_2}{x^2 + \lambda_2^2}\right] \qquad (76)$$

However, it is to be noted that the radial velocities are discontinuous across the B.T.E. sheet and their distributions are such that $-U_r(r, 0^+) = U_r(r, 0^-)$. The magnitude of the discontinuity in the radial velocity gives the strength of the vortex sheet at that point. By the Helmholtz laws, it is seen that $d\Gamma'/dr = \gamma(r) = 2\, U_r(r, 0^+)$, where $\Gamma'(r)$ is the blade bound vortex strength at radius r. $\Gamma'(r)$ is known at various radial stations along the B.T.E. sheet from previous calculations. A Fourier series is fitted to these values such that $d\Gamma'/dr = 0$ at $r = R_1^+$ and $r = R_2^-$. This is so because the vortex sheet strengths at these points must be equal to zero. The number of terms chosen in the Fourier series is the same as the number of points on the B.T.E. sheet at which $\Gamma'(r)$ is known. After fitting the Fourier series, the vortex strength and hence the radial velocity discontinuity at any point on the B.T.E. sheet can be evaluated. It can be shown that

$$\bar{U}_{r_{VS}}(X, 0^+) = -2\pi\, d\bar{\Gamma}'/dX, \text{ where } \bar{\Gamma}' = \Gamma'(X)/4\pi R_2 W.$$

Thus the values of the velocity components at the grid points on the edge $z = 0^+$, $R_1 < r < R_2$ are obtained without the need of further numerical integration techniques.

The values of the velocity components at the grid points on the outer edge of the network, that is, at $r = R_2^-$ and $0 < z \leq \pi R_2 \lambda_2 / b$, are obtained as follows. The velocity components U_z and U_ψ are discontinuous across the outer boundary sheet. Since the boundary

is also a stream surface, the radial velocities are zero at this edge. It can be shown that

$$\bar{U}_{z_{VS}}(1^-, \bar{z}) = \hat{\gamma}^0_{z_{nu}}(\bar{z}), \qquad 1^- = R_2^-/R_2, \tag{77}$$

$$\bar{U}_{\psi_{VS}}(1^-, \bar{z}) = G\left[\frac{\lambda_2}{1+\lambda_1^2} - \frac{\lambda_2}{1+\lambda_2^2}\right] - \hat{\gamma}^0_{\psi_{nu}}(\bar{z}), \tag{78}$$

and

$$\bar{U}_{r_{VS}}(1^-, \bar{z}) = 0, \tag{79}$$

where $\hat{\gamma}^0_{z_{nu}}$ and $\hat{\gamma}^0_{\psi_{nu}}$ are the nondimensional ring and line components of the nonuniform vortex sheet strengths at any point z on the outer boundary sheet. The above expressions are obtained by noting that the induced velocities are zero outside the outer boundary sheet and the strength of the uniform sheet is equal to the total sheet strength at the line of intersection. In order to evaluate the above expressions, a knowledge of the nonuniform sheet strengths at those particular grid points is required. However, from the solution of the set of simultaneous equations, the strengths of the filaments that represent the nonuniform vortex sheet strips and are located at the midpoints of these strips, are known. The strength of each of these vortex filaments is equal to the integral of sheet strength over the width of the strip which the filament replaces. The sheet strength can be evaluated from

a knowledge of the filament strengths by assuming a particular type of variation, e.g., linear or parabolic, for the sheet strengths over the width of the strip. For simplicity, it has been assumed that the sheet strength varies linearly over the width of the strip which the filament replaces. The sheet strengths at the required grid points on the boundary can then be evaluated using the trapezoidal rule for integration. A similar procedure is used to evaluate the nonuniform sheet strengths at the grid points on the inner boundary sheet.

The inner edge of the $\overline{zr}$-surface, mathematically represented as $r = R_1^+$ and $0 < z \leq \Pi R_2 \lambda_2 / b$, is now considered. The radial velocities at the grid points on this edge are zero since this boundary is also a stream surface. The axial and tangential velocities are discontinuous across the sheet. It is assumed that the axial and tangentail velocities on the boundary of the jet wake ($r = R_1^-$) do not vary in the axial direction and have the same value as that at the line of intersection of the B.T.E. sheet and inner boundary sheet. This assumption is a result of the mathematical model assumed for the jet wake. Using a procedure similar to that one used in the case of outer boundary sheet, the velocity components at the grid points on the inner boundary sheet are obtained as

$$\bar{U}_{r_{VS}}(R_1^+/R_2,\ z) = 0, \tag{80}$$

$$\bar{U}_{z_{VS}}(R_1^+/R_2,\ \bar{z}) = G[\lambda_2^2/(1+\lambda_2^2) - \lambda_1^2/(1+\lambda_1^2)] - \gamma^i_{z_{nu}}(\bar{z}), \qquad (81)$$

and

$$\bar{U}_{\psi_{VS}}(R_1^+/R_2,\ \bar{z}) = \hat{\gamma}^i_{\psi_{nu}}(\bar{z}), \qquad (82)$$

where $\hat{\gamma}^i_{z_{nu}}$ and $\hat{\gamma}^i_{\psi_{nu}}$ are the nondimensional ring and line components of the nonuniform vortex sheet strengths of the inner boundary. These are evaluated using the same arguments as were used at the outer boundary. The velocity components at the grid points on the remaining fourth edge of the $\overline{zr}$-surface are evaluated numerically.

The accuracy of the volume integrations is clearly dependent on the choice for I and J and the strip method used to derive the expression for the volume integral. As a check on the method, the induced axial velocity ($\bar{U}_z$) distribution on the $\overline{zr}$-surface is evaluated for particular values of λ_2, b, and m. Then the volume integral is evaluated using the strip method. This value is then compared with the exact value of the volume integral of $\bar{U}_z$ that was derived earlier. It was shown that,

$$\int_m^1 \int_0^1 \int_0^{2\pi} \bar{U}_z\, X dX\, d\bar{z}\, d\psi/2\pi = \frac{1}{2}[\kappa' + (1-G)(1-m^2)].$$

Thus the accuracy of the strip method can be checked. With values of I=10 and J=4, the volume integrals are evaluated and it was found that these values are acceptable from the standpoint of computation time and accuracy. Higher values tend to increase the computation time enormously with negligible gains in accuracy. The accuracy of the volume integrals is also checked by computing the volume integrals of $\bar{U}_z^2$, $\bar{U}_\psi^2$ and $\bar{U}_r^2$ for a particular λ_2 and 'm' but with increasing number of blades. These volume integrals should and do converge to the values corresponding to those of the infinite number of blades that are obtained later in the next chapter.

CHAPTER III

INFINITE-BLADED FAN

Wake Model And Its Solution

The vortex wake model of the optimum high by-pass ratio ducted fans with infinite number of blades is an extension of the wake model developed earlier for the fans with finite number of blades. The original work in this area was done by Gray[6]. The ultimate wake of these infinite bladed fans consists of the following elements: the jet wake, the fan wake and two cylindrical boundary vortex sheets. The jet wake model is exactly the same as the one used earlier. However, there are some distinct differences as far as the fan wake and boundary sheets are considered.

The wake of an infinitely bladed fan consists of a volume distribution of cylindrical vorticity. As was discussed earlier, the fan wake of an optimum high by-pass ratio ducted fan with finite number of blades consists of the helical vortex sheets of constant pitch shed from the trailing edges of the fan blades. As the number of blades increases, the helical vortex sheets become more and more closely spaced. In the limit for an infinite number of blades, these sheets completely fill the wake. The ultimate wake of a fan with an infinite number of blades can thus be viewed as cylindrical volume of vorticity, the volume being filled with an infinite number of helical vortex sheets shed from the trailing edges of the blades. The vorticity in the wake can be viewed as a combination of ring and line vorticity since the vortex cylinder is of constant

diameter. Following the same lines of arguments as were used in the case of the fan with a finite number of blades, the cylindrical fan wake is bounded on the inside by an inner cylindrical boundary vortex sheet of constant diameter shed from the trailing edge of the hub and on the outside by an outer cylindrical boundary vortex sheet of constant diameter shed from the trailing edge of the duct. These boundary vortex sheets move axially relative to the cylindrical fan wake and serve the same purposes as those in the case of a fan with finite number of blades.

Since the cylindrical fan wake can be thought of as a wake filled with infinite number of constant diameter helical vortex sheets of constant geometric pitch, the velocity relations that were obtained at points on helical vortex sheets of the finite bladed fans can be used everywhere in the wake of the infinite bladed fan. Consequently, the analysis of an infinite bladed fan wake is very much simplified. The strengths as well as the geometry and motion of the two cylindrical boundary vortex sheets can easily be determined once the velocity field in the ultimate fan wake is known. By using essentially the same arguments as were used in the case of the fan with finite number of blades, it can be shown that, for the flow to be irrotational outside the wake, the induced velocities outside of the wake should be equal to zero. As was done earlier, it is assumed that the net vorticity in the jet wake is equal to zero. In the case of the fan with finite number of blades, the uniform boundary vortex sheet strenghts as well as the pitch angles are determined by considering the velocity discontinuities at the lines of intersection between the B.T.E. sheets and the boundary vortex sheets. Therefore, in the case of the fan with an infinite number of blades, the B.T.E. sheets fill the

entire wake and hence, the boundary vortex sheet strengths as well as the pitch angles are the same as the sheet strengths and pitch angles of the corresponding uniform boundary sheets of the fan with finite number of blades.

At any point in the ultimate fan wake, that is for $R_1 < r < R_2$,

$$U_\xi = U_{\xi_1}, \sin\phi/\sin\phi_1, \tag{83}$$

$$U_\zeta = W \cos\phi, \tag{84}$$

and

$$U_r = 0. \tag{85}$$

For points outside the wake, that is for $r > R_2$,

$$U_\xi = U_\zeta = 0. \tag{86}$$

Equations (10) and (11) give the sheet strength and the pitch angle of the outer boundary sheet. Similarly Eqs. (16) and (17) give the corresponding values for the inner boundary sheet. The jet wake is treated exactly the same way as was done earlier.

Consider a line integral of the velocity along a closed contour $\overline{ABCA}$ on the surface of the cylinder of radius r, where $R_1 < r < R_2$. $\overline{ABC}$ is along the ξ direction and $\overline{CA}$ is along the ζ direction. C is the intersection point of a line in the helical direction, but on the same side of the vortex sheet, and a line in the ζ direction originating at A.

As per the velocity field, which has been discussed earlier, the components U_ξ and U_ζ are constant on a cylinder of radius 'r'.

$$\int_{ABCA} \vec{V}\cdot\vec{ds} = U_{\xi_r}(\xi_C - \xi_A) + U_{\zeta_r}(\zeta_A - \zeta_C)$$

However,
$$U_{\xi_r} = U_{\xi_1} \sin\phi/\sin\phi_1,$$

$$U_{\zeta_r} = W\cos\phi,$$

$$r\tan\phi = R_2\tan\phi_2 = \lambda_2 R_2,$$

$$(\xi_C - \xi_A) = 2\pi R_2\lambda_2\cos\phi\cot\phi,$$

and
$$(\zeta_C - \zeta_A) = 2\pi R_2\lambda_2\cos\phi.$$

Since the shed vorticity by convention is negative and since the net vorticity in the jet wake is zero, by Stoke's theorem

$$\int_{ABCA} \vec{V}\cdot\vec{ds} = -b\Gamma'(r),$$

where $\Gamma'(r)$ is the blade bound vortex strength at 'r' which is in fact the sum of all vortex filaments shed in board of radius 'r'. It is to be

be noted that b is infinite and $\Gamma'(r)$ is infinitesimal and therefore $b\Gamma'(r)$ is finite and represents the bound vortex strength of all the blades at r. Thus

$$-b\Gamma'(r) = (U_{\xi_1} \sin\phi/\sin\phi_1)(2\pi R_2\lambda_2 \cos\phi \cot\phi) - W \cos\phi \; 2\pi R_2\lambda_2 \cos\phi,$$

$$\frac{b\Gamma'(r)}{2\pi R_2\lambda_2 W} = \cos^2\phi - U_{\xi_1} \cos^2\phi/W \sin\phi_1,$$

and

$$K(X) = G \cos^2\phi,$$

where $G = 1 - U_{\xi_1}/W \sin\phi_1$. It can easily be shown that

$$K(X) = G \, X^2/(X^2 + \lambda_2^2) \tag{87}$$

and

$$K_0(X) = X^2/(X^2 + \lambda_2^2), \quad \text{where } X = r/R_2.$$

Thus, the Goldstein coefficients for the case of a fan with infinite number of blades can be easily computed. Since the velocity field in the ultimate wake is known, the vorticity in the wake can also be easily computed. Using Eqs. (83) through (86), it can be shown that for $R_1 < r < R_2$,

$$U_z = W[1 - G\lambda_2^2/(X^2 + \lambda_2^2)], \tag{88}$$

and

$$U_\psi = -GW\lambda_2 X/(X^2 + \lambda_2^2). \tag{89}$$

Therefore, the total velocity field in the ultimate wake is given by

$$\vec{Q}(X) = [V_\infty + W(1 - \frac{G\lambda_2^2}{X^2 + \lambda_2^2})]\,\vec{e}_z - \frac{GW\lambda_2 X}{(X^2 + \lambda_2^2)}\,\vec{e}_\psi, \tag{90}$$

where the velocities are with respect to a co-ordinate system fixed to the duct. The vorticity in the ultimate wake is given by $\vec{\nabla} \times \vec{Q} = \vec{\gamma}'$. Using the cylindrical coordinate system it can be shown that

$$\vec{\gamma}' = \vec{\nabla} \times \vec{Q} = -\frac{\partial v_z}{\partial r}\,\vec{e}_\psi + \frac{1}{r}\frac{\partial}{\partial r}(rv_\psi)\,\vec{e}_z, \text{ and therefore}$$

$$\vec{\gamma}'(X) = -\frac{2G\lambda_2^2 WX}{(X^2 + \lambda_2^2)^2 R_2}\,\vec{e}_\psi - \frac{2GW\lambda_2^3}{R_2(X^2 + \lambda_2^2)}\,\vec{e}_z \tag{91}$$

Converting to a helical coordinate system it is seen that

$$\gamma_\xi'(X) = -2GW\lambda_2^2/R_2(X^2 + \lambda_2^2)^{3/2},$$

and

$$\gamma'_{\zeta}(X) = 0,$$

where $\gamma'_{\xi}(X)$ is the vorticity per unit area. In order to get the vortex sheet strength in the ξ direction, γ'_{ξ} is multiplied by a characteristic length which for this case is given by $2\pi R_2\lambda_2 X/(X^2 + X_2^2)^{1/2}$

$$\hat{\gamma}_{\xi} = \gamma'_{\xi}(X)\ 2\pi R_2\lambda_2 X/\ (X^2 + \lambda_2^2)^{1/2} = (2\pi R_2\lambda_2)(-\frac{2GWX\lambda_2^2}{R_2(X^2+\lambda_2^2)^2})$$

This sheet strength is due to all blades of the fan. This expression can also be arrived yet another way, using the expression $\hat{\gamma}_{\xi}$ = $-bd\Gamma'(r)/dr$ and using Eq. (87). The assumption of infinite number of blades makes the flow field in the wake steady. The velocity field in the wake can be checked by evaluating the velocities due to the B.T.E. sheets, the inner and outer boundary vortex sheets and the jet wake, and then summing them. Having established the velocity field in the ultimate wake, the thrust and power coefficients can be evaluated using the integral theorems.

Estimation Of Thrust And Induced Power

As for the case of a fan with a finite number of blades, the momentum and energy integral theorems are used for the evaluation of the thrust and induced power coefficients. First, for the momentum integral theorem, it was shown earlier in Chapter II that the thrust due to the duct and fan system is given by

$$T_D = \frac{1}{\Delta t} \int_{\substack{\text{fan}\\\text{wake}}} (P - P_\infty) ds\, dt + \left(\frac{1}{\Delta t}\right) \int_{\substack{\text{fan}\\\text{wake}}} \rho(V_\infty U_z + U_z^2) ds\, dt$$

where ds is the elemental surface area. In the ultimate fan wake, $dt = dz/(V_\infty + W)$, and the characteristic time, $\Delta t = 2\pi/\Omega$. Defining $C_T = T_D/\rho\Omega^2 R_2^2 \pi R_2^2$ and $\bar{z} = z/2\pi R_2 \lambda_2$, it can be shown that

$$C_T = \frac{1}{\rho\pi\Omega^2 R_2^2} \int_m^1 \int_0^1 \int_0^{2\pi} (P - P_\infty) X dX\, d\bar{z}\, d\psi$$

$$+ \frac{\bar{W}^2}{\pi} \int_m^1 \int_0^1 \int_0^{2\pi} (\hat{V}_\infty \bar{U}_z + \bar{U}_z^2\, d\bar{z}\, d\psi \qquad (92)$$

where $\hat{V} = V_\infty/W$, $\bar{U}_z = U_z/W$, and $\bar{W} = W/\Omega R_2$. The second volume integral in the above expression can be evaluated in a straightforward fashion using Eq. (88). However, in order to evaluate the first integral the pressure terms must be expressed in terms of the known velocity field in the wake. This can be achieved by using Crocco's theorem which gives a relation between the variation of stagnation pressure and the velocity and vorticity in the ultimate wake. Then,

$$\vec{\nabla} h_0 = \vec{Q} \times \text{curl} \vec{Q}.$$

Neglecting the variations in temperature and noting that the pressure variation is in the radial direction, it can be shown that

$$1/\rho \; \partial P_0/\partial r \;=\; [Q_\psi \; \gamma_z' - Q_z \; \gamma_\psi'].$$

where $P_0 = P + \frac{1}{2} \rho Q^2$ and $Q^2 = Q_\psi^2 + Q_z^2$. Using Eq. (90), it can be shown that

$$\frac{dP_0}{dX} = \frac{2\rho G \lambda_2^2 (V_\infty W + W^2) X}{(X^2 + \lambda_2^2)^2} \tag{93}$$

and

$$P_0 = -2\rho G \lambda_2^2 (V_\infty W + W^2) \; /2(X^2 + \lambda_2^2) + \text{constant}.$$

The constant is evaluated by considering P_0 at $r = \bar{R_2}$ where $P_0 = P_0' = P_\infty + \frac{1}{2} \rho Q_{R_2}^2$. After some algebraic manipulation, it can be shown that

$$\frac{(P - P_\infty)}{\rho} = \frac{G^2 W^2 \lambda_2^2 (X^2 - 1)}{2(1 + \lambda_2^2)(X^2 + \lambda_2^2)} . \tag{94}$$

Substituting Eq. (94) into Eq. (92) and using the expression for $\bar{U}_z$, C_T can be evaluated in closed form as

$$C_T = \overline{W}^2 \left[\frac{G^2\lambda_2^2(1 - m^2)}{2(1 + \lambda_2^2)} + \frac{G^2\lambda_2^4(1 - m^2)}{(m^2 + \lambda_2^2)(1 + \lambda_2^2)} + (1 - m^2)(\lambda_2/\overline{W}) \right.$$

$$\left. -G\lambda_2^2[1 + \lambda_2/\overline{W} + G/2] \operatorname{Ln}\left((1 + \lambda_2^2)/(m^2 + \lambda_2^2) \right) \right]. \quad (95)$$

Thus for a given λ_2 and $\overline{W}$, C_T can be evaluated from this equation. It was also found that for $m = 0$, that is, for a fan with no hub, Eq. (95) reduces to the expression obtained by Gray[6] for a ducted fan with infinite number of blades and without any hub.

Induced Power

As for the case of a fan with a finite number of blades, the ideal power required by the optimum high by-pass ratio ducted fan with infinite number of blades, excluding the jet, can be obtained through a consideration of the induced energy loss in the fan wake. Using the same arguments as were used in Chapter II, it can be shown that the induced energy loss in the wake is given by

$$E_D = \frac{\Omega}{2\Pi(V_\infty + W)} \int_{\substack{\text{vol. of} \\ \text{fan wake}}} \left[\frac{1}{2} \rho v^2 V_\infty + \left(\frac{1}{2} \rho v^2 + (P - P_\infty) \right) U_z \right] d(\text{volume})$$

Defining $e = E_D/\rho(\Omega R_2)^3 \Pi R_2^2$ and nondimensionalizing the other variables, it can be shown that

$$e = \frac{\bar{W}^3}{2\Pi} \int_m^1 \int_0^1 \int_0^{2\Pi} \bar{v}^2 [\hat{V}_\infty + U_z] X dX \, d\bar{z} \, d\psi$$

$$+ \frac{\bar{W}}{\Pi \Omega^2 R_2^2} \int_m^1 \int_0^1 \int_0^{2\Pi} \left(\frac{P - P_\infty}{\rho}\right) \bar{U}_z \, X dX \, d\bar{z} \, d\psi \qquad (96)$$

where $\bar{v}^2 = \bar{U}_z^2 + \bar{U}_\psi^2$ using Eqs. (88), (89) and (94), Eq. (96) can be evaluated in closed form as

$$e = \frac{\bar{W}^2 \lambda_2}{2} \left[(1 - m^2) + \frac{2G^2 \lambda_2^3 \bar{W}(1 - m^2)}{(1 + \lambda_2^2)(m^2 + \lambda_2^2)} + \frac{G^2 \lambda_2 \bar{W}(1 - m^2)}{1^2 + \lambda_2^2} \right.$$

$$\left. - G \lambda_2 (2 \lambda_2 + \bar{W} - G \lambda_2 + G \bar{W} + \frac{G^2 \bar{W} \lambda_2^2}{(1 + \lambda_2^2)}) \, \mathrm{Ln}\left(\frac{1 + \lambda_2^2}{m^2 + \lambda_2^2}\right) \right]. \qquad (97)$$

The induced power coefficient can then be obtained as

$$C_p = (\lambda_2 - \bar{W}) C_T + e. \qquad (98)$$

The induced power coefficient for a constant diameter wake of the ducted fan can also be obtained by the application of the Kutta-Joukowski theorem. It was shown in Chapter II that

$$C_{P_{KJ}} = G\,\bar{W}\,\lambda_2^2[\kappa_0' - G\,\bar{W}\,\lambda_2\,\mu_0']$$

and

$$C_{T_p} = G\,\bar{W}\,\lambda_2[\kappa_0' - G\,\bar{W}\,\mu_0'\,\lambda_2/2].$$

For the ducted fan with infinite number of blades, it was shown earlier that $K_0(X) = X^2/(X^2 + \lambda_2^2)$. Using this expression for $K_0(X)$ and the definitions of κ_0' and μ_0', it is shown that

$$C_{P_{KJ}} = G\,\bar{W}\,\lambda_2^2\left[(1 - m^2) + \frac{G\,\bar{W}\,\lambda_2^3(1 - m^2)}{(1 + \lambda_2^2)(m^2 + \lambda_2^2)} - (\lambda_2^2 + G\,\bar{W}\,\lambda_2)\right.$$

$$\left.\mathrm{Ln}\left(\frac{1 + \lambda_2^2}{m^2 + \lambda_2^2}\right)\right]. \quad (99)$$

and

$$C_{T_p} = G\,\bar{W}\,\lambda_2\left[(1 - m^2) + \frac{G\,\bar{W}\,\lambda_2^3(1 - m^2)}{2(1 + \lambda_2^2)(m^2 + \lambda_2^2)} - (\lambda_2^2 + G\,\bar{W}\,\lambda_2/2)\right.$$

$$\left.\mathrm{Ln}\left(\frac{1 + \lambda_2^2}{m^2 + \lambda_2^2}\right)\right]. \quad (100)$$

After some algebraic manipulation, it can be shown that Eqs. (98) and

(99) are in fact equivalent though they were derived differently. It was also found that these expressions reduce to the expressions (from unpublished work by Gray[6]) for the fan with no hub ($m = 0$).

Thus, unlike the case of the fan with finite number of blades where extensive numerical procedures are needed to evaluate C_T, C_p and $K_0(X)$, the analysis of the ducted fan with infinite number of blades is much more simplified.

CHAPTER IV

RESULTS

Having established the method as well as the numerical parameters necessary to evaluate the blade bound vortex strength distribution, K(X), the method for the generation as well as the solution of the system of equations was programmed for a digital computer. First, it was necessary to check the method used. Therefore, the general computer program has been used to obtain the $K_o(X)$ distribution for the special case of a fan with no hub. Wright[2] generated the data for such a fan. The Goldstein coefficient distribution, that is, $K_o(X)$, was evaluated for a fan with $\lambda_2 = 0.5$ and $b = 2$ and compared in Fig. 11 with that due to Wright. It can be seen from Fig. 11 that the agreement between the two sets of results is excellent. Figure (12) shows another such comparison for a fan with $\lambda_2 = 0.75$ and $b = 4$. The general computer program was then used to obtain the nondimensional bound vorticity distribution, $K_o(X)$, for high by-pass ratio ducted fans for various values of λ_2, m and the number of blades, b. Some of the data, especially the one corresponding to $m = \frac{1}{3}$, is presented in the form of tables at the end of this chapter. A value of $m = \frac{1}{3}$ relates to a ducted fan with a by-pass ratio of approximately 9, which was considered to be in the range of the by-pass ratios which are of interest from the point of view of applicability of the method presented in this thesis. The values of λ_2 and b chosen for this 'm' are also arrived at from a practical

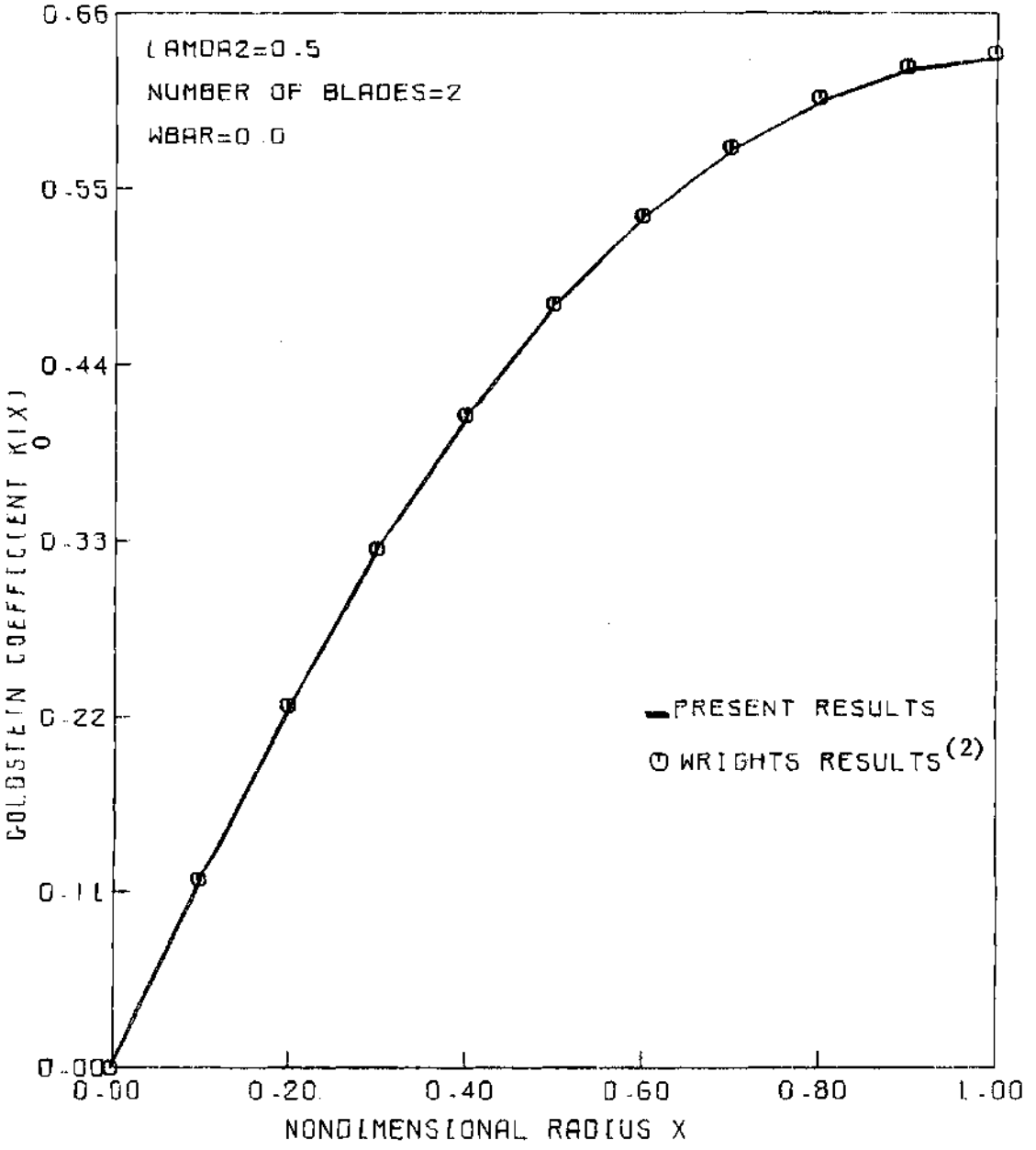

FIGURE 11. COMPARISON OF WRIGHTS RESULTS FOR $K_0(X)$ WITH THE PRESENT VALUES

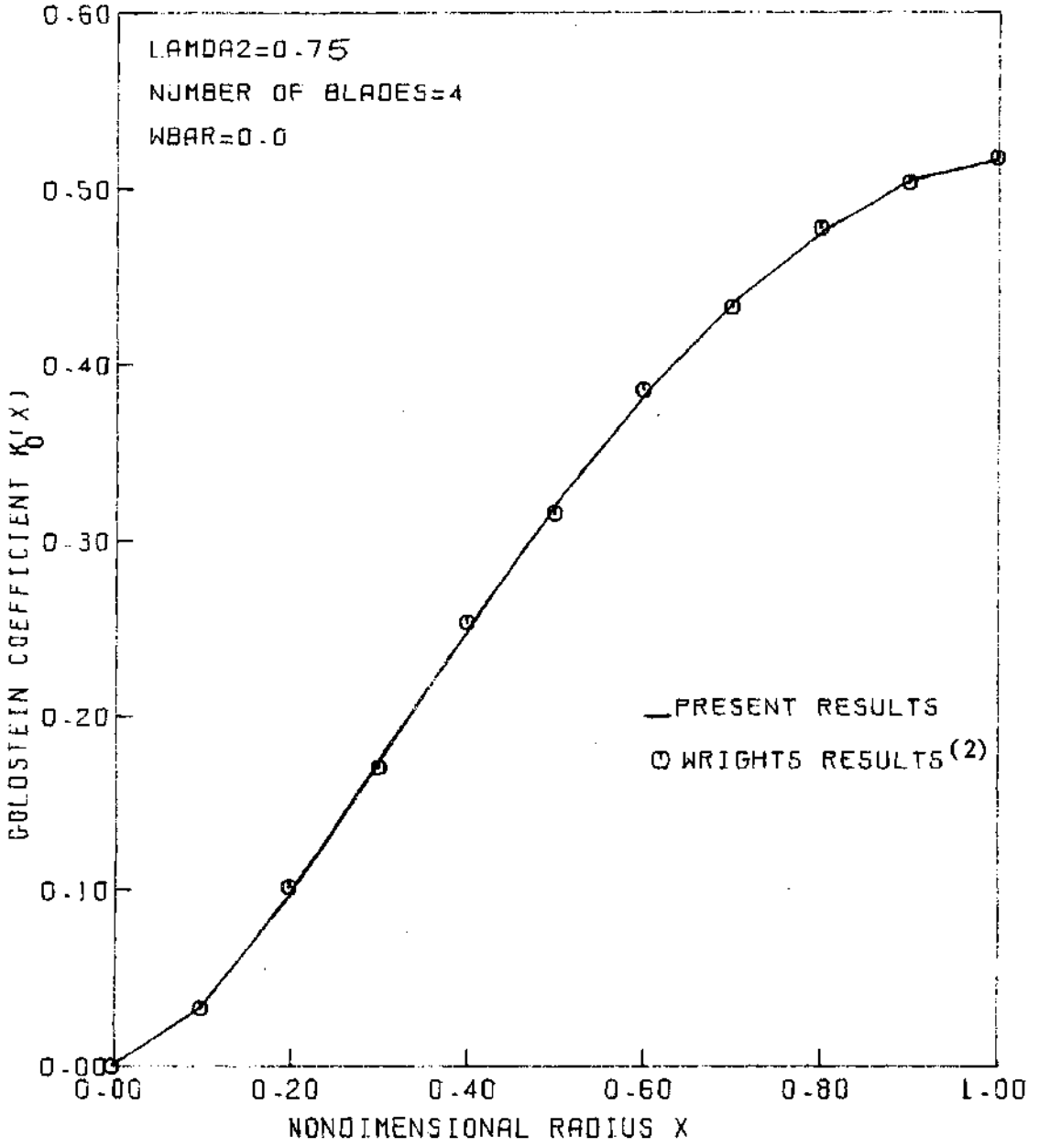

FIGURE 12. COMPARISON OF WRIGHTS RESULTS FOR $K_0(X)$ WITH THE PRESENT VALUES

view point. For example, the high by-pass ratio ducted fans in use today have a value of λ_2 in the range of 0·5 to 1·0. The data presented in these tables will be helpful from the point of view of design of such fans. The $K_o(X)$ distribution for fans with different values of m was also evaluated. Figures 13, 14, 15 and 16 show the $K_o(X)$ distributions for different values of λ_2 and m and, for each of these values, how these distributions converge with increasing blade number to that corresponding to an infinite number of blades. The $K_o(X)$ distribution for the fan with infinite number of blades was evaluated using the method outlined in Chapter III. These figures clearly show that for all values of λ_2 and m considered, the convergence is very good. It is also seen from Fig. 14 that in the case of a fan with m = 0.75 (low by-pass ratio), the $K_o(X)$ distribution is rather flat which is expected since for fans with a large value of m, the flow field and the vortex strengths are more uniform across the fan wake.

An estimation of the amount of computational time involved in the generation of the data was made. Typically, for a fan with λ_2 = 0.5, m = $\frac{1}{4}$, and b = 2, it takes about 180 seconds on the Cyber 74 computer to obtain the $K_o(X)$ distribution. For a fan with λ_2 = 0.5, m = $\frac{1}{4}$, and b = 12, it takes about 1027 seconds to obtain the $K_o(X)$ distribution. For a given by-pass ratio and blade number the computer time decreases with increasing values of λ_2. This is due to the fact that the stipulated numerical accuracies are met with a lower number of computations for fans with higher values of λ_2. The computational time does not change appreciably with m.

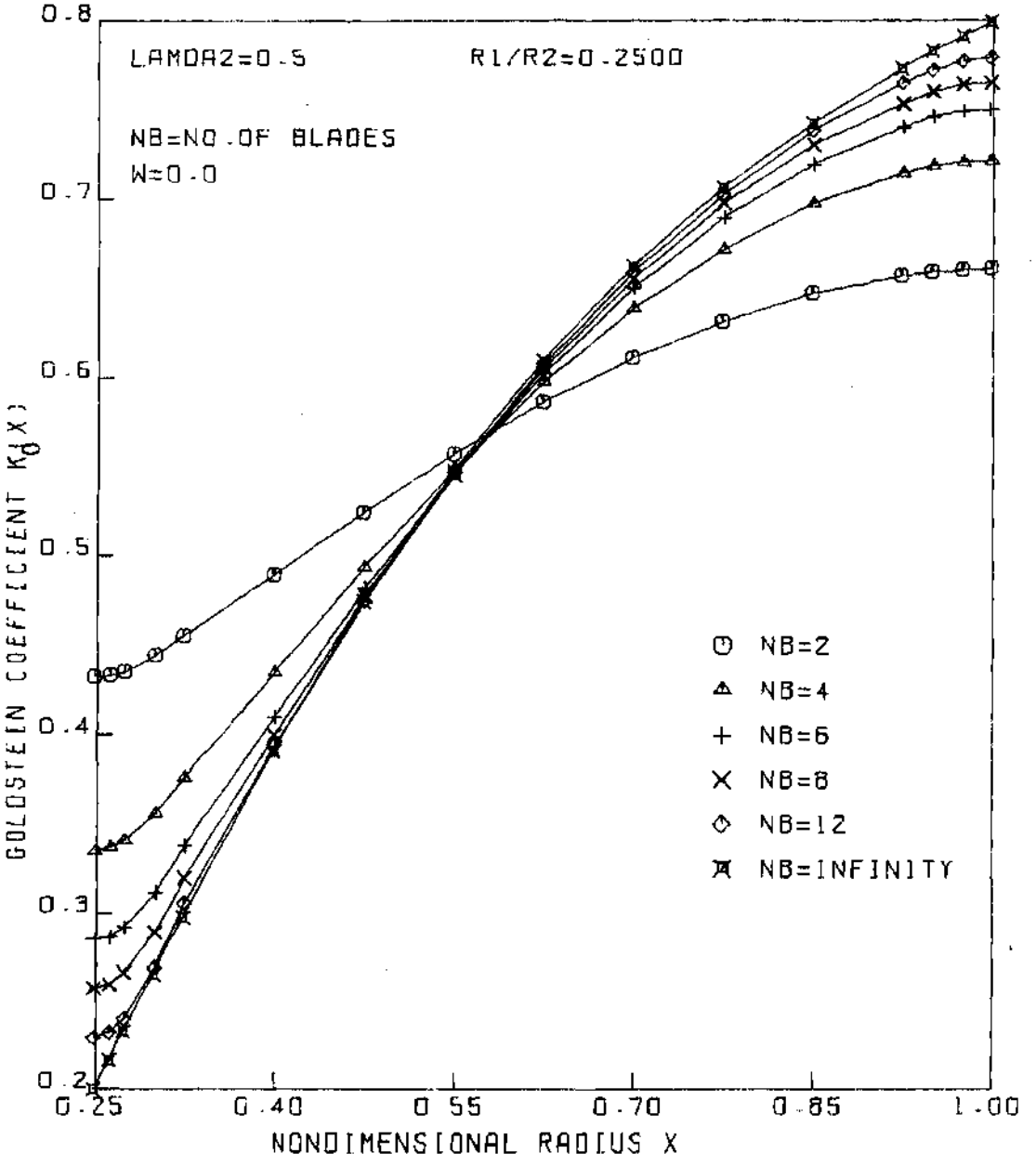

FIGURE 13. VARIATION OF $K_0(X)$ WITH NUMBER OF BLADES

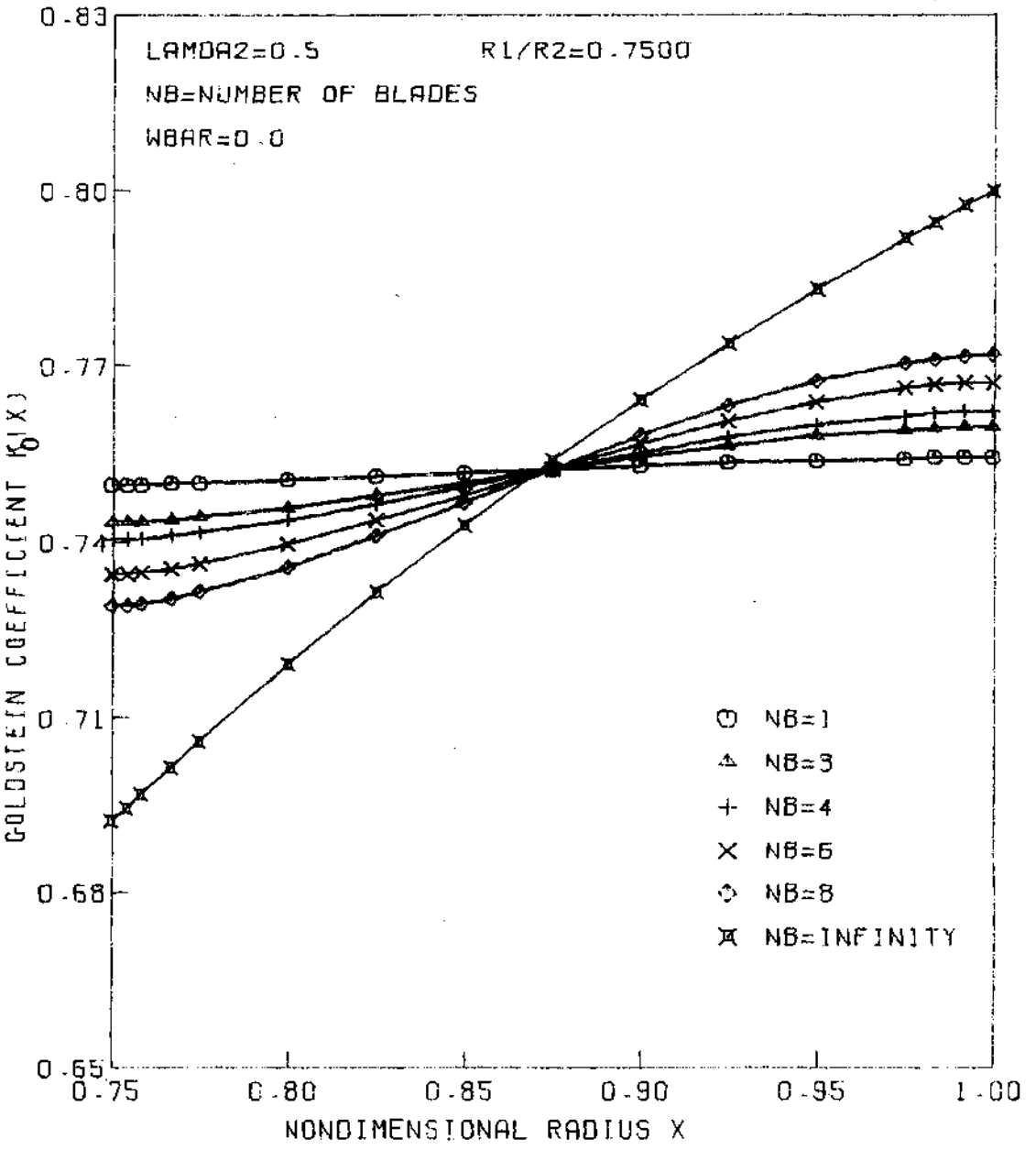

FIGURE 14. VARIATION OF $K_0(X)$ WITH NUMBER OF BLADES

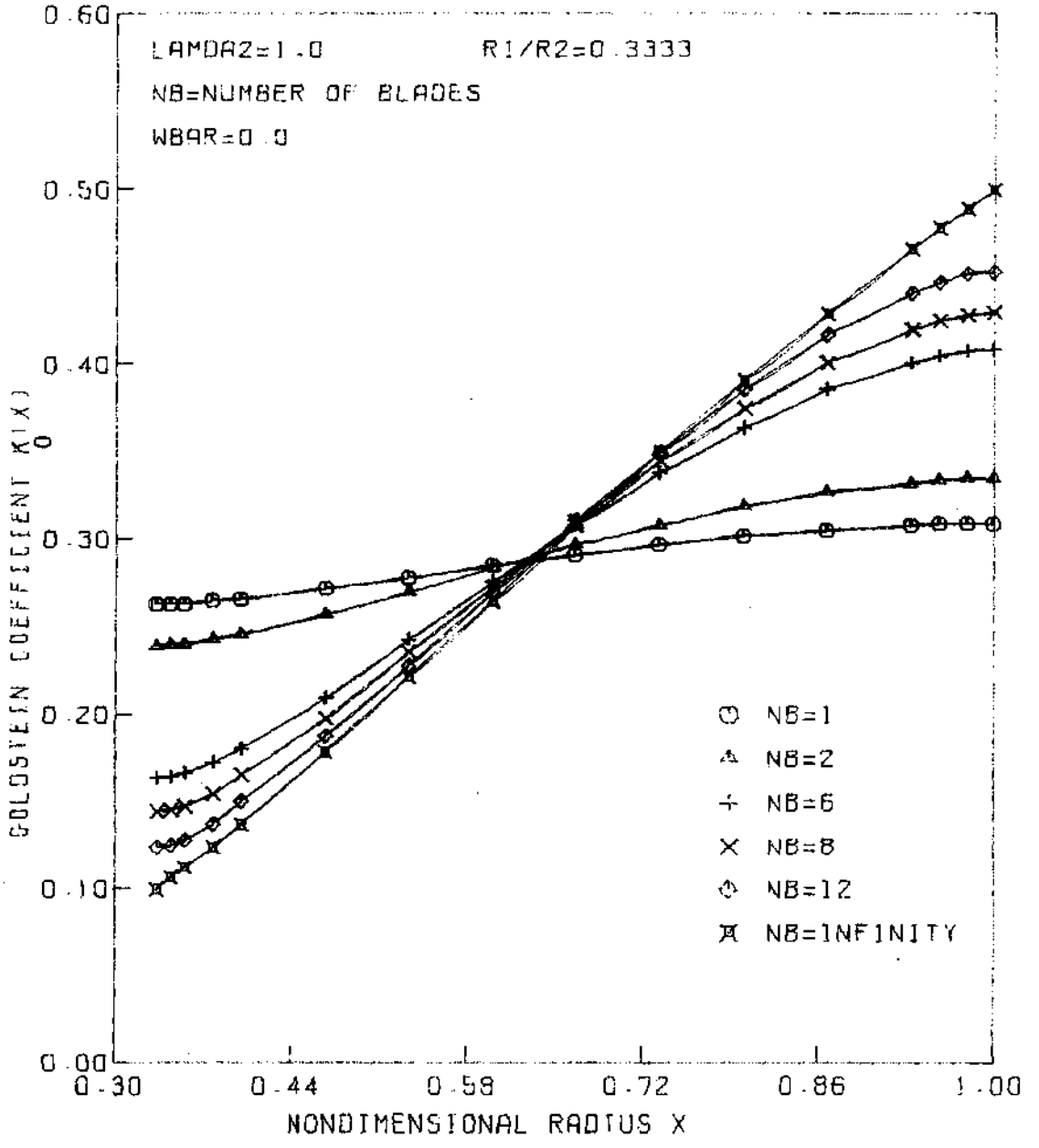

FIGURE 15. VARIATION OF $K_0(X)$ WITH NUMBER OF BLADES

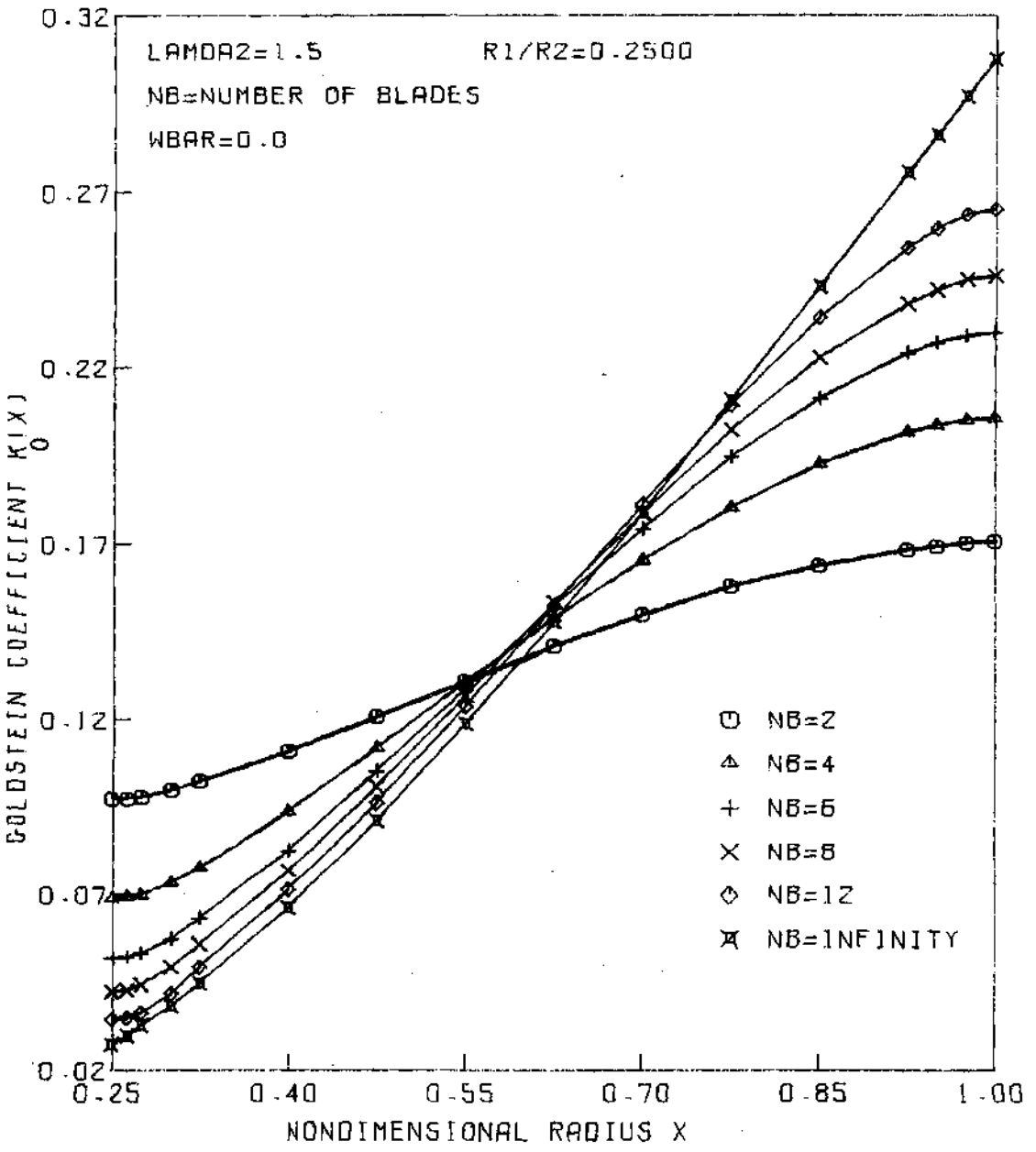

FIGURE 16. VARIATION OF $K_0(X)$ WITH NUMBER OF BLADES

As was shown earlier, the $K_o(X)$ distributions for larger and larger blade number converge to that of the infinite-bladed fan. This becomes very important since it takes only a few seconds to generate the data for the infinite-bladed fan. Therefore for fans with a large number of blades, instead of spending an inordinate amount of computer time in generating the data, it is more economical, as well as quicker, to approximate such fans with corresponding infinite-bladed fans. Another test of convergence of the data with increasing blade number can be made by considering the mass coefficient, κ_o'. It is seen from Fig. 17 that the mass coefficient, κ_o', also converges rapidly to that of the infinite-bladed fan for $\lambda_2 = 0.5$ and $m = \frac{1}{4}$. This is found to be true regardless of the values of λ_2 and m chosen in generating the data, thus establishing the accuracy of the numerical procedures used.

In Chapter II, a detailed description of the method for obtaining C_T, C_p, η_i, and C_{T_p}/C_T in terms of the volume integrals of the velocity distribution in the wake was given. This method was programmed for the digital computer and the program was used to evaluate numerically C_T, C_p, η_i, etc. This program was designed to first evaluate the velocity field in the wake from a knowledge of the vortex strength distributions. After obtaining the velocity field, the required volume integrals are evaluated numerically. The values of C_T, C_p and η_i were obtained for various values of load parameter, $\overline{W}/\lambda_2$, which varies from 0.0 to 1.0, with $\overline{W}/\lambda_2 = 1$ being the case where the flight speed is zero (static case). As before, the data corresponding to a fan with no hub was generated as a special case to serve as the test case. Figures 18 through 21 show that the agreement between Wright's[2] data and the

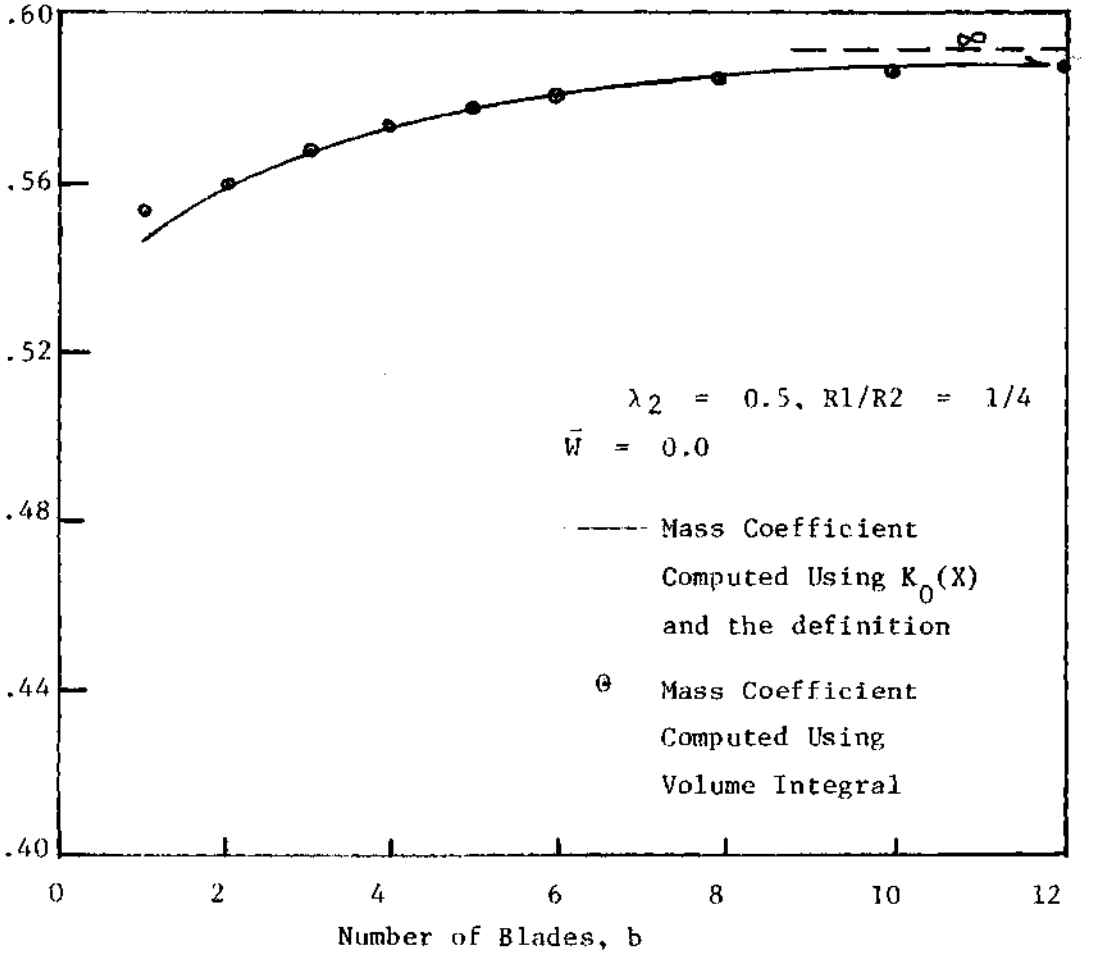

Figure 17. Variation Of Mass Coefficient, κ_0' With Number Of Blades.

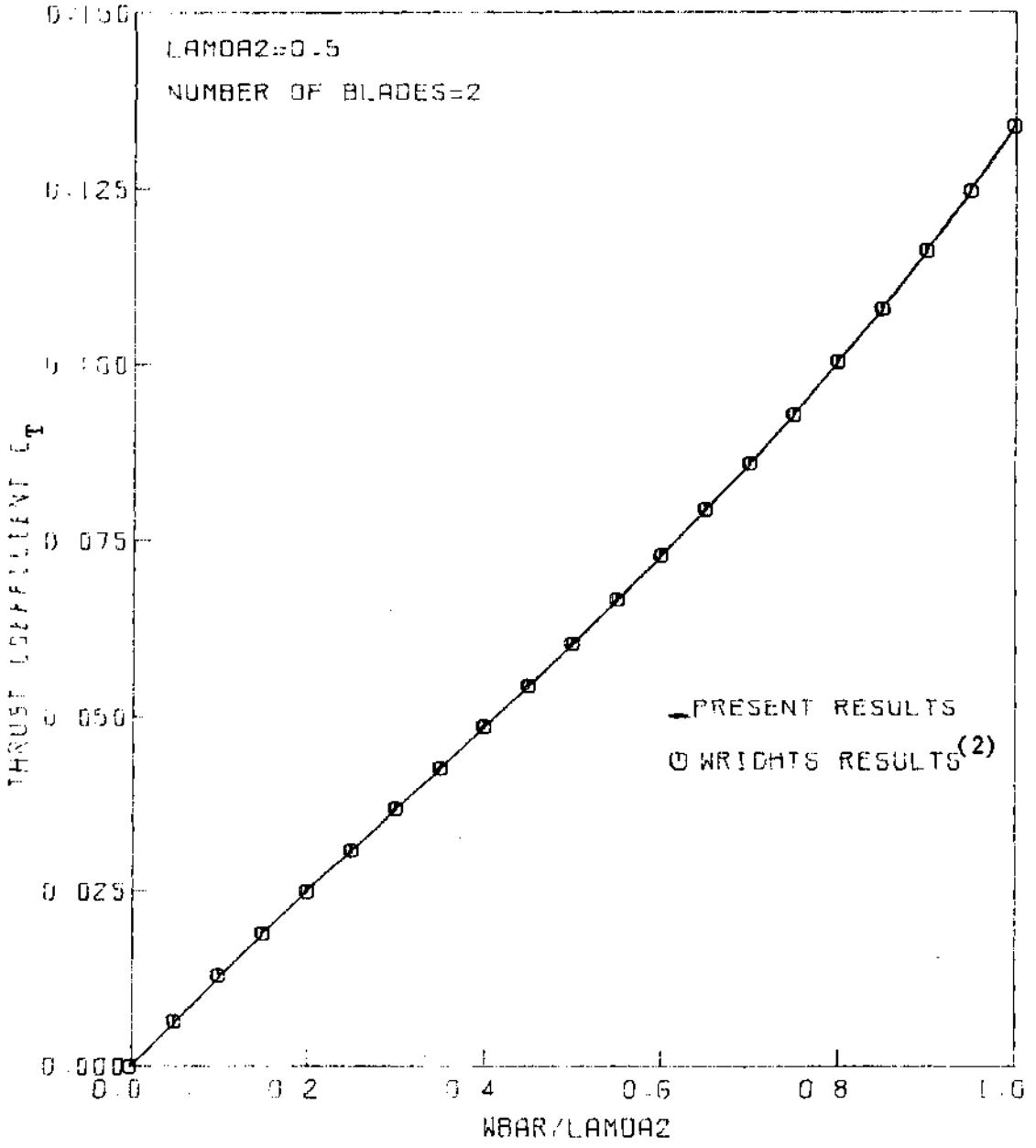

FIGURE 18. COMPARISON OF WRIGHTS RESULTS FOR C_T WITH THE PRESENT VALUES

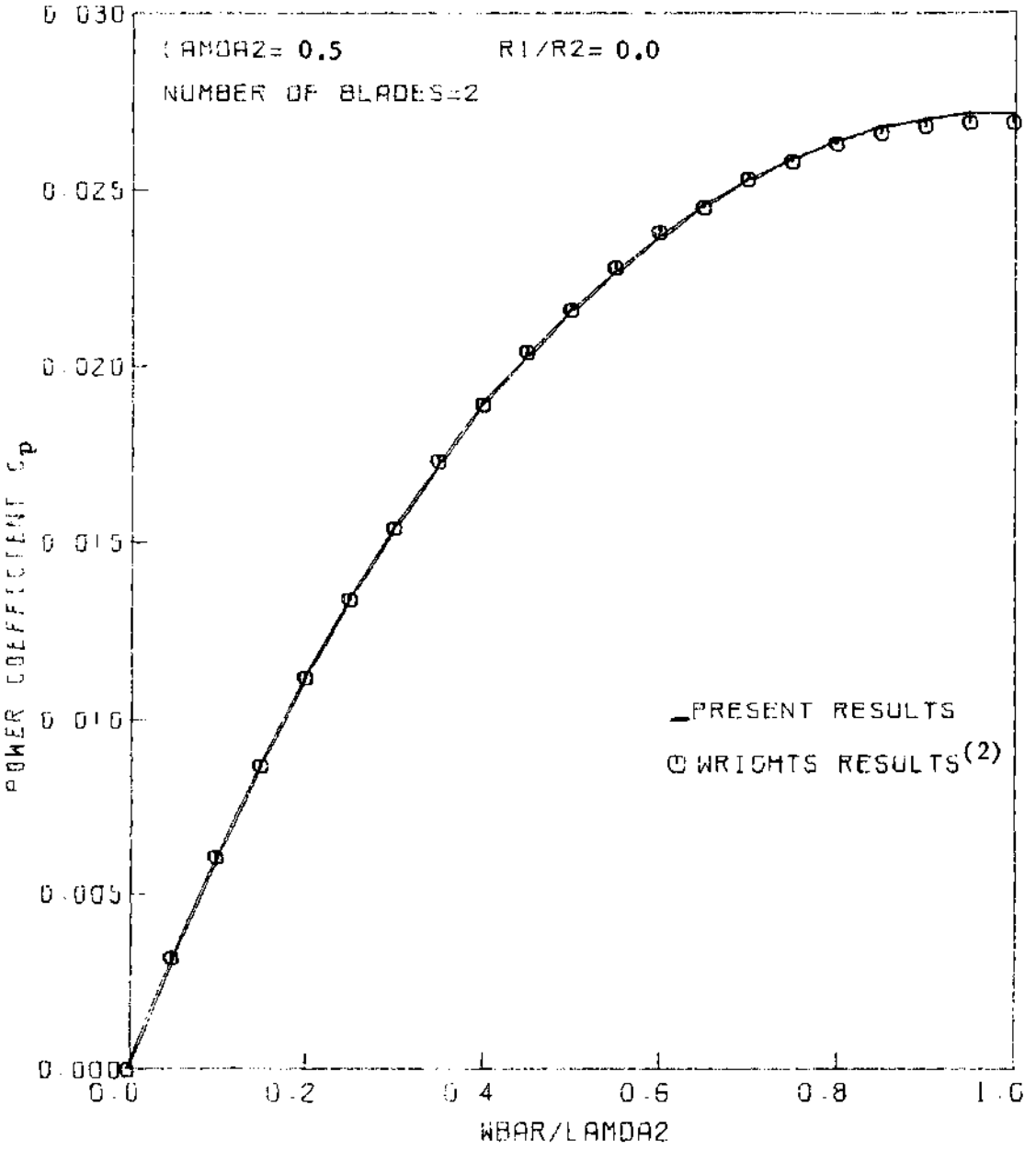

FIGURE 19. COMPARISON OF WRIGHTS RESULTS FOR C_p WITH THE PRESENT VALUES

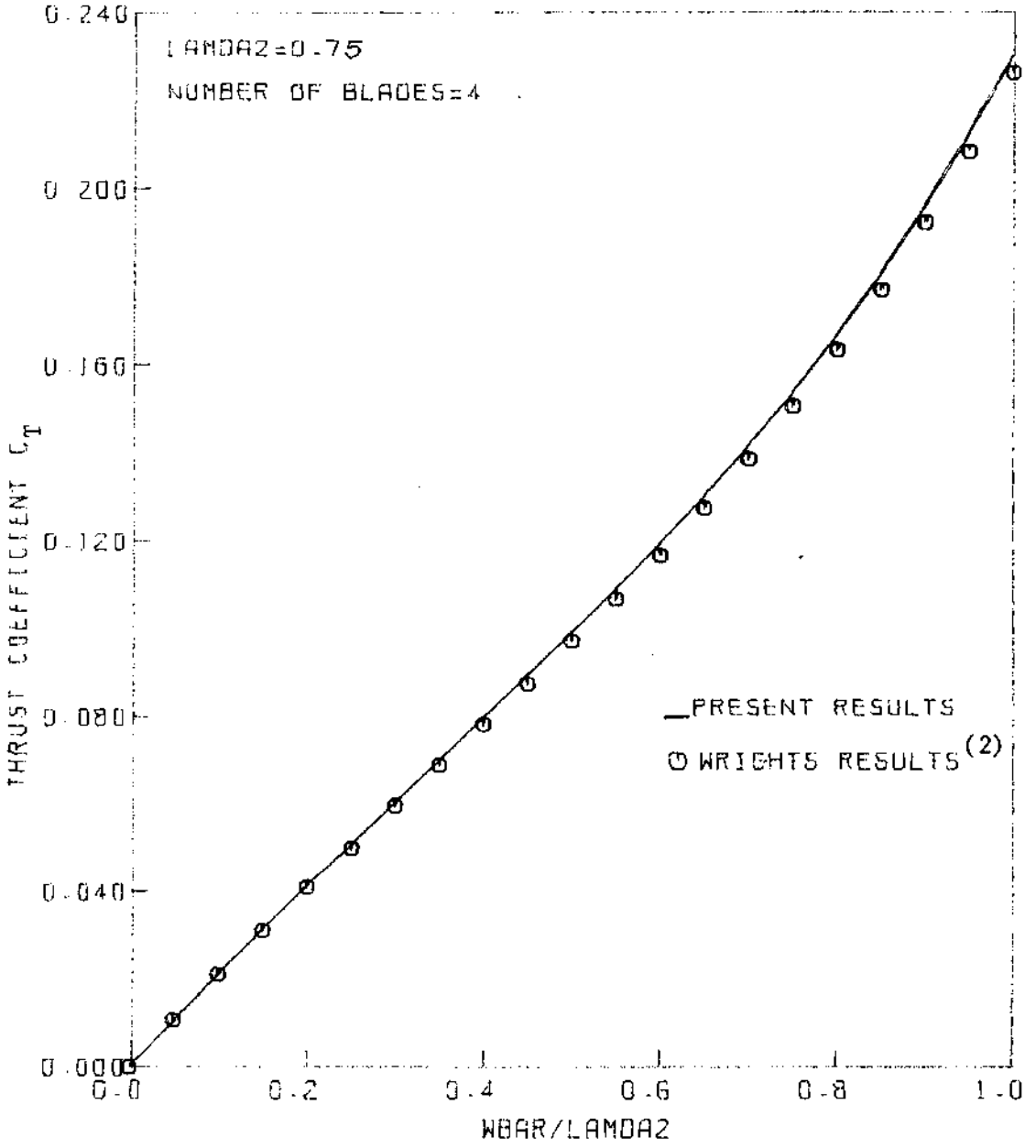

FIGURE 20. COMPARISON OF WRIGHTS RESULTS FOR C_T WITH THE PRESENT VALUES

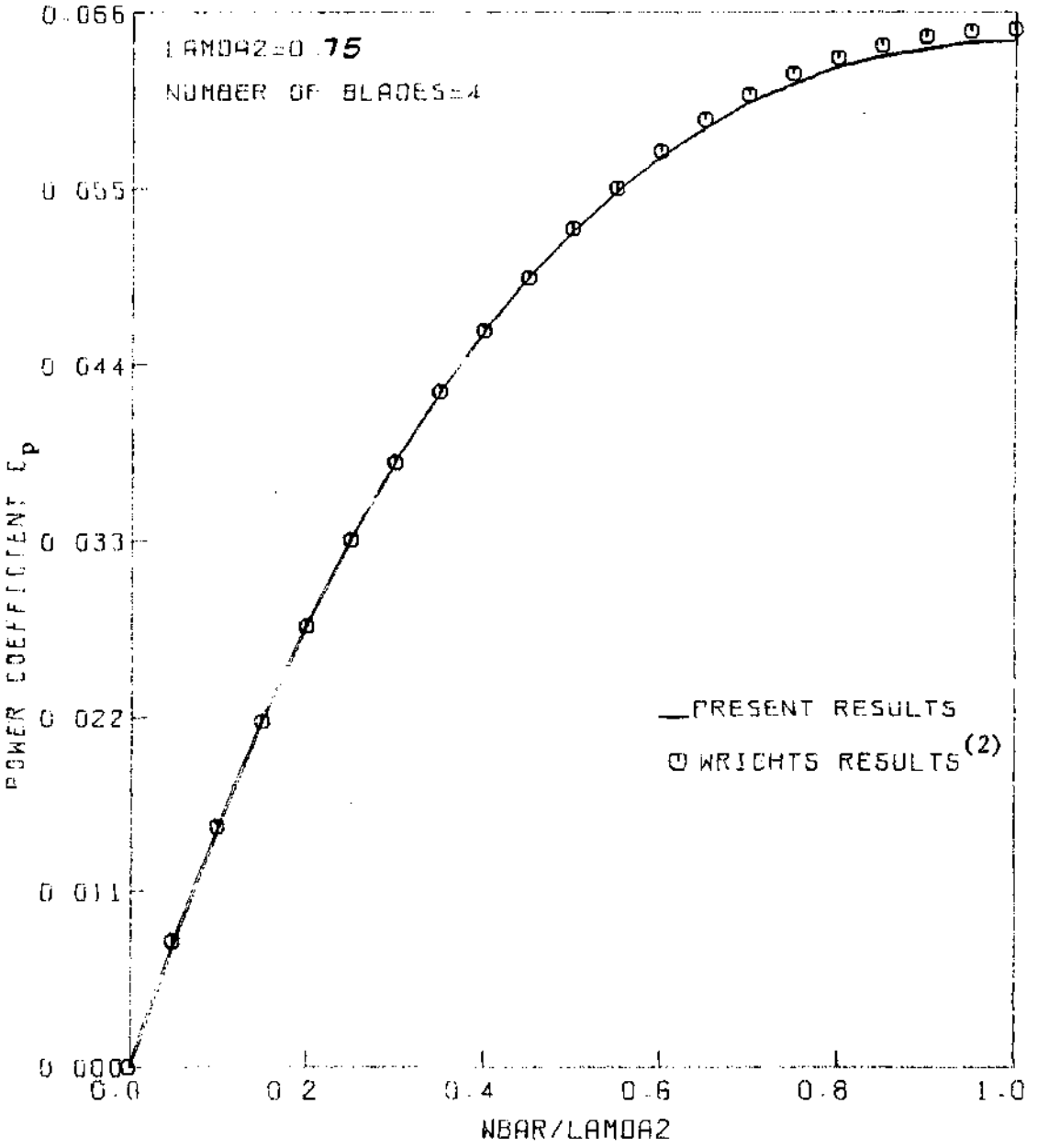

FIGURE 21. COMPARISON OF WRIGHTS RESULTS FOR C_p WITH THE PRESENT VALUES

present data is very good for both C_T and C_p. The observed differences are probably due to the differences in the numerical procedures.

The accuracy of the numerical evaluation of volume integrals can be established by evaluating $\int U_z \, dvol'$ numerically and comparing it with the exact value given in terms of the mass coefficient (Eq. (60)). For $\lambda_2 = 0.5$, $m = \frac{1}{4}$, and $\bar{W} = 0$, Fig. 17 shows that the agreement between the mass coefficient computed using $K_o(X)$ and the value computed using the volume integral of $\bar{U}_{z_{vs}}$ and λ_2, is excellent. In fact, this check was made for all the data generated and it was found that in every case these values agreed to within one percent.

As an additional check on the volume integrals as well as on the convergence of the data with increasing blade number, the values of ε_z, ε_ψ, and ε_r were evaluated for various values of λ_2, m and blade number, b, and compared with those of the corresponding infinite-bladed fan. The values for the infinite-bladed fan were obtained using the velocity field given in Chapter III. For the case of fans with finite number of blades, ε_z, ε_ψ, and ε_r were obtained using the numerical computations of the volume integrals. Figures 22 and 23 show that ε_z converges satisfactorily to that of the infinite bladed fan for both the cases of $\bar{W}/\lambda_2 = 0.0$ and $\bar{W}/\lambda_2 = 1.0$. In fact, this is true for all the values of λ_2 and m considered except for the case of a fan with $\lambda_2 = 0.5$ and $m = 0.75$. In this particular case, due to the relatively uniform velocity field in the wake, ε_z does not change appreciably with b. In the case of ε_ψ (Fig. 24), it does converge to the value corresponding to the infinite-bladed fan with increasing blade number. For the case of

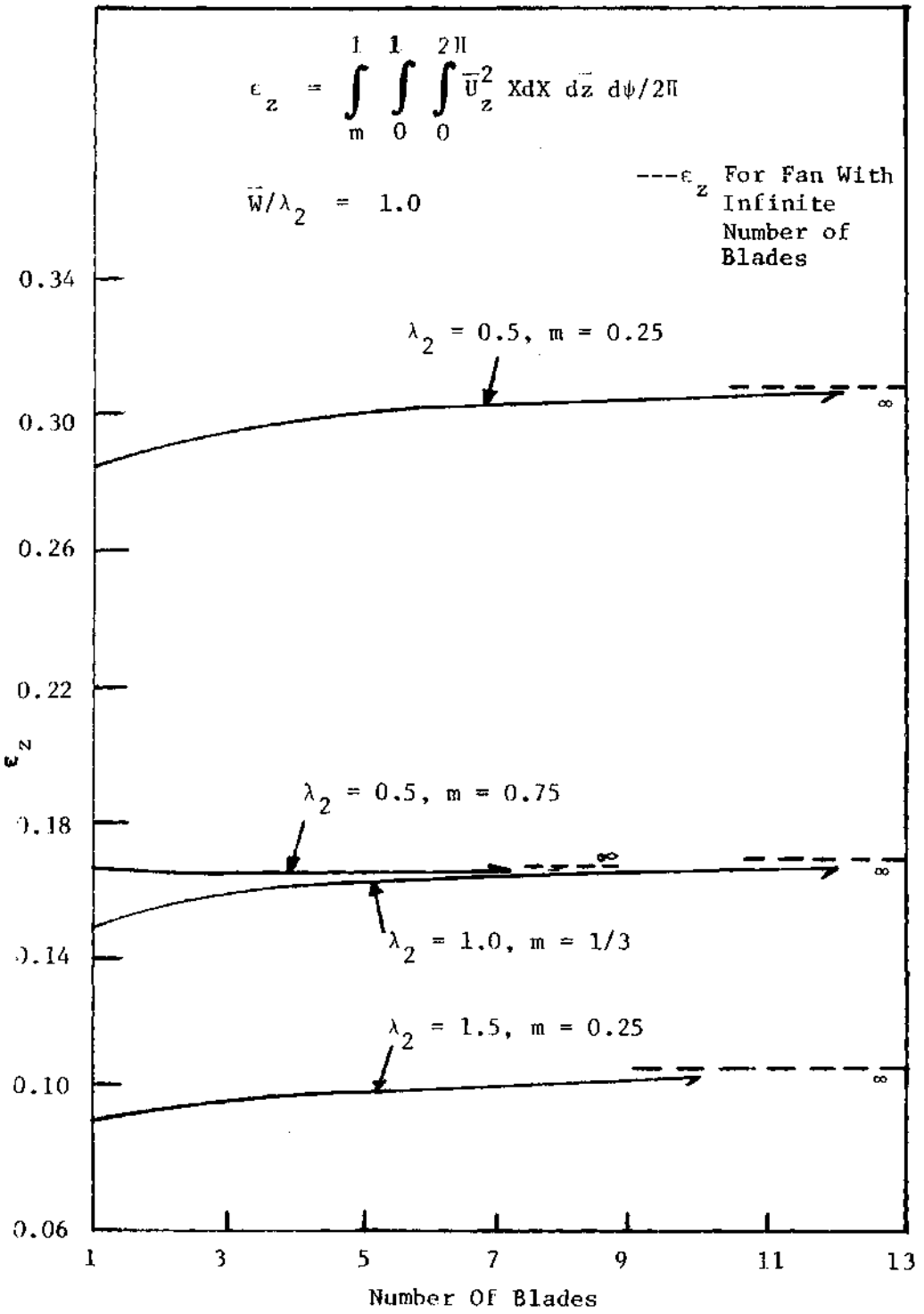

Figure 22. Variation of ϵ_z With Number Of Blades.

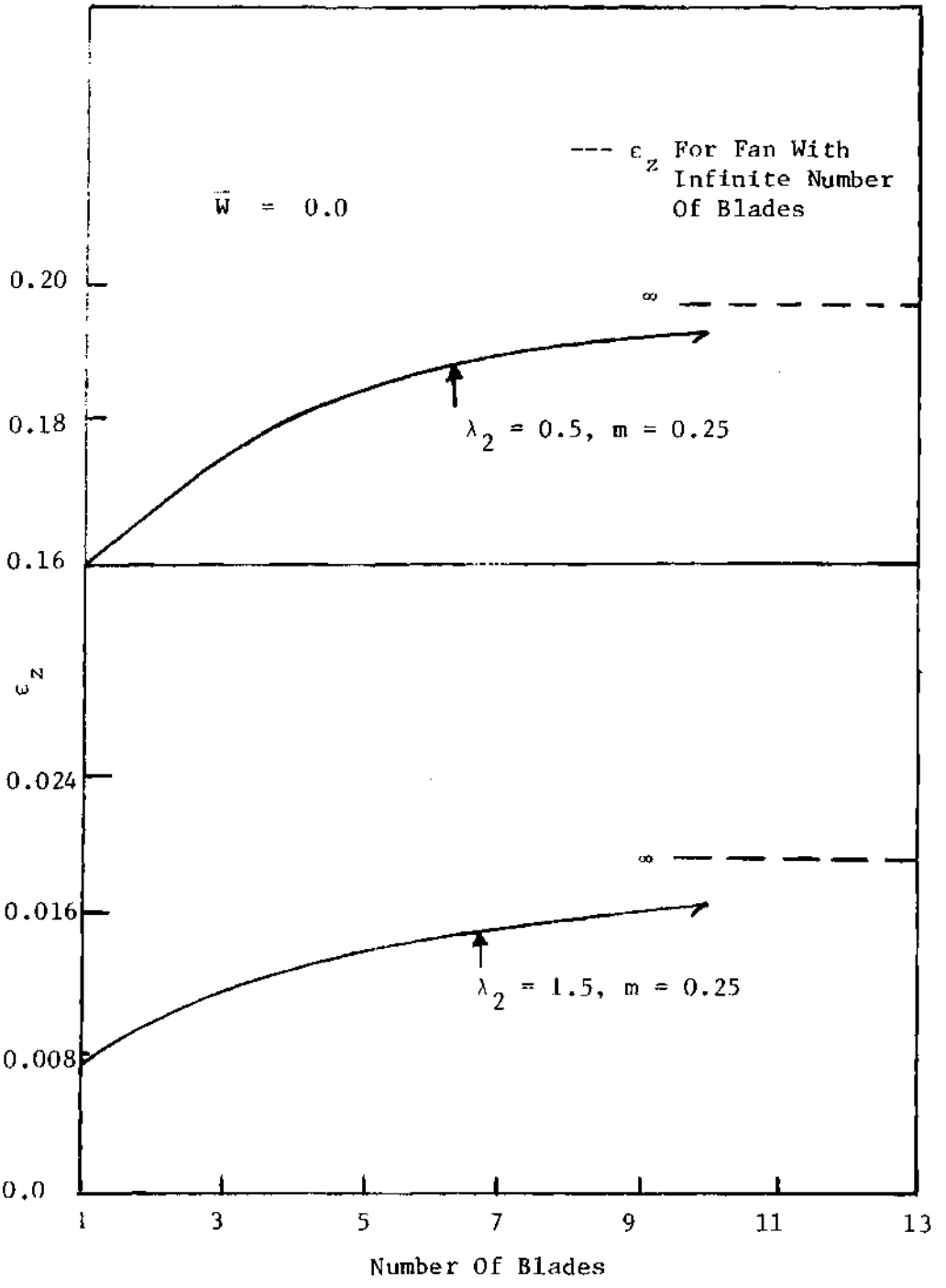

Figure 23. Variation Of ϵ_z With Number Of Blades.

the fan with $\lambda_2 = 0.5$ and $m = 0.75$ as shown in Fig. 24, the value of ε_ψ does not change appreciably with b. This may be due to the relatively uniform flow field associated with high values of m. It is also seen here that, unlike in the case of ε_z, the convergence is not monotonic (in a few cases) with a dip in the curve at the lower values of blade number (see Fig. 24). This may be due to the inner boundary sheet which induces tangential velocities in the fan wake and that at lower values of b, its effects might be more pronounced. Figure 25 shows that ε_r converges to zero which is the value corresponding to the infinite-bladed fan for all values of λ_2 and m. Once again the convergence is not monotonic for reasons that are not clear.

A third case for the check on the accuracy of the volume integrals can be made by comparing the values of the power coefficient, C_p, obtained from two different methods. In one method as was described earlier in Chapter II, C_p was computed using C_T and the induced energy loss, e, in the wake which involves the computation of several volume integrals. In the other case as was also described in Chapter II, C_p was computed using the Kutta-Joukowski theorem. As shown in Fig. 26, the agreement between the two sets of values for the case of a fan with $\lambda_2 = 0.5$ and $m = 0.25$, is very good. It was found that the two sets of values of C_p obtained from the two methods agreed to within one percent for most of the cases considered.

After establishing the accuracy of numerical volume integrations, the values of C_T, C_p, C_{T_p}/C_T, and η_i were computed for different combinations of λ_2 and m. For each λ_2, m, and b, these quantities were computed

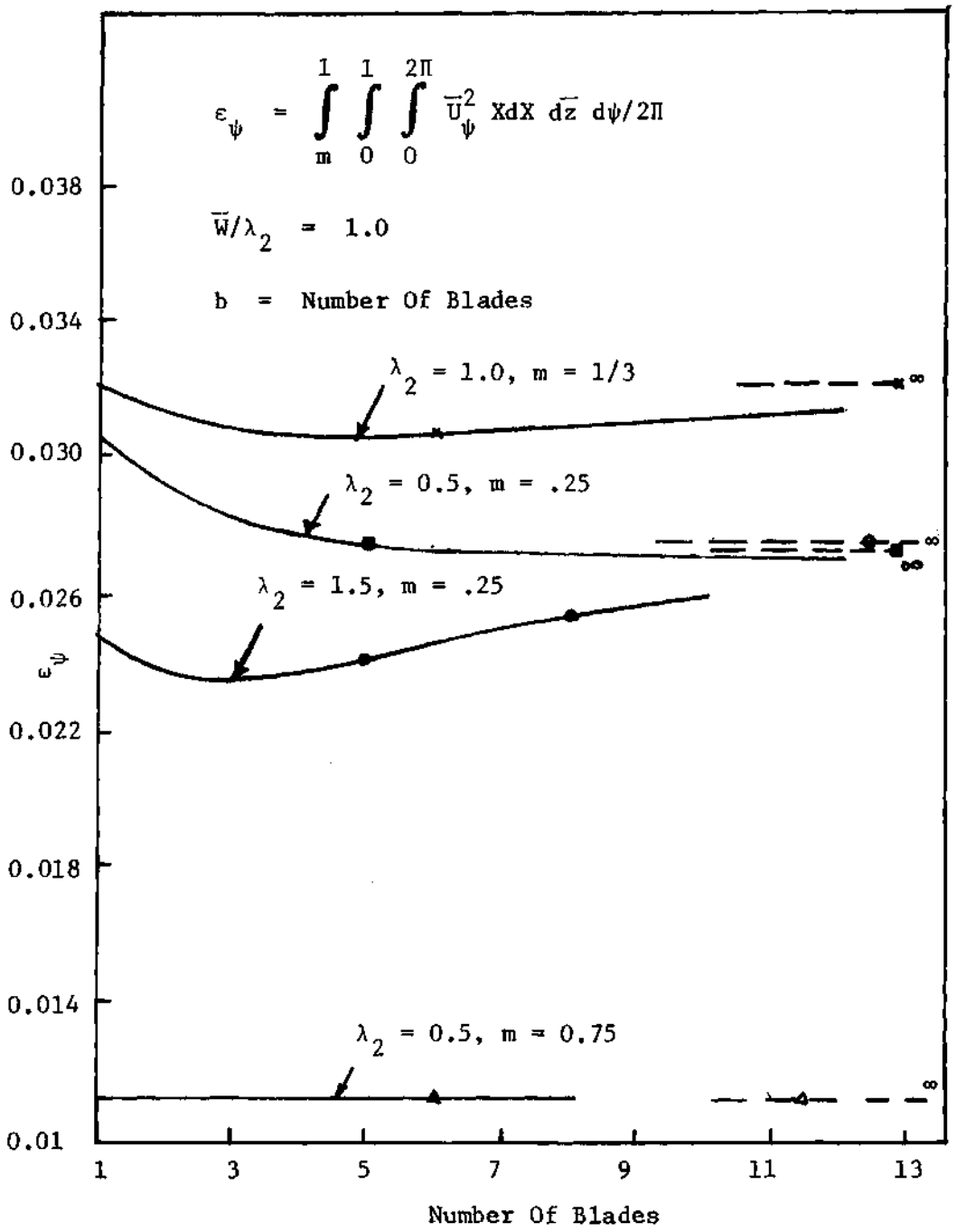

Figure 24. Variation Of ε_ψ With Number Of Blades.

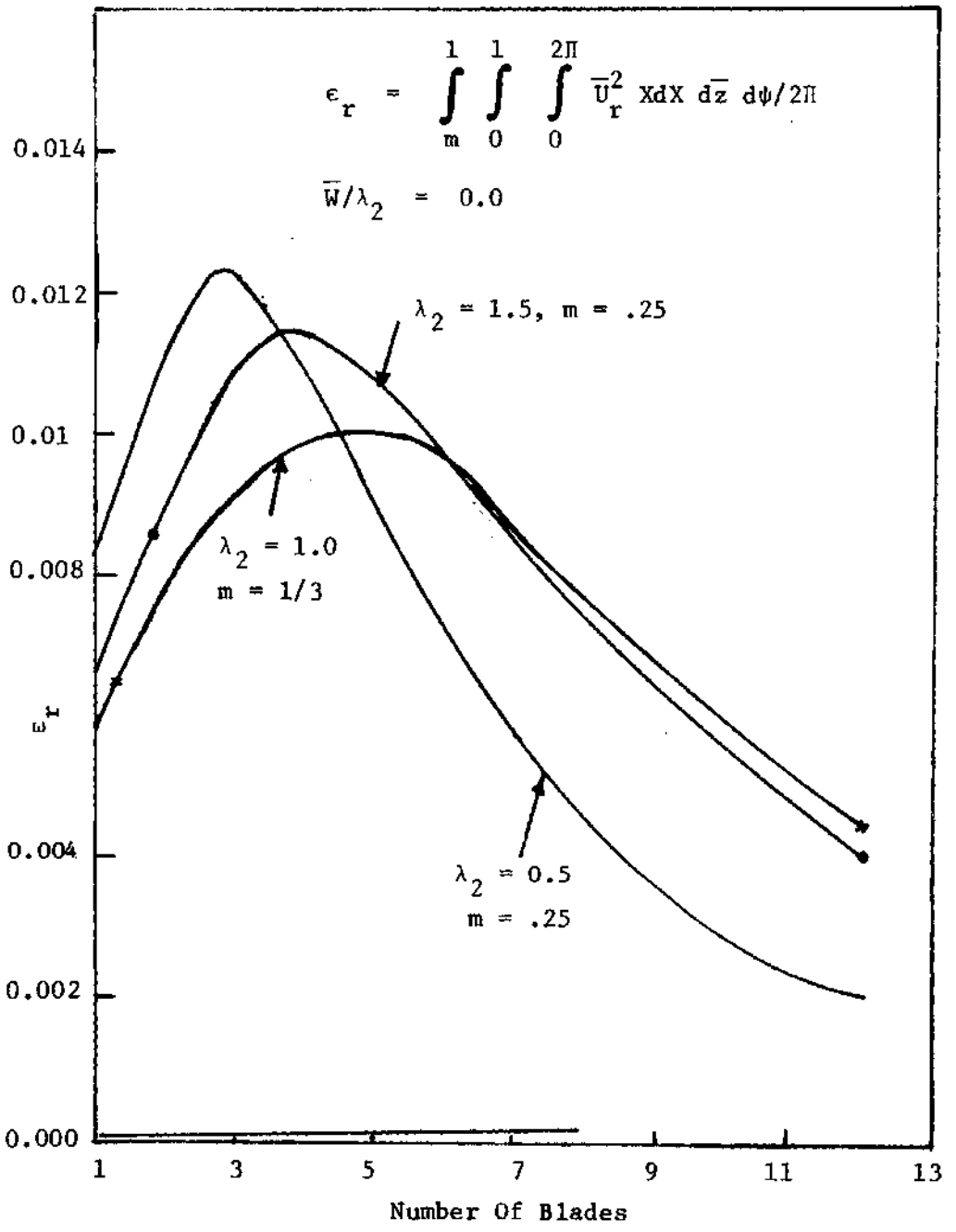

Figure 25. Variation Of ϵ_r With Number Of Blades.

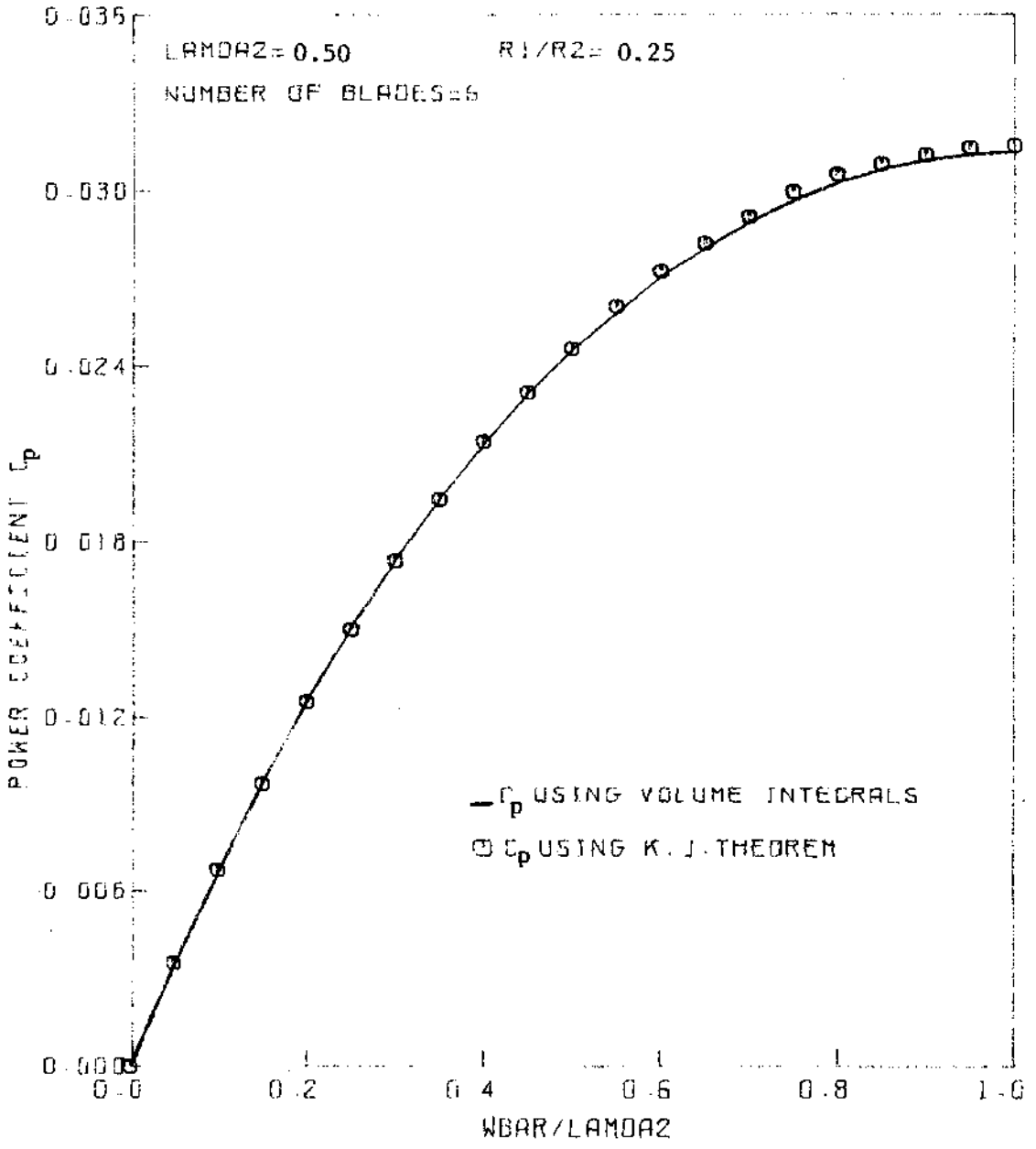

FIGURE 26. COMPARISON OF POWER COEFFICIENTS COMPUTED USING TWO DIFFERENT METHODS

for values of $\overline{W}/\lambda_2$ ranging from 0.0 to 1.0. An index to the data presented in the form of tables, is given in Table 1. Figures 27 through 34 show the variations with the blade number of C_T and C_p with $\overline{W}/\lambda_2$ for various combinations of λ_2 and m. As expected, these variations converge to that of the infinite-bladed fan. In the case of the fan with $\lambda_2 = 0.5$, and $m = 0.75$ (Figs. 29 and 30), it is seen that the values of C_T and C_p do not change significantly with an increase in the number of blades. As was discussed earlier, there is a significance to the convergence seen in these figures. It not only demonstrates the validity of the wake model and the method used but also makes it possible to approximate a ducted fan with a large number of blades with that of a corresponding infinite-bladed fan. This latter consequence is very significant considering the large amount of computer time involved in these calculations for finite-bladed fans. For example, it takes about 900 secs on the Cyber 74 to generate C_T, C_p, C_{T_p}/C_t, etc. for $\overline{W}/\lambda_2$ from 0.0 to 1.0 for a fan with $\lambda_2 = 0.5$, $m = 0.25$ and $b = 2$. However, if the number of blades is increased from 2 to 12 keeping the other parameters constnat, it takes about 4200 secs to generate the same data. These computational times do not include those required for the generation of the data for $K_o(X)$. It is to be borne in mind that it takes only a few seconds of computer time to generate the similar data for an infinite-bladed fan. These observations regarding the computational time hold generally true for all values of λ_2 and m that were considered. Figure 35 shows the variations of induced efficiency, η_i, with the load parameter, $\overline{W}/\lambda_2$, for a fan with $\lambda_2 = 0.5$ and $m = 0.25$

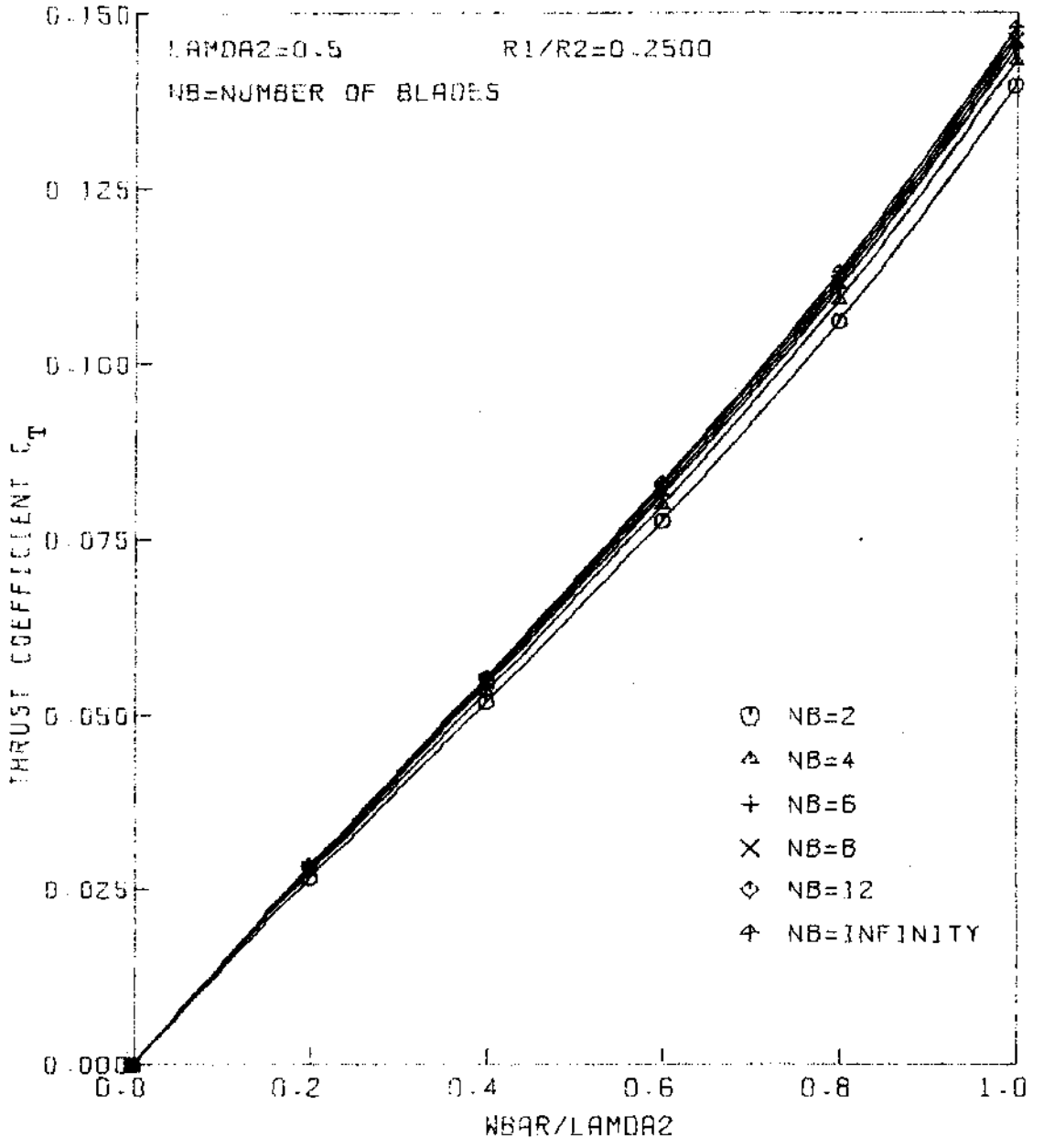

FIGURE 27. VARIATION OF THRUST COEFFICIENT WITH LOAD FOR FANS WITH VARYING NUMBER OF BLADES

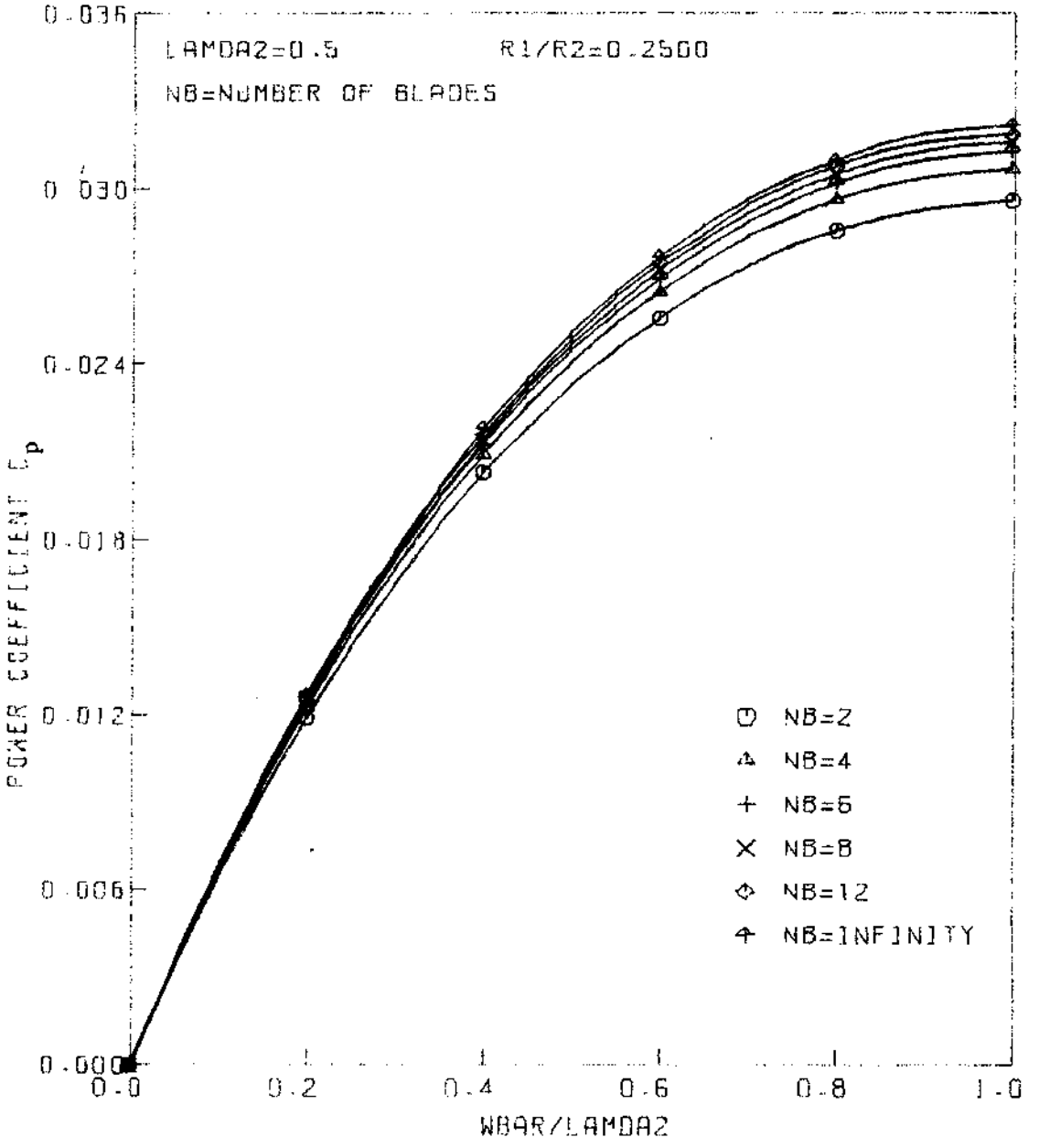

FIGURE 28. VARIATION OF POWER COEFFICIENT WITH LOAD FOR FANS WITH VARYING NUMBER OF BLADES

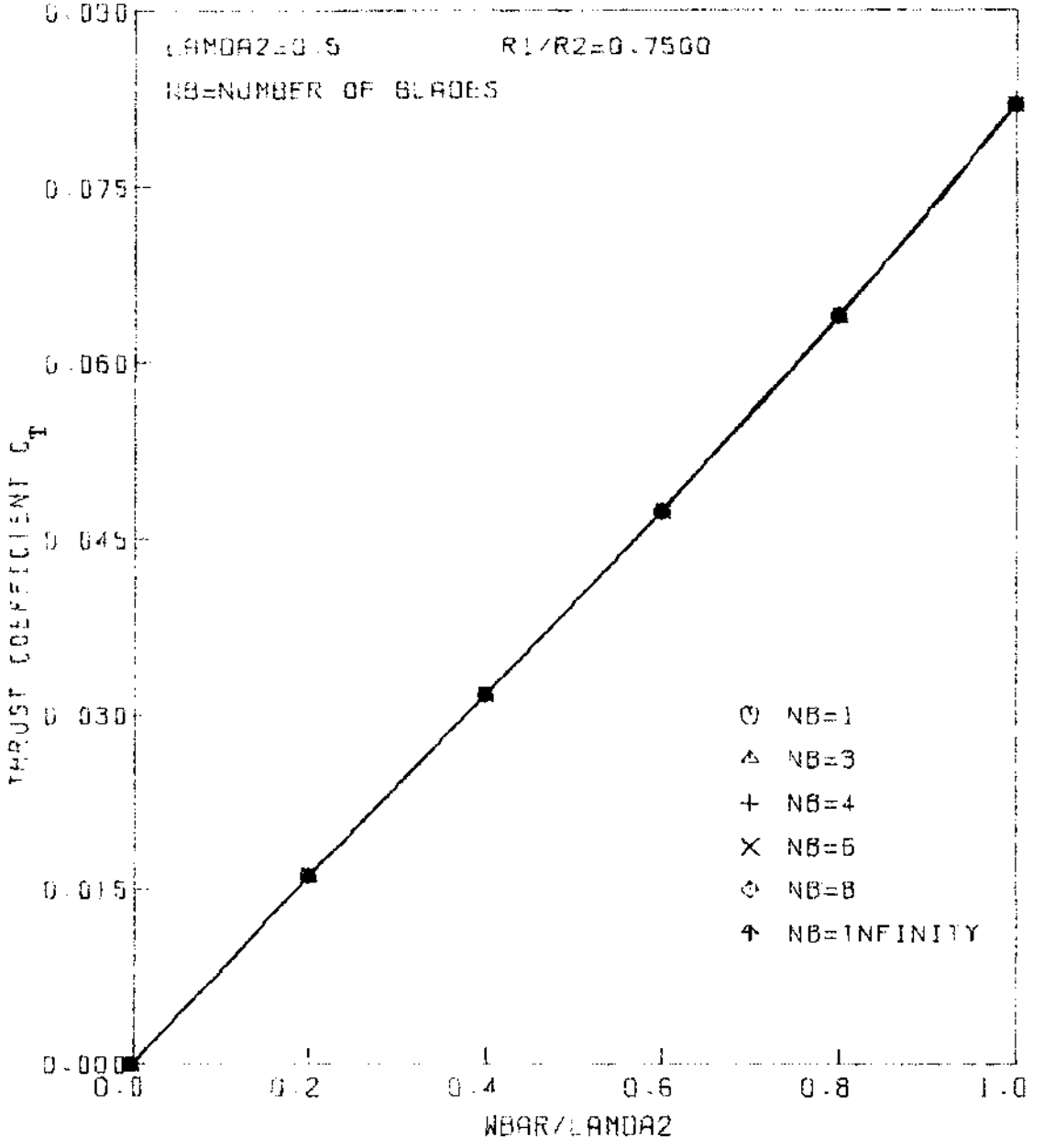

FIGURE 29. VARIATION OF THRUST COEFFICIENT WITH LOAD FOR FANS WITH VARYING NUMBER OF BLADES

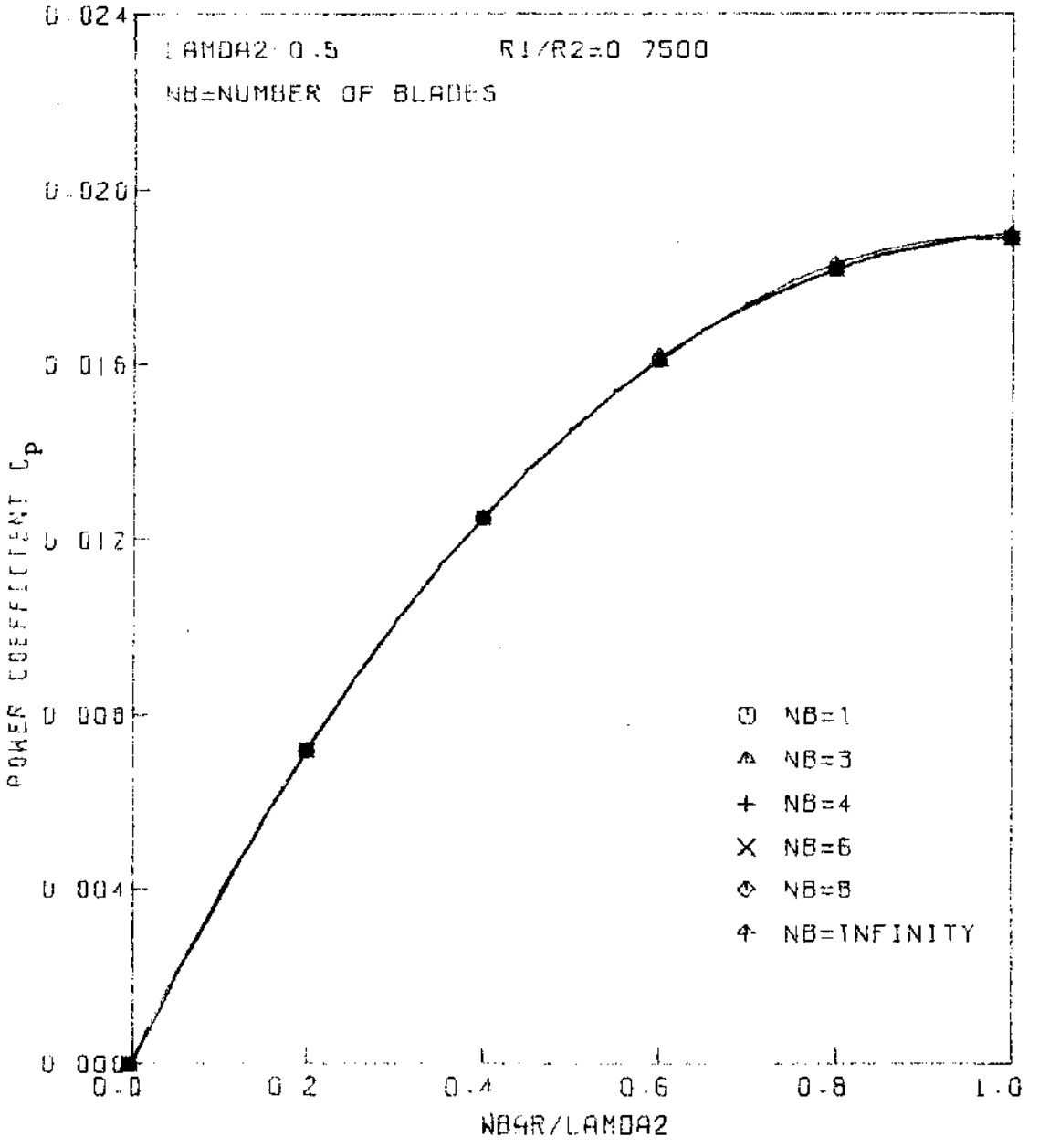

FIGURE 30 VARIATION OF POWER COEFFICIENT WITH LOAD FOR FANS WITH VARYING NUMBER OF BLADES

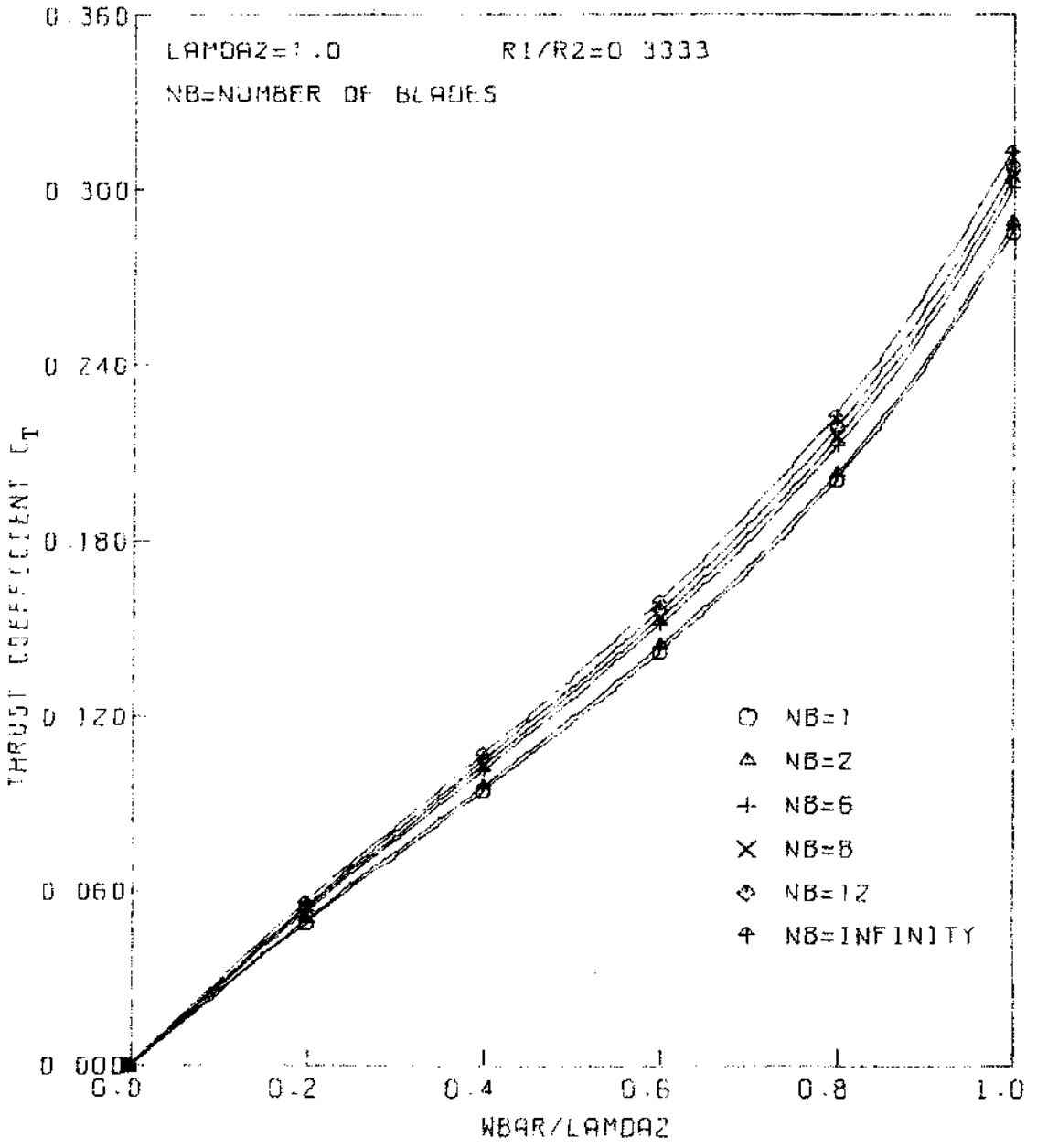

FIGURE 31. VARIATION OF THRUST COEFFICIENT WITH LOAD FOR FANS WITH VARYING NUMBER OF BLADES

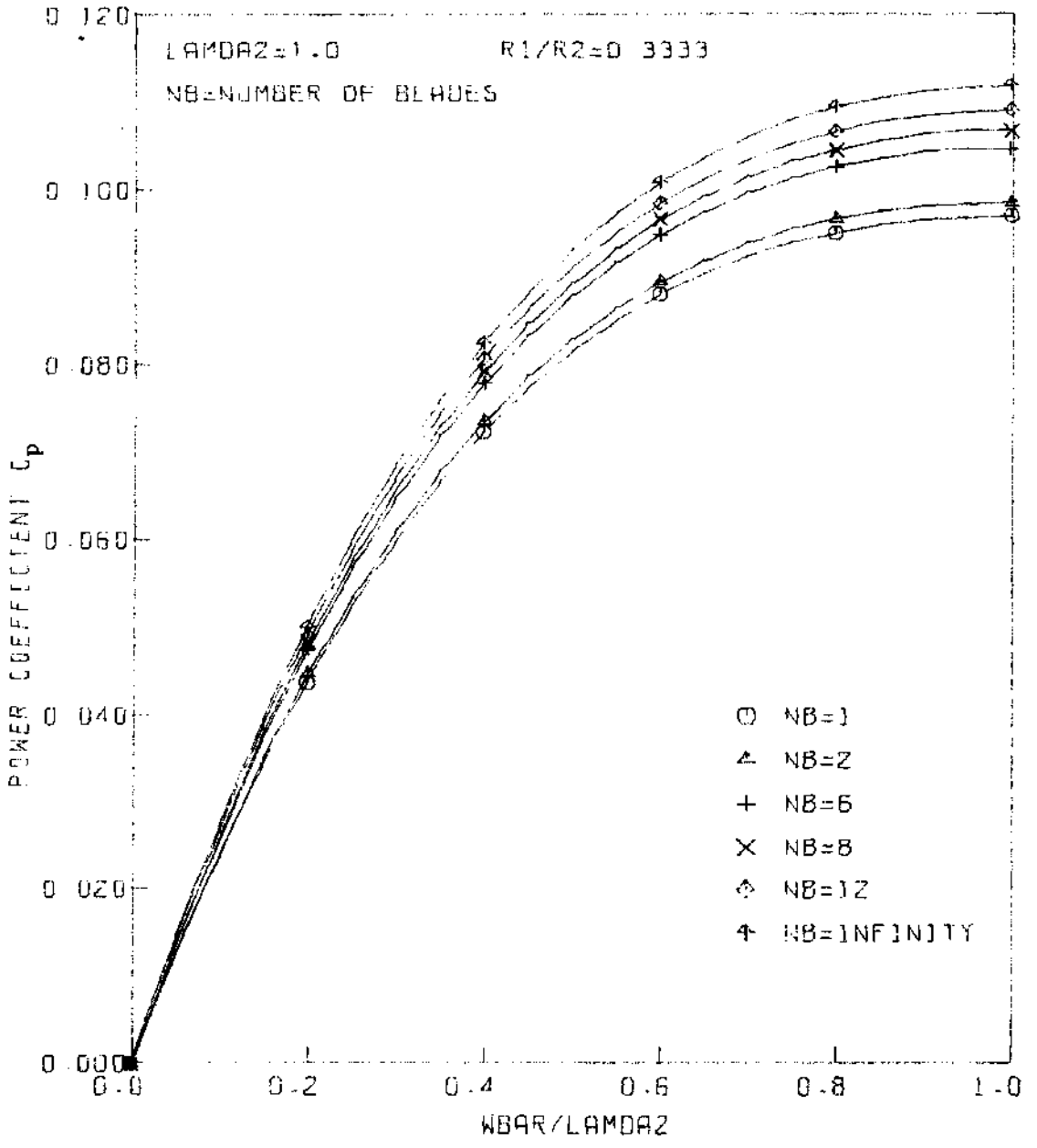

FIGURE 32 VARIATION OF POWER COEFFICIENT WITH LOAD FOR FANS WITH VARYING NUMBER OF BLADES

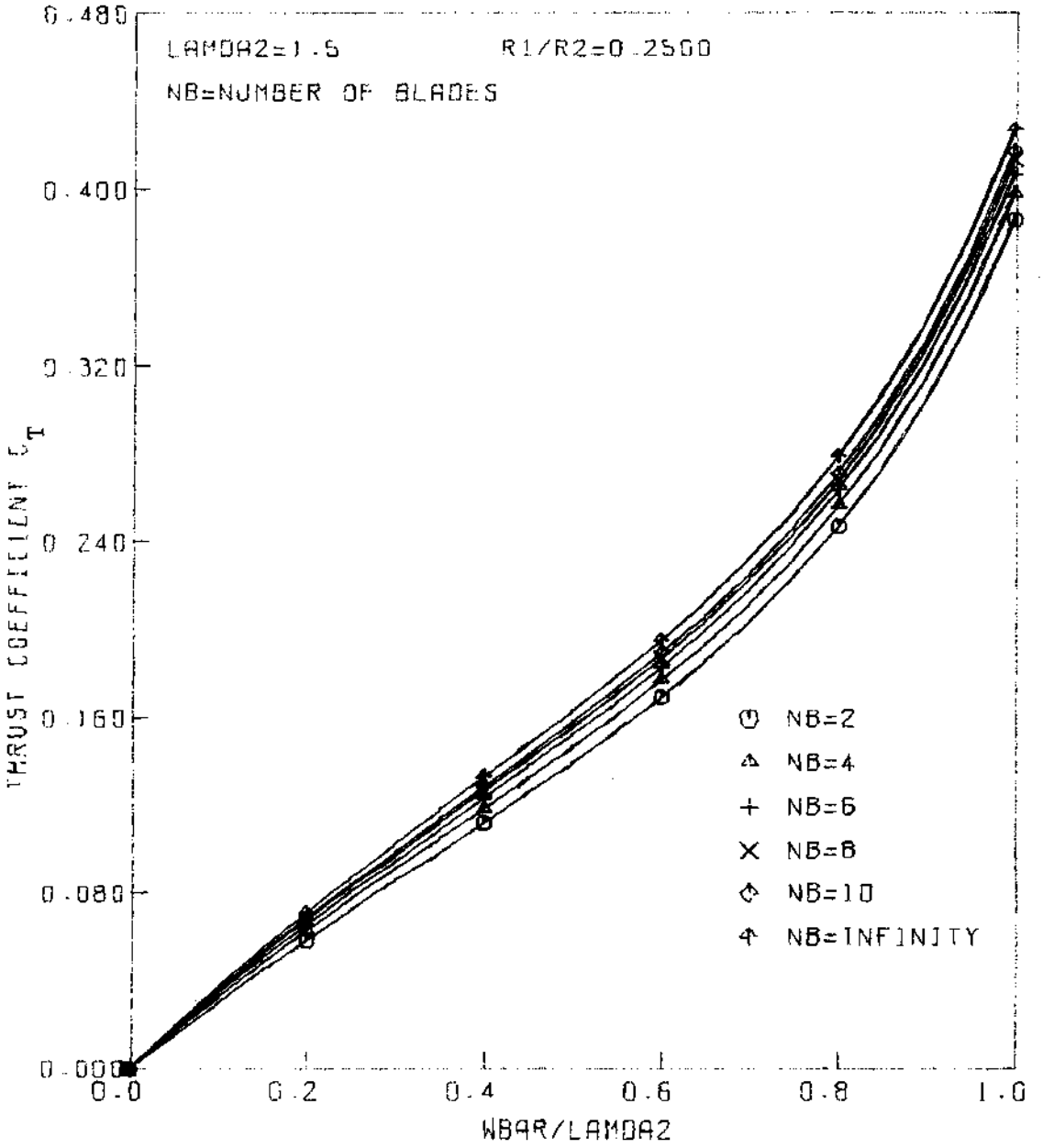

FIGURE 33. VARIATION OF THRUST COEFFICIENT WITH LOAD FOR FANS WITH VARYING NUMBER OF BLADES

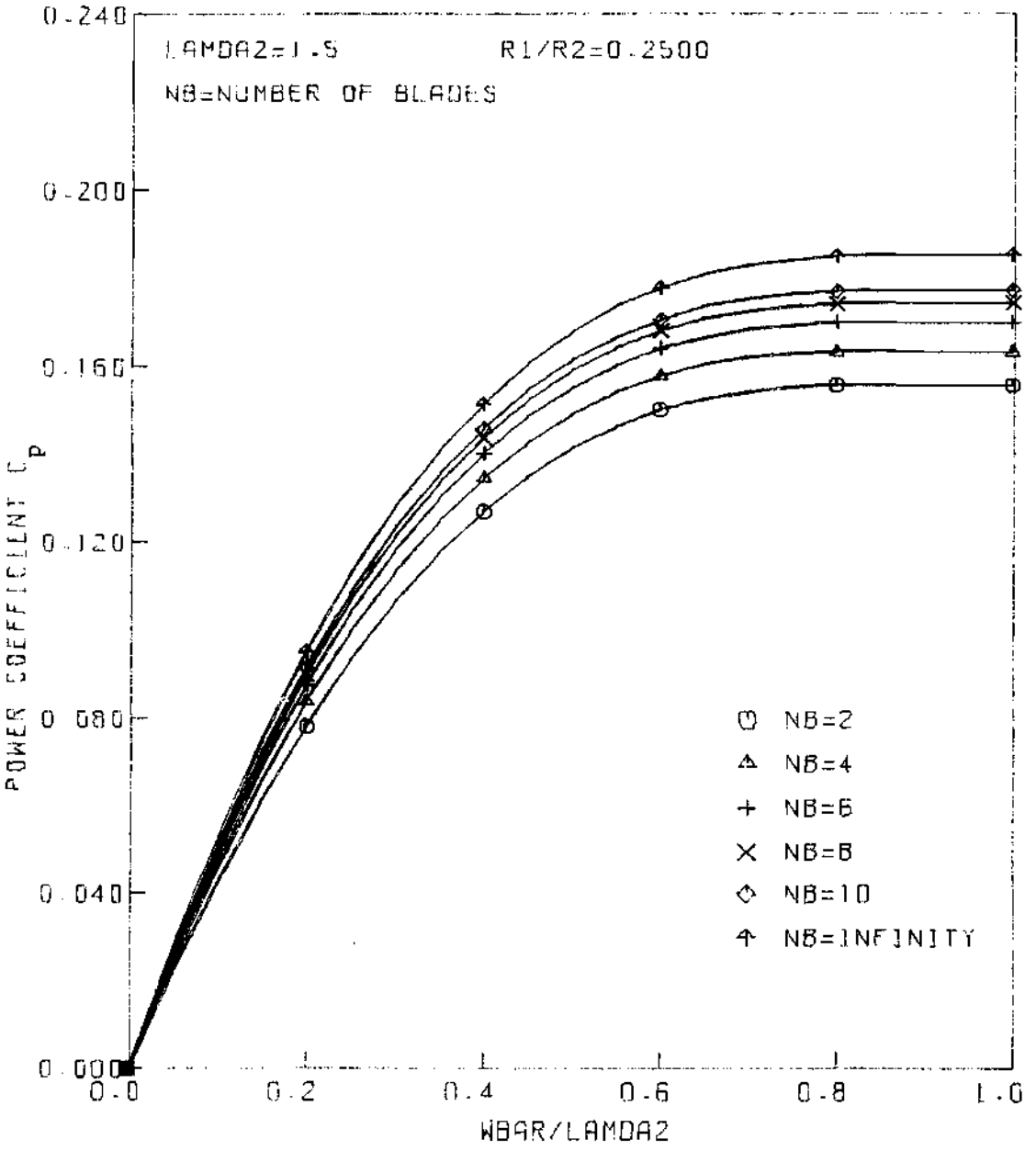

FIGURE 34. VARIATION OF POWER COEFFICIENT WITH LOAD FOR FANS WITH VARYING NUMBER OF BLADES

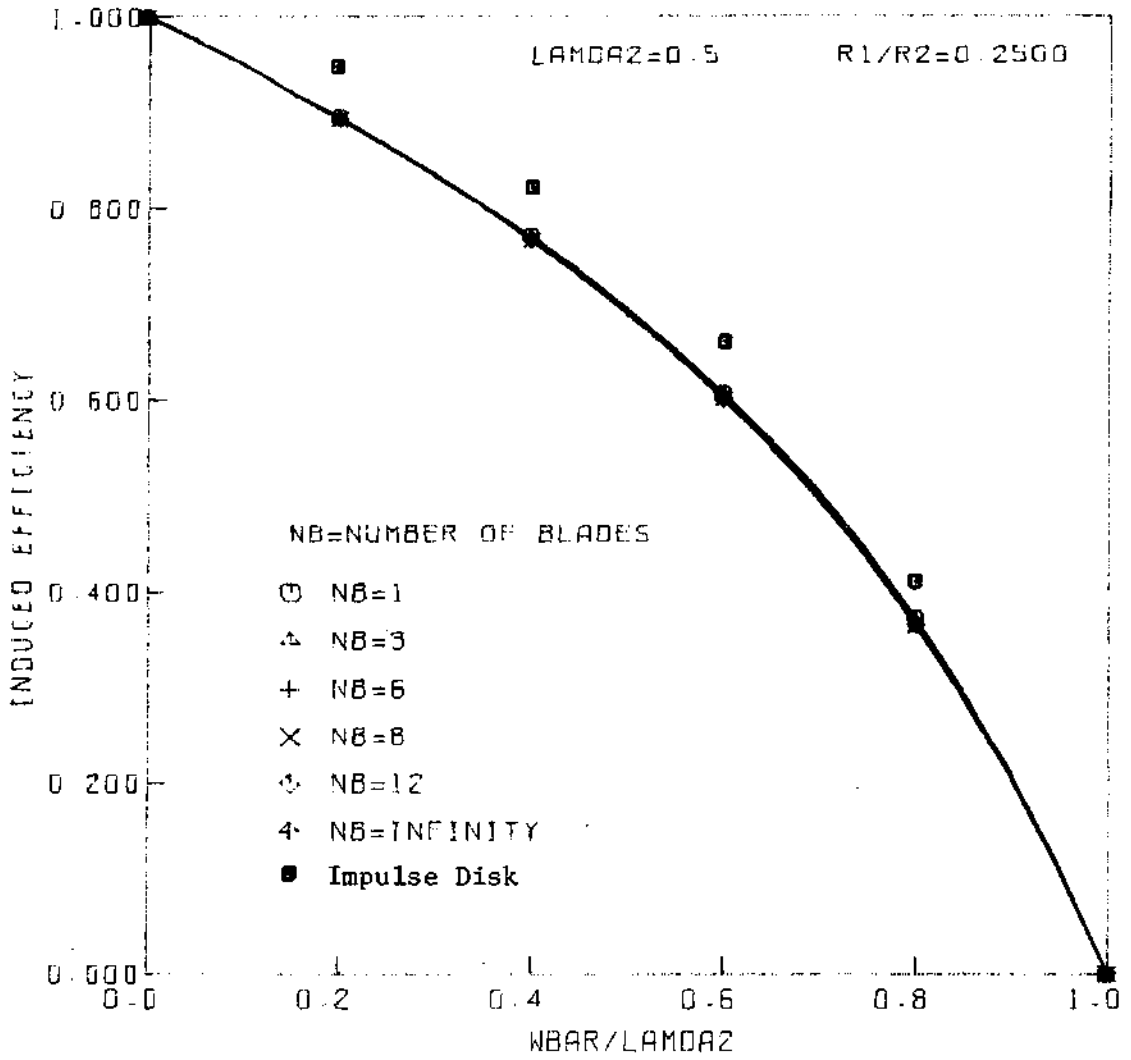

FIGURE 35. VARIATION OF INDUCED EFFICIENCY WITH LOAD FOR FANS WITH VARYING NUMBER OF BLADES

and for increasing blade number. It is seen that these variations do not change significantly with b inspite of the fact that the magnitude of the radial velocities in the wake decrease with increasing blade number and becomes zero in the limiting case of an infinite number of blades. This is so because with increasing of blades the thrust developed also changes and hence the effect of a decrease in ϵ_r cannot be clearly seen in the Fig. 35. The induced efficiency of a single rotation, optimum ducted fan, such as the one considered here is also compared with that of an impulse disk developing the same thrust. In the latter case, the tangential velocities are absent in the ultimate wake and the axial velocity is uniform across the wake. As shown in Fig. 35, the induced efficiencies of the impulse disk are higher (by about 3 to 4%) than those of the single-rotation fan with no stator vanes.

The variation of C_{T_p}/C_T with $\overline{W}/\lambda_2$ is shown in Fig. 36. It is seen from this figure that at lighter loads, most of the thrust is developed by the fan blades and as the load parameter, $\overline{W}/\lambda_2$, increases, the proportion of the thrust developed by the fan to that of the duct decreases.

The data for $K_o(X)$, C_T, C_p, C_{T_p}/C_T, etc., for fans with $m = \frac{1}{3}$ but with different values of λ_2 and b are presented in tables at the end of the thesis.

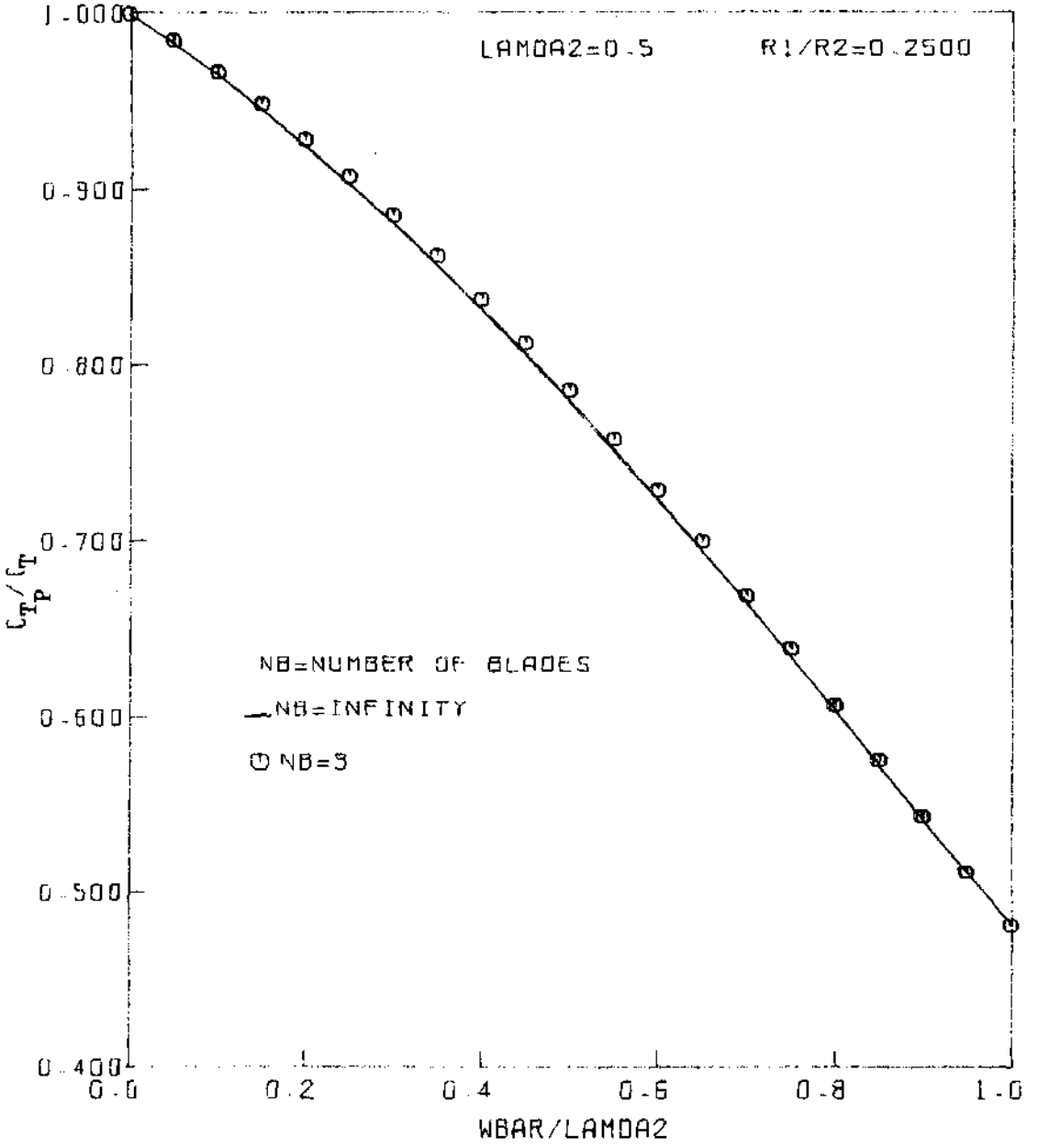

FIGURE 36. VARIATION OF C_{T_P}/C_T WITH LOAD

CHAPTER V

DUCT/FAN DESIGN

Preliminary Discussion

In the earlier chapters, the ultimate wake of optimum, high by-pass ratio ducted fans with a finite as well as an infinite number of blades was solved for the vortex strength distributions and velocity fields. However, from a practical point of view, it is necessary to design a duct which is compatible with the given ultimate wake. In the following discussion, a tentative and approximate procedure is suggested for the design of such a duct. The design is based on the assumption that the flow is incompressible and potential. The real fluid effects such as viscosity and compressibility[11] can be incorporated into the design after the preliminary design based on the potential flow.

The design of the duct involves determining its bound vortex strength distribution as well as its mean camber surface. It is to be noted that there are, in general, two types of ducts that have a wide application. The duct can be used either to accelerate or decelerate the flow to the fan. In accelerating ducts, such as bell mouths, the thrust of the combination of duct and fan is increased over that of the fan alone. In the past decelerating ducts were used in marine propellers where their main purpose was to delay cavitation. However, most of the commercial fan engines of today have ducts which first decelerate and then accelerate the flow. In high-speed subsonic flight where these

engines are mostly used, the incoming air flow is decelerated to the entrance to the fan where the fan adds energy to the flow. The flow is then accelerated downstream of the fan. These ducted fans are driven by coaxial core engines which are gas turbines. The wakes of the ducted fan engines therefore consist of a hot jet exhaust surrounded by a relatively cold fan exhaust.

The flow field in the duct of any finite-bladed ducted fan is unsteady. Therefore, to design the duct, it is suggested that the actual wake system of a ducted fan with finite number of blades be replaced by that of an equivalent (developing the same thrust) ducted fan with infinite number of blades. With the infinite bladed approximation, the flow field with respect to a coordinate system fixed to the duct is steady and is approximately equal to the time average flow of the actual unsteady flow field. The duct design will therefore be based on the ultimate wake of an infinite bladed ducted fan. After the duct design is established, the fan is then designed using the wake for a finite number of blades. The wake model and its solution for a ducted fan with infinite number of blades is given in Chapter III.

The wake of an optimum, high by-pass ratio, ducted fan with infinite number of blades consists of semi-infinite coaxial cylindrical vortex sheets. These cylinders of vorticity shed from the fan blades and the duct surround the jet wake from the core engine. The fan, in principle, can be at any axial location in the duct. Unlike commercial fan engines, no stator blades are assumed to be present in the duct-fan system. The effect of a tip clearance between the fan blades and the

duct is assumed to be negligible.

The design of the duct-fan system can be based on either the available power or the thrust developed. The latter case is considered here. It is assumed that the flight velocity, V_∞, the angular velocity of the fan, Ω, the number of blades, b, and the core engine characteristics are given. With regard to the core engine, it is assumed that the core engine geometry (R_1 and its inlet geometry, see Fig. 37), mass flow rate, and power output are given. The by-pass ratio is also assumed to be given. The outer radius, R_2, of the ultimate fan wake is then obtained. In the following discussion, an outline of the design of a decelerating-accelerating duct, such as those used in high by-pass ratio commercial fan engines is given. The amount of deceleration is assumed to be given. It is to be noted that the procedure to be described is also applicable to accelerating ducts.

Design Outline

The procedure is similar to the one given by Gray[4] for a lightly loaded ducted fan with counter rotating propellers. It has been suitably modified to take into account the decelerating-accelerating duct.

(i) Calculation of the Thrust coefficient, C_T: Determine

$$C_T = T_D/\rho \quad \pi R_2^2 \Omega^2 R_2^2,$$

where T_D is the given thrust of the duct-fan system.

(ii) Determination of the wake parameter, W: Since the duct is designed for an equivalent infinite-bladed fan, Eq. (95) is employed to obtain $\bar{W}$ using C_T from (1). The Modified False Position method of Ref. 10 can be used to obtain $\bar{W}$. Using this value of $\bar{W}$, the vortex strengths of the wake cylinders as well the velocity field in the ultimate wake are determined.

(iii) Determination of the Compatible Duct: A schematic diagram of the fan engine configuration and the vortex wake near the trailing edge of the duct is shown in Fig. 37. The duct contour and its bound vortex strength distribution are obtained by an iterative procedure. As shown in Fig. 37, the fan and the inlet (LJ) of the core engine are assumed to lie in the same plane. In the first iteration, (refer Fig. 37), it is assumed that the constant diameter wake cylinders of the ultimate wake extend up to the duct exit plane, AB. As shown in Fig. 37, the annular fan wake is divided into a finite number of semi-infinite cylindrical sheets. Between the fan and the duct exit plane, the wake filaments contract depending on the shape of the duct aft of the fan. It is assumed that the nondimensional local radii of these wake filaments (based on the outer radius) remain the same as the filaments move through the duct. The vortex strengths of these filaments are determined by the sheet strengths of the vortex cylinders at AB using the principle of conservation of circulation. These wake vortex sheets between the fan and the duct exit plane are replaced by a set of equivalent vortex rings for the purpose of the design.

For design purposes, the effect of the center body is taken into

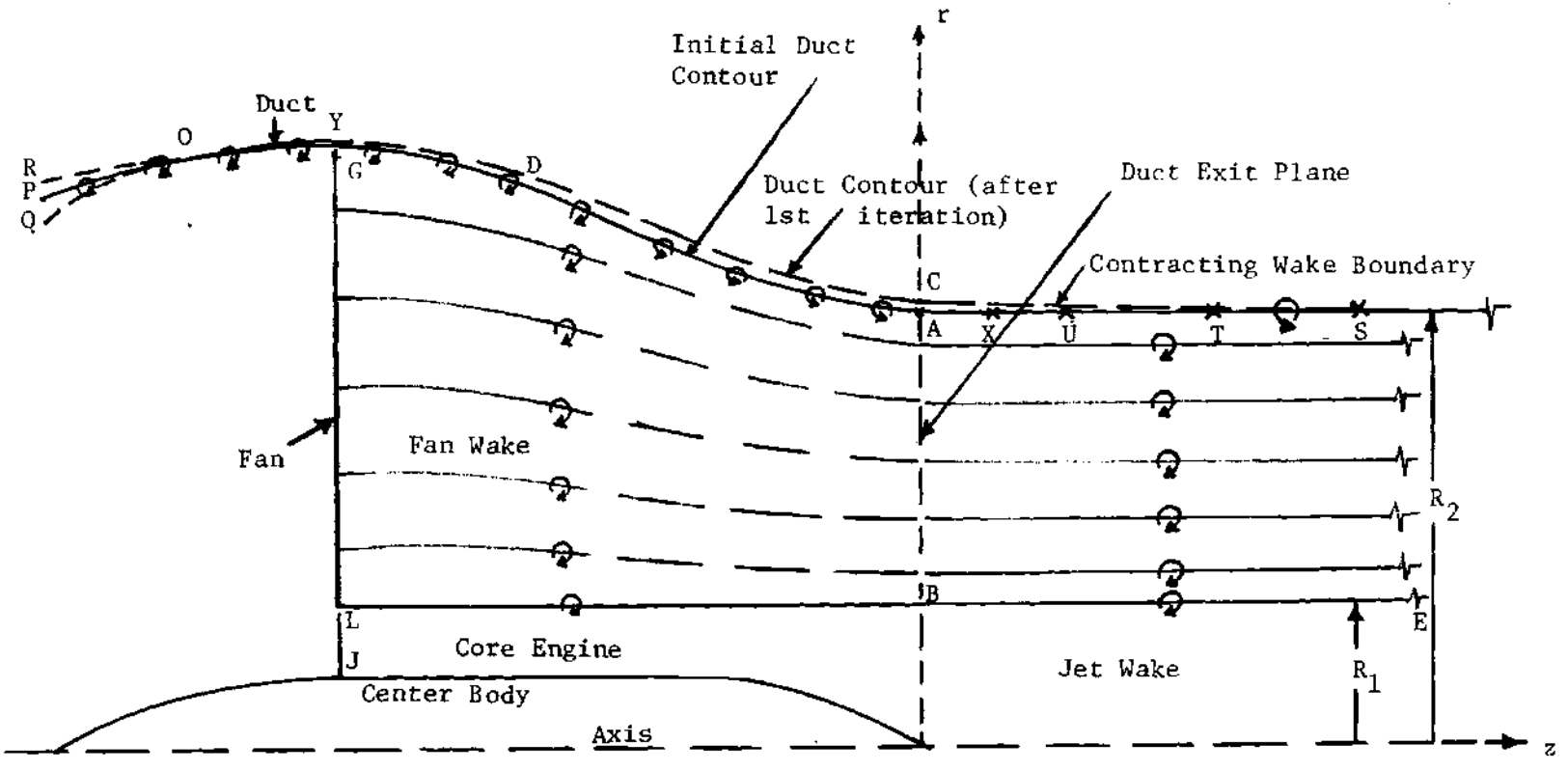

Figure 37. Schematic Diagram Of A Fan Engine And Its Wake And Duct Contour After First Iteration.

account by a suitable singularity distribution along the axis of the engine. The strengths of the singularities are determined by the shape of the center body. The flow through the core engine will also have an effect on the design of the duct and is taken into account by a sink distribution on the annulus, LJ (see Fig. 37). Thus the various singularities ahead of the duct exit plane are identified.

Step I

It is assumed that the amount of deceleration of the flow to the fan is given. Based on a one dimensional theory, the radius of the duct in the fan plane is determined from the given amount of deceleration using the continuity theorem. The radius of the duct at the trailing edge, R_2, is known. Between points A and G (see Fig. 37), a smooth contour is drawn and is used as the initial contour of the duct. The inlet portion (GP) of the duct is chosen such that there is a smooth entry of flow at its leading edge. However, in the first iteration its shape is not known. As can be seen later, its shape (GOP) is fixed by the bound vortex strengths near the leading edge. For the first iteration, a smooth contour (GOP) as shown in Fig. 37 is chosen. Having assumed the duct contour (AGP), a bound vortex strength distribution which is compatible with the contour, AGP, and satisfies the required mass flow condition at the duct exit plane, AB, is determined.

In the first iteration, the semi-infinite constant diameter, fan wake cylinders extending downstream from the duct exit plane give rise to an axial velocity distribution such that $U_z(o, r) = \frac{1}{2} U_z(\infty, r)$ where $z = o$ represents the duct exit plane and hence in order to conserve

the mass the other half of the axial velocities must be supplied by the various singularities ahead of the duct exit plane. This mass conservation is satisfied by requiring that $(\Psi_A - \Psi_B) = \frac{1}{2}$ (volume flow in the ultimate fan wake), where Ψ_A and Ψ_B are the total stream functions due to all the singularities including the duct bound vortex strengths ahead of the duct exit plane at A and B respectively.

For the purposes of the design, the duct contour (AGP) is divided into a finite number of strips. The unknown bound vorticity distribution of the duct is replaced by a set of ring vortex filaments of unknown strength which are placed at the midpoints of the segments that the ring filaments replace. A set of control points is chosen such that their number is one less than that of the unknown vortex rings. Control points are located between adjacent vortex filaments (except A and R).

In the first iteration, the effects of center body and the core engine on the duct design are neglected. Using the Biot-Savart law, the strengths of the bound ring vortex filaments are determined such that, at the control points,

$$(dr/dz) = U_r/(V_\infty + U_z)$$

and the mass flow condition at the exit is satisfied. Thus, the contour and the bound vortex strengths of the duct are obtained in the first iteration.

Step II

For the duct to be compatible with the assumed wake model aft of its trailing edge, the radial induced velocities at the wake boundary near the trailing edge of the duct must be zero. If the axial induced valocities just outside the wake boundary near the trailing edge of the duct are different from zero, the vortex sheet strength of the outer boundary will be different from that in the ultimate wake. Therefore, the radial and the axial induced velocity components are computed at several points, X, U, T, S (see Fig. 37), just outside of the wake boundary. These velocities must be zero for a compartible duct. However, these radial and axial induced velocities will be small but not zero. Therefore, the wake must contract (or expand) for a short distance (about one duct exit diameter) downstream from the duct trailing edge. The effects of this small contraction (or expansion) can be approximated however. This contraction (or expansion) is evaluated using the computed radial induced velocities at the points, X, U, and T.

In the second iteration and starting from the point, S, which is about one diameter away from the duct trailing edge, (the actual distance being selected such that the induced velocities just outside the wake boundary are negligibly small in comparison with the wake velocities), a new wake contour, SC, and duct contour, CDYP, are chosen to take into account the contraction computed earlier. It is also to be noted that the pressure should be continuous across the contour, SC. This necessitates an adjustment to the strength of the

vortex sheet, SC, which is determined by the axial induced velocities computed earlier. Depending on the shape of SC, the geometry of the inner wake vortex cylinders also change and must be taken into account.

Step III

Using the new duct contour, CDYP, the bound vortex strengths are determined in exactly the same way as was done in step I taking into account the slight contraction or expansion of the wake near the duct trailing edge. The mass flow condition, in this second iteration, is satisfied in the plane, SE. After finding the new set of bound vortex strengths, the test for compatibility is made as outlined in step II. Steps II and III are repeated until the computed geometry of the wake near the trailing edge of the duct does not change between two successive iterations. The duct so determined will have a slightly contracting (or expanding) wake and the vortex sheet strength distributions in this portion of the wake are different from those in the ultimate wake. Thus, a compatible duct with constant diameter wake cylinders extending downstream from its exit plane will never occur.

After obtaining the approximately compatible duct, the inlet, OP, of the duct is adjusted either by increasing or decreasing the leading edge radius to give a new contour, OR or OQ respectively, so that the strength of the leading edge vortex ring is small compared with the other rings and that its circulatory field is such that it decelerates the oncoming flow. This ensures an approximately smooth entry of flow at the leading edge. The effects of the core engine and center body can now be incorporated into the design by an iterative procedure. However, these will slightly change the duct contour and the

wake shape near the trailing edge of the duct. The final duct contour and the wake geometry are obtained using an iterative procedure.

As an example of the procedure, an approximately compatible, low-speed duct mean camber surface design was attempted and the result at the end of the first iteration is shown in Fig. 37 as PYC. It was found that the contraction is small (approximately 5%) and the radial induced velocities just outside the wake boundary at a distance of one diameter from the trailing edge of the duct are small (within 1% of the wake velocities).

(iv) Duct Thickness Distribution: A surface of finite thickness wrapped around the duct mean camber surface may slightly change the wake shape near the trailing edge of the duct. However, for a thin duct the effect will be negligible. The following procedure, originally due to Gray[4] is used to find the thickness distribution.

(a) Construct a reasonable inner contour using elements of existing airfoil sections being careful to match slopes and radii of curvature where different sections are joined.

(b) Equidistant on either side of and very close to the duct mean camber surface determined in iii, place a doublet ring. The location of the doublet must be well within the thickness distribution. Using the stream function data of doublet rings, determine the strength of the doublet which will locally, that is, in the plane of the doublet ring move the streamline through the trailing edge radially inward to the assumed contour. This involves the computation of the stream

function due to all the singularities including those of the wake at the surface point.

(c) A corresponding outer point may be determined in the plane of the doublet ring by adding the stream function due to the doublet ring to the values of the stream function outside of the mean camber surface. The required point is obtained where the total stream function is equal to that at the trailing edge. The outer contour is determined by connecting a few such points by a smooth curve. This is an approximate method and does not furnish the solution for the pressure distribution on the duct.

(v) Fan design: Once the duct is designed, the equivalent infinite-bladed fan need not be used. In fact, the fan is designed for the specified number of blades. The wake of the finite-bladed fan, as was described in Chapter II, is completely determined since $\bar{W}$ is known. Therefore this wake along with the duct designed earlier, is used in the design of the fan blades. In principle, since the strengths of all the singularity distributions in the wake as well as in the duct and the engine are known, the induced velocity distribution at the fan blades can be obtained. The required bound vorticity distribution of the blades is known from the wake analysis of Chapter II. From the wake analysis, the bound vorticity distribution $\Gamma'(X)$ is obtained from the corresponding $K(X)$ distribution according to the definition,

$$\Gamma'(X) = \frac{2\Pi(V_\infty + W)W}{b\Omega} K(X).$$

From the Kutta-Joukowski theorem,

$$L'(X) = \rho_\infty V\Gamma'(X) = \frac{1}{2}\rho V^2 C\, C_\ell ,$$

where $L'(X)$ = local lift per unit span,

C_ℓ = local section lift coefficient,

C = local blade chord,

and V = local total velocity.

From the above two formulae, it can be shown that

$$\sigma\, C_\ell = \frac{2W(V_\infty + W)K(X)}{\Omega r\, V} ,$$

where $\sigma = bc/2\Pi r$ - local solidity.

If the local lift coefficient distribution is specified, the chord distribution can be obtained from the last equation.

The design of the fan as well as that of the duct presented here was very much simplified and as such involved several assumptions. However the procedure detailed here is certainly helpful in the preliminary design which can be used as a first step in the complicated design of fan engines.

In practice, the ducts of the fan engines are designed using semi-empirical procedures. The real fluid effects such as viscosity and compressibility are taken into acocunt. However, the design procedure outlined here provides a basis for incorporating the real fluid effects.

It also gives a preliminary estimate of the duct contour and the bound vortex strength distribution of the duct if the compressibility effects are not large.

CHAPTER VI

CONCLUDING REMARKS

A few conclusions are made based on the analysis of the ultimate wake of a single-rotation ducted fan with finite as well as infinite number of blades. Some of these are,

(i) In order that the jet wake be compatible with the ultimate fan wake, it has to satisfy certain conditions at its interface with the helical vortex system of the fan wake. The jet wake should provide a certain combination of induced velocity components, V_j and U_{ψ_j}, at its interface with the fan wake. However, there are several such combinations of V_j and U_{ψ_j}, which satisfy the necessary compatibility relationships.

(ii) Design criteria for the single-rotation high by-pass ratio ducted fan with the highest possible induced efficiency for the assumed non-contracting ultimate wake were obtained numerically. In the case of the ducted fan with infinite number of blades, the design criteria were obtained analytically. The accuracy of the numerical procedures used in determining the vortex strength distribution, the thrust and the induced power for a fan with finite number of blades, is supported by the rapid convergence of this data to that of the infinite number of blades. This convergence also makes the approximation of a finite bladed fan with a large number of blades by an equivalent infinite

bladed fan valid. The distinct advantage in making such an approximation is the considerable saving in the computational time associated with the generation of the data of a finite bladed fan with a large number of blades. This can be very helpful in the design of a compatible duct.

(iii) The assumed ultimate fan wake gives rise to the highest possible induced efficiency for a single-rotation ducted fan. It should be noted that a fan-stator combination will have a higher induced efficiency than a single-rotation fan developing the same thrust, since the tangential wake velocities in the former case will be much smaller. However, the row of stator blades increases the weight, profile drag, and cost of the ducted fan. The saving in weight, profile drag, and cost of a single-rotation ducted fan without any stator blades may prove to be more desirable from a complete cost-benefit analysis viewpoint. However, a thorough investigation has to be made regarding the comparative advantages of these two types of ducted fans before reaching any conclusions.

(iv) The design procedure suggested is based on the potential, incompressible wake model and therefore furnishes a preliminary estimate of the compatible duct. Real fluid effects such as compressibility and viscosity as well as the effects of a finite blade-tip clearance are to be taken into account for a comprehensive design of the duct-fan system.

(v) The analysis presented is valid for the static case as well as for flight speeds at which the induced velocities are small enough to neglect compressibility effects.

Table 1. Index To Data Tables.

Table No.	λ_2	m	b
2	0·500	0·333	2
3	0·500	0·333	3
4	0·500	0·333	6
5	0·500	0·333	∞
6	0·625	0·333	2
7	0·625	0·333	6
8	0·625	0·333	∞
9	0·750	0·333	1
10	0·750	0·333	2
11	0·750	0·333	4
12	0·750	0·333	∞
13	1·000	0·333	1
14	1·000	0·333	2
15	1·000	0·333	6
16	1·000	0·333	8
17	1·000	0·333	12
18	1·000	0·333	∞
19	1·000	0·250	2
20	1·000	0·250	∞
21	1·000	0·500	2
22	1·000	0·500	∞

Table 2.

$\lambda_2 = .50, m = .333, b = 2$

X	$K_0(x)$	$\bar{W}/\lambda_2$	C_T	$C_{P_{VI}}$	C_{T_P}/C_T	G
		0.00	0.00	0.00	1.00	1.00
0.3333	.5223	0.05	.0069	.0034	.9834	.980
		0.10	.0136	.0065	.9657	.959
0.4000	.5356	0.15	.0202	.0094	.9468	.938
		0.20	.0267	.0120	.9268	.917
0.4667	.5571	0.25	.0332	.0144	.9056	.895
		0.30	.0395	.0166	.8832	.873
0.5333	.5803	0.35	.0459	.0186	.8597	.850
		0.40	.0522	.0204	.8350	.827
0.6000	.6027	0.45	.0585	.0220	.8094	.804
		0.50	.0649	.0235	.7827	.780
0.6667	.6230	0.55	.0714	.0248	.7550	.756
		0.60	.0781	.0259	.7266	.732
0.7333	.6405	0.65	.0848	.0269	.6975	.708
		0.70	.0917	.0277	.6677	.683
0.8000	.6550	0.75	.0989	.0284	.6373	.657
		0.80	.1063	.0290	.6066	.632
0.8667	.6663	0.85	.1140	.0294	.5756	.606
		0.90	.1220	.0297	.5445	.580
0.9333	.6738	0.95	.1303	.0299	.5133	.554
1.0000	.6770	1.00	.1390	.0300	.4822	.528

Table 3.

$\lambda_2 = .50, m = .333, b = 3$

X	$K_0(x)$	$\bar{W}/\lambda_2$	C_T	$C_{P_{VI}}$	C_{T_P}/C_T	G
		0.00	0.00	0.00	1.00	1.00
0.3333	.4809	0.05	.0070	.0034	.9834	
		0.10	.0137	.0065	.9657	
0.4000	.5006	0.15	.0204	.0094	.9469	
		0.20	.0270	.0121	.9268	
0.4667	.5317	0.25	.0335	.0145	.9056	
		0.30	.0399	.0167	.8833	
0.5333	.5651	0.35	.0463	.0188	.8598	
		0.40	.0527	.0206	.8352	
0.6000	.5972	0.45	.0591	.0222	.8096	
		0.50	.0655	.0237	.7830	
0.6667	.6262	0.55	.0721	.0250	.7554	
		0.60	.0787	.0261	.7271	
0.7333	.6513	0.65	.0855	.0272	.6980	
		0.70	.0925	.0280	.6682	
0.8000	.6721	0.75	.0997	.0287	.6380	
		0.80	.1072	.0293	.6073	
0.8667	.6881	0.85	.1149	.0297	.5764	
		0.90	.1229	.0300	.5453	
0.9333	.6991	0.95	.1313	.0302	.5142	
1.0000	.7038	1.00	.1401	.0303	.4832	

Table 4.

$\lambda_2 = .5$, $m = .333$, $b = 6$

X	$K_0(x)$	$\bar{W}/\lambda_2$	C_T	$C_{P_{VI}}$	C_{T_P}/C_T	G
		0.00	0.00	0.00	1.00	1.00
0.3333	.4025	0.05	.0071	.0034	.9831	
		0.10	.0140	.0066	.9651	
0.4000	.4375	0.15	.0207	.0096	.9460	
		0.20	.0274	.0123	.9258	
0.4667	.4883	0.25	.0340	.0148	.9044	
		0.30	.0406	.0170	.8819	
0.5333	.5406	0.35	.0471	.0191	.8584	
		0.40	.0536	.0210	.8338	
0.6000	.5894	0.45	.0601	.0227	.8082	
		0.50	.0667	.0242	.7816	
0.6667	.6329	0.55	.0734	.0255	.7542	
		0.60	.0801	.0267	.7260	
0.7333	.6703	0.65	.0871	.0277	.6971	
		0.70	.0942	.0286	.6676	
0.8000	.7014	0.75	.1015	.0293	.6376	
		0.80	.1090	.0299	.6072	
0.8667	.7259	0.85	.1168	.0304	.5765	
		0.90	.1249	.0307	.5457	
0.9333	.7431	0.95	.1334	.0309	.5148	
1.0000	.7511	1.00	.1422	.0310	.4840	

Table 5.

$\lambda_2 = .50$, $m = .333$, $b = \infty$

X	$K_0(x)$	$\bar{W}/\lambda_2$	C_T	$C_{P_{VI}}$	C_{T_P}/C_T	G
		0.00	0.00	0.00	1.00	1.00
0.3333	.3077	0.05	.0071	.0035	.9826	
		0.10	.0142	.0067	.9641	
0.4000	.3902	0.15	.0211	.0097	.9446	
		0.20	.0278	.0125	.9240	
0.4667	.4656	0.25	.0346	.0150	.9024	
		0.30	.0412	.0173	.8797	
0.5333	.5322	0.35	.0479	.0194	.8560	
		0.40	.0545	.0214	.8313	
0.6000	.5902	0.45	.0611	.0231	.8057	
		0.50	.0678	.0247	.7792	
0.6667	.6400	0.55	.0746	.0260	.7519	
		0.60	.0815	.0272	.7238	
0.7333	.6827	0.65	.0886	.0283	.6951	
		0.70	.0958	.0292	.6658	
0.8000	.7191	0.75	.1032	.0300	.6360	
		0.80	.1108	.0306	.6059	
0.8667	.7503	0.85	.1187	.0310	.5756	
		0.90	.1269	.0314	.5450	
0.9333	.7770	0.95	.1354	.0316	.5145	
1.0000	.8000	1.00	.1442	.0316	.4840	

Table 6.

$\lambda_2 = .625, m = .333, b = 2$

X	$K_0(x)$	$\bar{W}/\lambda_2$	C_T	$C_{P_{VI}}$	C_{T_P}/C_T	G
		0.00	0.00	0.00	1.00	1.00
0.3333	.4257	0.05	.0089	.0054	.9855	.985
		0.10	.0176	.0104	.9696	.970
0.4000	.4368	0.15	.0261	.0150	.9525	.952
		0.20	.0344	.0192	.9339	.934
0.4667	.4556	0.25	.0425	.0230	.9140	.914
		0.30	.0506	.0264	.8926	.893
0.5333	.4764	0.35	.0586	.0295	.8697	.870
		0.40	.0666	.0323	.8454	.845
0.6000	.4968	0.45	.0746	.0348	.8196	.820
		0.50	.0828	.0370	.7925	.793
0.6667	.5157	0.55	.0911	.0389	.7641	.764
		0.60	.0996	.0406	.7346	.735
0.7333	.5323	0.65	.1084	.0420	.7039	.704
		0.70	.1175	.0432	.6723	.672
0.8000	.5463	0.75	.1269	.0442	.6399	.640
		0.80	.1369	.0450	.6069	.607
0.8667	.5572	0.85	.1473	.0456	.5736	.574
		0.90	.1584	.0461	.5400	.540
0.9333	.5645	0.95	.1701	.0463	.5063	.506
1.0000	.5677	1.00	.1826	.0464	.4729	.473

Table 7.

$\lambda_2 = .625, m = .333, b = 6$

X	$K_0(x)$	$\bar{W}/\lambda_2$	C_T	$C_{P_{VI}}$	C_{T_P}/C_T	G
		0.00	0.00	0.00	1.00	1.00
0.3333	.3129	0.05	.0092	.0056	.9855	
		0.10	.0182	.0108	.9696	
0.4000	.3425	0.15	.0270	.0156	.9525	
		0.20	.0356	.0199	.9340	
0.4667	.3878	0.25	.0441	.0239	.9142	
		0.30	.0525	.0275	.8929	
0.5333	.4365	0.35	.0608	.0307	.8701	
		0.40	.0691	.0336	.8460	
0.6000	.4837	0.45	.0775	.0362	.8205	
		0.50	.0859	.0385	.7936	
0.6667	.5270	0.55	.0945	.0405	.7655	
		0.60	.1033	.0423	.7362	
0.7333	.5652	0.65	.1124	.0438	.7059	
		0.70	.1217	.0451	.6747	
0.8000	.5977	0.75	.1315	.0462	.6427	
		0.80	.1417	.0470	.6100	
0.8667	.6236	0.85	.1524	.0477	.5770	
		0.90	.1637	.0481	.5437	
0.9333	.6419	0.95	.1756	.0484	.5104	
1.0000	.6505	1.00	.1883	.0485	.4773	

Table 8.

$\lambda_2 = .625, m = .333, b = \infty$

X	$K_0(x)$	$\bar{W}/\lambda_2$	C_T	$C_{P_{VI}}$	C_{T_P}/C_T	G
		0.00	0.00	0.00	1.00	1.00
0.3333	.2214	0.05	.0095	.0058	.9848	
		0.10	.0181	.0111	.9684	
0.4000	.2906	0.15	.0277	.0160	.9508	
		0.20	.0366	.0204	.9318	
0.4667	.3580	0.25	.0453	.0245	.9116	
		0.30	.0539	.0282	.8900	
0.5333	.4213	0.35	.0625	.0316	.8671	
		0.40	.0710	.0346	.8429	
0.6000	.4796	0.45	.0797	.0373	.8173	
		0.50	.0883	.0397	.7906	
0.6667	.5322	0.55	.0972	.0418	.7626	
		0.60	.1062	.0437	.7336	
0.7333	.5793	0.65	.1155	.0453	.7036	
		0.70	.1251	.0466	.6727	
0.8000	.6210	0.75	.1350	.0478	.6411	
		0.80	.1454	.0487	.6089	
0.8667	.6579	0.85	.1563	.0494	.5763	
		0.90	.1678	.0499	.5436	
0.9333	.6904	0.95	.1798	.0502	.5107	
1.0000	.7191	1.00	.1926	.0503	.4779	

Table 9.

$\lambda_2 = .75, m = .333, b = 1$

X	$K_0(x)$	$\bar{W}/\lambda_2$	C_T	$C_{P_{VI}}$	C_{T_P}/C_T	G
		0.00	0.00	0.00	1.00	1.00
0.3333	.3823	0.05	.0104	.0076	.9861	.984
		0.10	.0205	.0146	.9709	.967
0.4000	.3870	0.15	.0304	.0210	.9544	.949
		0.20	.0400	.0268	.9365	.931
0.4667	.3947	0.25	.0495	.0321	.9171	.912
		0.30	.0588	.0368	.8961	.893
0.5333	.4036	0.35	.0681	.0410	.8734	.873
		0.40	.0774	.0447	.8491	.852
0.6000	.4125	0.45	.0867	.0480	.8231	.831
		0.50	.0962	.0509	.7955	.809
0.6667	.4209	0.55	.1059	.0534	.7663	.786
		0.60	.1159	.0556	.7355	.763
0.7333	.4284	0.65	.1263	.0574	.7035	.739
		0.70	.1372	.0589	.6702	.714
0.8000	.4346	0.75	.1487	.0601	.6359	.689
		0.80	.1609	.0611	.6008	.663
0.8667	.4393	0.85	.1740	.0619	.5651	.637
		0.90	.1880	.0624	.5292	.610
0.9333	.4425	0.95	.2031	.0627	.4933	.583
1.0000	.4442	1.00	.2195	.0628	.4576	.551

Table 10.

$\lambda_2 = .75$, $m = .333$, $b = 2$

X	$K_0(x)$	$\bar{W}/\lambda_2$	C_T	$C_{P_{VI}}$	C_{T_P}/C_T	G
		0.00	0.00	0.00	1.00	1.00
0.3333	.3486	0.05	.0106	.0078	.9867	
		0.10	.0209	.0149	.9721	
0.4000	.3580	0.15	.0310	.0214	.9561	
		0.20	.0408	.0273	.9387	
0.4667	.3738	0.25	.0504	.0326	.9197	
		0.30	.0599	.0375	.8990	
0.5333	.3917	0.35	.0693	.0418	.8768	
		0.40	.0787	.0456	.8528	
0.6000	.4095	0.45	.0881	.0489	.8270	
		0.50	.0977	.0519	.7996	
0.6667	.4263	0.55	.1075	.0544	.7706	
		0.60	.1177	.0566	.7400	
0.7333	.4413	0.65	.1282	.0585	.7080	
		0.70	.1392	.0600	.6747	
0.8000	.4540	0.75	.1508	.0613	.6404	
		0.80	.1632	.0623	.6052	
0.8667	.4641	0.85	.1764	.0630	.5696	
		0.90	.1905	.0636	.5336	
0.9333	.4711	0.95	.2058	.0639	.4976	
1.0000	.4741	1.00	.2222	.0640	.4618	

Table 11.

$\lambda_2 = .75, m = .333, b = 4$

X	$K_0(x)$	$\bar{W}/\lambda_2$	C_T	$C_{P_{VI}}$	C_{T_P}/C_T	G
		0.00	0.00	0.00	1.00	1.00
0.3333	.2881	0.05	.0109	.0080	.9873	
		0.10	.0215	.0153	.9733	
0.4000	.3060	0.15	.0319	.0220	.9579	
		0.20	.0419	.0280	.9410	
0.4667	.3359	0.25	.0518	.0336	.9225	
		0.30	.0615	.0385	.9023	
0.5333	.3693	0.35	.0712	.0429	.8804	
		0.40	.0808	.0468	.8568	
0.6000	.4027	0.45	.0905	.0503	.8314	
		0.50	.1003	.0533	.8042	
0.6667	.4340	0.55	.1103	.0559	.7754	
		0.60	.1206	.0581	.7451	
0.7333	.4620	0.65	.1314	.0600	.7132	
		0.70	.1426	.0616	.6801	
0.8000	.4860	0.75	.1544	.0630	.6459	
		0.80	.1670	.0640	.6109	
0.8667	.5050	0.85	.1804	.0648	.5752	
		0.90	.1947	.0653	.5392	
0.9333	.5184	0.95	.2102	.0657	.5032	
1.0000	.5244	1.00	.2268	.0658	.4674	

Table 12.

$\lambda_2 = .75$, $m = .333$, $b = \infty$

X	$K_0(x)$	$\bar{w}/\lambda_2$	C_T	$C_{P_{VI}}$	C_{T_P}/C_T	G
		0.00	0.00	0.00	1.00	1.00
0.3333	.1649	0.05	.0115	.0084	.9868	
		0.10	.0227	.0161	.9723	
0.4000	.2215	0.15	.0336	.0232	.9564	
		0.20	.0442	.0296	.9391	
0.4667	.2791	0.25	.0547	.0354	.9204	
		0.30	.0650	.0407	.9000	
0.5333	.3358	0.35	.0752	.0455	.8780	
		0.40	.0854	.0497	.8544	
0.6000	.3902	0.45	.0956	.0534	.8291	
		0.50	.1060	.0567	.8023	
0.6667	.4414	0.55	.1166	.0596	.7739	
		0.60	.1275	.0620	.7440	
0.7333	.4888	0.65	.1388	.0642	.7128	
		0.70	.1505	.0659	.6803	
0.8000	.5322	0.75	.1628	.0674	.6469	
		0.80	.1759	.0686	.6126	
0.8667	.5718	0.85	.1897	.0695	.5777	
		0.90	.2045	.0700	.5425	
0.9333	.6076	0.95	.2203	.0705	.5071	
1.0000	.6400	1.00	.2373	.0706	.4720	

Table 13.

$\lambda_2 = 1.0, m = .333, b = 1$

X	$K_0(x)$	$\bar{W}/\lambda_2$	C_T	$C_{P_{VI}}$	C_{T_P}/C_T	G
		0.00	0.00	0.00	1.00	1.00
0.3333	.2625	0.05	.0128	.0125	.9867	.987
		0.10	.0252	.0239	.9722	.974
0.4000	.2657	0.15	.0373	.0344	.9565	.960
		0.20	.0491	.0438	.9394	.945
0.4667	.2712	0.25	.0607	.0523	.9208	.929
		0.30	.0720	.0598	.9005	.912
0.5333	.2776	0.35	.0833	.0665	.8784	.895
		0.40	.0946	.0723	.8544	.877
0.6000	.2843	0.45	.1059	.0773	.8284	.858
		0.50	.1175	.0815	.8004	.838
0.6667	.2906	0.55	.1295	.0851	.7702	.817
		0.60	.1419	.0881	.7380	.795
0.7333	.2963	0.65	.1550	.0906	.7038	.772
		0.70	.1690	.0925	.6678	.748
0.8000	.3011	0.75	.1842	.0941	.6302	.723
		0.80	.2006	.0952	.5914	.697
0.8667	.3048	0.85	.2187	.0961	.5517	.671
		0.90	.2386	.0967	.5115	.643
0.9333	.3075	0.95	.2608	.0970	.4713	.615
1.0000	.3090	1.00	.2854	.0971	.4316	.586

Table 14.

$\lambda_2 = 1.0$, $m = .333$, $b = 2$

X	$K_0(x)$	$\bar{W}/\lambda_2$	C_T	$C_{P_{VI}}$	C_{T_P}/C_T	G
		0.00	0.00	0.00	1.00	1.00
0.3333	.2390	0.05	.0132	.0128	.9880	
		0.10	.0259	.0246	.9749	
0.4000	.2453	0.15	.0382	.0352	.9604	
		0.20	.0503	.0448	.9444	
0.4667	.2567	0.25	.0620	.0534	.9268	
		0.30	.0736	.0610	.9074	
0.5333	.2699	0.35	.0850	.0678	.8862	
		0.40	.0964	.0736	.8629	
0.6000	.2834	0.45	.1079	.0787	.8375	
		0.50	.1196	.0829	.8099	
0.6667	.2963	0.55	.1316	.0866	.7780	
		0.60	.1441	.0896	.7479	
0.7333	.3080	0.65	.1574	.0920	.7137	
		0.70	.1715	.0940	.6777	
0.8000	.3181	0.75	.1868	.0955	.6399	
		0.80	.2034	.0967	.6007	
0.8667	.3262	0.85	.2216	.0975	.5606	
		0.90	.2418	.0981	.5200	
0.9333	.3317	0.95	.2641	.0984	.4793	
1.0000	.3344	1.00	.2890	.0985	.4391	

Table 15.

$\lambda_2 = 1.0$, $m = .333$, $b = 6$

X	$K_0(x)$	$\bar{W}/\lambda_2$	C_T	$C_{P_{vz}}$	C_{T_P}/C_T	G
		0.00	0.00	0.00	1.00	1.00
0.3333	.1638	0.05	.0140	.0137	.9900	
		0.10	.0276	.0262	.9787	
0.4000	.1809	0.15	.0407	.0375	.9661	
		0.20	.0534	.0476	.9518	
0.4667	.2095	0.25	.0658	.0567	.9358	
		0.30	.0779	.0648	.9179	
0.5333	.2422	0.35	.0899	.0718	.8980	
		0.40	.1019	.0780	.8759	
0.6000	.2756	0.45	.1139	.0834	.8515	
		0.50	.1260	.0879	.8247	
0.6667	.3079	0.55	.1386	.0918	.7955	
		0.60	.1516	.0950	.7640	
0.7333	.3376	0.65	.1653	.0976	.7301	
		0.70	.1800	.0997	.6942	
0.8000	.3638	0.75	.1957	.1014	.6565	
		0.80	.2129	.1027	.6172	
0.8667	.3853	0.85	.2316	.1036	.5769	
		0.90	.2523	.1043	.5359	
0.9333	.4010	0.95	.2752	.1047	.4948	
1.0000	.4084	1.00	.3007	.1048	.4540	

Table 16.

$\lambda_2 = 1.0$, $m = .333$, $b = 8$

X	$K_0(x)$	$\bar{W}/\lambda_2$	C_T	$C_{P_{VI}}$	C_{T_P}/C_T	G
		0.00	0.00	0.00	1.00	1.00
0.3333	.1447	0.05	.0143	.0139	.9901	
		0.10	.0280	.0266	.9790	
0.4000	.1652	0.15	.0414	.0381	.9665	
		0.20	.0543	.0484	.9523	
0.4667	.1980	0.25	0.0668	.0576	.9365	
		0.30	.0792	.0658	.9187	
0.5333	.2350	0.35	.0914	.0730	.8989	
		0.40	.1035	.0793	.8769	
0.6000	.2729	0.45	.1157	.0848	.8527	
		0.50	.1280	.0894	.8260	
0.6667	.3098	0.55	.1407	.0934	.7970	
		0.60	.1539	.0967	.7656	
0.7333	.3442	0.65	.1678	.0994	.7319	
		0.70	.1826	.1015	.6961	
0.8000	.3749	0.75	.1986	.1033	.6585	
		0.80	.2159	.1046	.6194	
0.8667	.4006	0.85	.2348	.1056	.5792	
		0.90	.2556	.1063	.5383	
0.9333	.4196	0.95	.2787	.1067	.4973	
1.0000	.4290	1.00	.3043	.1068	.4566	

Table 17.

$\lambda_2 = 1.0$, $m = .333$, $b = 12$

X	$K_0(x)$	$\bar{W}/\lambda_2$	C_T	$C_{P_{VI}}$	C_{T_P}/C_T	G
		0.00	0.00	0.00	1.00	1.00
0.3333	.1248	0.05	.0145	.0141	.9901	
		0.10	.0285	.0270	.9789	
0.4000	.1501	0.15	.0421	.0387	.9664	
		0.20	.0552	.0492	.9522	
0.4667	.1872	0.25	.0680	.0586	.9364	
		0.30	.0806	.0670	.9186	
0.5333	.2280	0.35	.0930	.0744	.8989	
		0.40	.1053	.0808	.8769	
0.6000	.2695	0.45	.1177	.0864	.8528	
		0.50	.1302	.0911	.8262	
0.6667	.3104	0.55	.1431	.0952	.7973	
		0.60	.1566	.0986	.7661	
0.7333	.3493	0.65	.1707	.1014	.7326	
		0.70	.1857	.1036	.6970	
0.8000	.3850	0.75	.2018	.1054	.6596	
		0.80	.2193	.1068	.6207	
0.8667	.4160	0.85	.2384	.1079	.5807	
		0.90	.2594	.1086	.5401	
0.9333	.4401	0.95	.2826	.1090	.4992	
1.0000	.4528	1.00	.3083	.1091	.4587	

Table 18.

$\lambda_2 = 1.0$, $m = .333$, $b = \infty$

X	$K_0(x)$	$\bar{W}/\lambda_2$	C_T	$C_{P_{VI}}$	C_{T_P}/C_T	G
		0.00	0.00	0.00	1.00	1.00
0.3333	.1000	0.05	.0148	.0144	.9900	
		0.10	.0290	.0275	.9787	
0.4000	.1379	0.15	.0428	.0394	.9661	
		0.20	.0562	.0502	.9519	
0.4667	.1788	0.25	.0693	.0598	.9360	
		0.30	.0821	.0684	.9182	
0.5333	.2214	0.35	.0947	.0759	.8984	
		0.40	.1073	.0825	.8765	
0.6000	.2647	0.45	.1199	.0882	.8524	
		0.50	.1327	.0932	.8260	
0.6667	.3077	0.55	.1459	.0974	.7972	
		0.60	.1595	.1009	.7662	
0.7333	.3497	0.65	.1739	.1038	.7329	
		0.70	.1891	.1062	.6975	
0.8000	.3902	0.75	.2054	.1081	.6604	
		0.80	.2231	.1095	.6218	
0.8667	.4289	0.85	.2424	.1106	.5821	
		0.90	.2636	.1114	.5417	
0.9333	.4656	0.95	.2870	.1118	.5011	
1.0000	.5000	1.00	.3129	.1119	.4607	

Table 19.

$\lambda_2 = 1.0, m = .25, b = 2$

X	$K_0(x)$	$\bar{W}/\lambda_2$	C_T	$C_{P_{VI}}$	C_{T_P}/C_T	G
		0.00	0.00	0.00	1.00	1.00
.250	.1873	0.05	.0127	.0124	.9876	
		0.10	.0250	.0238	.9739	
.325	.1969	0.15	.0370	.0341	.9590	
		0.20	.0486	.0434	.9425	
.400	.2134	0.25	.0600	.0517	.9245	
		0.30	.0712	.0591	.9047	
.475	.2319	0.35	.0823	.0656	.8829	
		0.40	.0935	.0712	.8591	
.550	.2502	0.45	.1047	.0761	.8330	
		0.50	.1161	.0802	.8048	
.625	.2676	0.55	.1280	.0831	.7742	
		0.60	.1403	.0865	.7414	
.700	.2831	0.65	.1534	.0889	.7064	
		0.70	.1675	.0907	.6695	
.775	.2964	0.75	.1828	.0922	.6309	
		0.80	.1994	.0933	.5909	
.850	.3069	0.85	.2179	.0941	.5500	
		0.90	.2383	.0946	.5087	
.925	.3141	0.95	.2611	.0949	.4675	
1.00	.3175	1.00	.2867	.0950	.4269	

Table 20.

$\lambda_2 = 1.0$, $m = .25$, $b = \infty$

X	$K_0(x)$	$\bar{w}/\lambda_2$	C_T	$C_{P_{VI}}$	C_{T_P}/C_T	G
		0.00	0.00	0.00	1.00	1.00
.250	.0588	0.05	.0149	.0146	.9901	
		0.10	.0294	.0279	.9789	
.325	.0955	0.15	.0434	.0399	.9663	
		0.20	.0569	.0508	.9521	
.400	.1379	0.25	.0701	.0605	.9363	
		0.30	.0831	.0691	.9185	
.475	.1840	0.35	.0959	.0768	.8987	
		0.40	.1086	.0834	.8767	
.550	.2322	0.45	.1214	.0892	.8524	
		0.50	.1344	.0942	.8257	
.625	.2809	0.55	.1477	.0984	.7967	
		0.60	.1616	.1019	.7652	
.700	.3289	0.65	.1762	.1048	.7316	
		0.70	.1918	.1072	.6958	
.775	.3752	0.75	.2085	.1091	.6581	
		0.80	.2267	.1106	.6190	
.850	.4194	0.85	.2466	.1117	.5788	
		0.90	.2686	.1124	.5379	
.925	.4611	0.95	.2928	.1128	.4968	
1.000	.5000	1.00	.3197	.1130	.4561	

Table 21.

$\lambda_2 = 1.0$, $m = .50$, $b = 2$

x	$K_0(x)$	$\bar{W}/\lambda_2$	C_T	$C_{P_{VI}}$	C_{T_P}/C_T	G
		0.00	0.00	0.00	1.00	1.00
.500	.3265	0.05	.0131	.0127	.9886	
		0.10	.0257	.0244	.9759	
.550	.3293	0.15	.0380	.0350	.9619	
		0.20	.0499	.0446	.9466	
.600	.3342	0.25	.0616	.0532	.9296	
		0.30	.0731	.0608	.9109	
.650	.3402	0.35	.0844	.0676	.8904	
		0.40	.0957	.0736	.8681	
.700	.3467	0.45	.1070	.0787	.8436	
		0.50	.1185	.0832	.8172	
.750	.3530	0.55	.1302	.0869	.7881	
		0.60	.1423	.0901	.7580	
.800	.3589	0.65	.1551	.0927	.7253	
		0.70	.1686	.0949	.6909	
.850	.3640	0.75	.1829	.0966	.6548	
		0.80	.1984	.0979	.6174	
.900	.3682	0.85	.2153	.0989	.5789	
		0.90	.2336	.0995	.5398	
.950	.3711	0.95	.2538	.0999	.5004	
1.00	.3726	1.00	.2760	.1000	.4612	

Table 22.

$\lambda_2 = 1.0, m = .50, b = \infty$

X	$K_0(x)$	$\bar{W}/\lambda_2$	C_T	$C_{P_{VI}}$	C_{T_P}/C_T	G
		0.00	0.00	0.00	1.00	1.00
.500	.2000	0.05	.0138	.0134	.9896	
		0.10	.0271	.0257	.9780	
.550	.2322	0.15	.0399	.0367	.9650	
		0.20	.0525	.0468	.9505	
.600	.2647	0.25	.0647	.0559	.9344	
		0.30	.0767	.0639	.9166	
.650	.2970	0.35	.0885	.0710	.8969	
		0.40	.1003	.0773	.8752	
.700	.3289	0.45	.1121	.0827	.8514	
		0.50	.1240	.0875	.8256	
.750	.3600	0.55	.1362	.0914	.7975	
		0.60	.1488	.0949	.7673	
.800	.3902	0.65	.1620	.0977	.7350	
		0.70	.1759	.0999	.7008	
.850	.4194	0.75	.1907	.1018	.6650	
		0.80	.2067	.1032	.6277	
.900	.4475	0.85	.2239	.1044	.5893	
		0.90	.2428	.1051	.5502	
.950	.4744	0.95	.2634	.1055	.5108	
1.00	.5000	1.00	.2860	.1057	.4715	

BIBLIOGRAPHY

1. Weetman, R. J., and Cromack, D. E., "Ducted Propellers: A Review and Description of Current Investigations," Massachusetts University, Jan. 1970.

2. Wright, T., "Determination of the Design Parameters for Optimum Heavily Loaded Ducted Fans," Ph.D Thesis, School of Aerospace Engineering, Georgia Institute of Technology, Nov. 1969.

3. Betz, A., "Screw Propellers With Minimum Energy Loss," Technical Translation 736, National Research Council of Canada, Ottawa, Canada, 1958.

4. Gray, R. B., "An Investigation of an Approach to the Problem of Determining the Optimum Design of Shrouded Propellers," TREC 60-44, May 1960, U. S. Army Transportation Research Command, Fort Eustis, Va.

5. Gray, R. B., "An Investigation of a Digital Computer Method of Determining the Optimum Design Parameters of Shrouded Propellers," TREC 61-124, Oct. 1961, U. S. Army Transportation Research Command, Fort Eustis, Va.

6. Gray, R. B., "Analysis of a Heavily Loaded Ducted Fan With an Infinite Number of Blades," Unpublished.

7. Theodorsen, T., Theory of Ducted Propellers, McGraw-Hill Book Company, Inc., New York, N. Y., 1968.

8. Lamb, H., Hydrodynamics, Dover Publications, New York, N. Y., 1945.

9. Cranahan, B., Luther, H. A., and Wilkes, O. J., Applied Numerical Methods, John Wiley & Sons, Inc., 1969.

10. Hamming, R. W., Numerical Methods for Scientists and Engineers, McGraw-Hill Book Company, Inc., 1973.

11. Lieblein, S., and Stockman, N. O., "Compressibility Correction for Internal Flow Solutions," Journal of Aircraft, Vol. 9, No. 4, April 1972, pp. 312-313.

VITA

Damaraju Subramanya Janakiram was born in May, 1949 in Repalle, India. He had his early education in Vizianagaram, India. He graduated from M.R.M.P. School in 1965 and subsequently joined the Andhra University Engineering College. He earned his Bachelor of Engineering degree in 1970 with distinction in Mechanical Engineering.

He joined the Indian Institute of Science in 1970 where he did his postgraduate work in Aeronautical Engineering. He graduated from the Indian Institute of Science in 1972 with distinction.

He entered the Georgia Institute of Technology in the fall of 1972. He is a student member of AIAA.